Calcium Carbonate as a Functional Filler in Polyamide 12
-
Manipulation of the thermal and mechanical properties

by

Fabio Mauro Ippolito

A Thesis submitted in fulfilment for the degree of

Doctor of Philosophy in Mechanical Engineering

October 2021

University of Swansea
College of Engineering

In collaboration with

Hochschule der Medien Stuttgart
Department of Print and Media

Swansea University
Prifysgol Abertawe

HOCHSCHULE DER MEDIEN

Acknowledgements

I wish to thank the supervisors of this research project, Dr. Tim Claypole and Dr. Gunter Hübner. They made this study possible and their support, encouragement, guidance, and wise words have been continuous throughout the course of this work.

I also wish to express sincere gratitude to Dr. Patrick Gane for his support, the many useful discussions, his assistance and friendship during my journey.

A special thanks to my research colleague Rene Blum. With his friendship, support and assistance throughout the years, he kept me pushing forward and stopped me from losing sight. I would not stand where I am today without his endless support and wisdom.

Many thanks to the people working in Omya's research laboratories for their help, patience and for always keeping up with my special requests.

To Samantha, Emilia and Liara, my family for all their love and encouragement and for being able to cope with my absence and 'not always so pleasant when under stress' self. I would not have been able to finish this journey without them and this work is dedicated to them.

Publications

F. Ippolito, S. Rentsch, G. Hübner, T. Claypole, P. Gane, **Influence of calcium carbonate on polyamide 12 regarding melting, formability and crystallisation properties**, Composites Part B: Engineering 164 (**2019**) 158-167.
https://doi.org/10.1016/j.compositesb.2018.11.079

F. Ippolito, G. Hübner, T. Claypole, P. Gane, **Influence of the Surface Modification of Calcium Carbonate on Polyamide 12 Composites**, Polymers 12(6) (**2020**) 1295.
https://doi.org/10.3390/polym12061295

F. Ippolito, G. Hübner, T. Claypole, P. Gane, **Impact of Bimodal Particle Size Distribution Ratio of Functional Calcium Carbonate Filler on Thermal and Flowability Properties of Polyamide 12**, Applied Sciences 11(2) (**2021**) 641.
https://doi.org/10.3390/app11020641

F. Ippolito, G. Hübner, T. Claypole, P. Gane, **Calcium Carbonate as Functional Filler in Polyamide 12 - Manipulation of the Thermal and Mechanical Properties**, Processes 9(6) (**2021**) 937.
https://doi.org/10.3390/pr9060937

Table of Contents

List of Figures

List of Tables

List of Abbreviations

AM	Additive Manufacturing	
CAD	Computer-aided design	
LS	Laser Sintering	
SLS	Selective Laser Sintering	
GCC	Ground Calcium Carbonate	
PCC	Precipitated Calcium Carbonate	
sc-PCC	Scalenohedral Precipitated Calcium Carbonate	
pr-PCC	Prismatic Precipitated Calcium Carbonate	
$CaCO_3$	Calcium Carbonate	
CaO	Calcium Oxide	
CO_2	Carbon Dioxide	
A_n	Andrew Number	
P_{LS}	Laser Power	
v_{LS}	Laser beam scan speed	
d_{LS}	Laser overlap	
rpm	rotational speed, rounds per minute	
EOS PA2200	Polyamide 12 Grade for SLS from Company EOS	
PA12	Polyamide 12	
DPM	Degree of Particle Melt	
vc-G	very coarse GCC grade	
c-G	coarse GCC grade	- same batch throughout all investigations
m-G	medium sized GCC grade	- same batch throughout all investigations
s-G	small sized GCC grade	- same batch throughout all investigations
vs-G	very small sized GCC grade	- same batch throughout all investigations
es-G	extra small sized GCC grade	- same batch throughout all investigations
us-G	ultra-small sized GCC grade	- same batch throughout all investigations
c-P	coarse PCC grade	
s-P	small sized PCC grade	
d_{v50}	volume based median particle size	
SSA	specific surface area	
TGA	Thermogravimetric analysis	
TMA	Thermal mechanical analysis	
Tism	Thermal melting inflection slope	
DSC	Differential Scanning Calorimetry	
MFI	Melt Flow Index	
EaB	Tensile Elongation at Break	
kgf	kilogram-force or kilopond	

Abstract

Controlling and adjusting the thermal response properties of a polymeric compound is a key driver for improving its usability for an additive manufacturing process such as selective laser sintering, optimising the final part density as well as hardness. Adding mineral fillers to polymers was originally aimed at cost reduction. However, fillers are often used to fulfil a functional role, such as improved thermal or mechanical properties of the polymer composite.

The influence of particle size distribution, filler morphology and filler amount of calcium carbonate as a mineral functional filler particle on the thermal properties in a compression-moulded polyamide 12 matrix was investigated. The possibility to combine precisely defined particle size distributions, thereby combining the benefits which each particle size range within the chosen material size distribution contributes to the matrix, was evaluated.

The loss of ductility, occurring as a common downside of the introduction of a non-flexing mineral filler, has been investigated. The effect of an optimised coupling agent on the mechanical properties of a compression-moulded compound, containing polyamide 12 filled with surface modified calcium carbonate was also determined. Mineral filler modifier, namely 6-amino hexanoic acid, ε-caprolactam, L-arginine and glutamic acid, were chosen to investigate their coupling effect.

The melt flowability at 190°C, the melting speed, melting and crystallisation point, degradation temperature, crystallisation time at 170 and 172°C, as well as the elongation at break were analysed.

The melt properties of a polyamide 12 matrix show a significant dependency on the filler volume-based particle size. The finer and the narrower the particle size distribution of the calcium carbonate particles in the polymer matrix become, the less influence the filler has on the melting properties, influencing the melt flow less significantly than the same surface amount of broad size distribution coarse calcium carbonate filler particles. However, due to increased nucleation, the crystallisation behaviour on cooling showed a markedly more rapid onset in the case of fine sub-micrometre filler particle size. The overall thermal and flow properties can be optimised, by adjusting the morphology and particle size distribution of a coarse and fine calcium carbonate filler, blended in an optimised functional filler ratio. With an optimised surface modifying agent and/or filler morphology, the tensile strength as well as elongation at break can be improved in comparison with uncoated filler implementation, such that up to 60% of the loss of ductility and toughness of a final part when using an untreated filler could be regained using the correct amount of an optimised surface modifier.

The improvements were demonstrated with a twin-screw extruded compound, indicating the potential for the usage of a functional filler within a polymer matrix as an optimised composite for additive manufacturing.

1 Introduction

1.1 Innovation Opportunity

The successful introduction of a product into the market requires short development time to fast and safe production of high-quality products. The time between the product idea and production is crucial for companies to be able to react to the market demands. The demand for individualised and more complex products requires flexibility in development and production. Subtractive methods, such as cutting, drilling or erosion, require tooling for the production, are limited in the development of complex inner structures/geometries and the quick adjustment in the production of individual customer-oriented products. Furthermore, these processes often result in a significant material loss (e.g. milling chips), which have a disadvantageous economic effect on the production.

A principal advantage of the additive manufacturing process is the potential to manufacture parts with greater complexity / geometry than capable through traditional subtractive processes, without the need for mould tooling. Geometries that are difficult or impossible to produce through the conventional techniques can be produced as effortlessly and at similar costs as producing uncomplicated shapes [1, 2]. As no tooling is required during the production, the design constraints existing with the conventional subtractive methods are significantly reduced, providing advantages in the design, performance and implementation of products [3]. In addition, by eliminating tooling and mould structures, the economics of production are optimised, enabling low volume production and even completely customised products [4]. Using traditional forming processes, manufacturers need to produce a greater quantity of parts in order to amortize the costs of tooling. Parts with only moderate complexity can amount to $50,000 of tooling and a lead time of two or more months [5].

Comparing these expenses with those of additive processes where there is no tooling cost and therefore the cost per part is no longer dependent upon the production volume [5, 6].

In addition, in additive processes, parts can be instantly modified, or products can be switched even during a build, significantly reducing the lead-times for a product.

A major sector of AM employs selective laser sintering (SLS), which readily interfaces with computer-aided design (CAD) as the print template formed from a powder bed by fusing the layers of powder together adopting a laser beam of material-selective absorbing wavelength.

Many investigations have been carried out to define the limitations and crucial factors, which can prevent successful processing through selective laser sintering [7-13]. The most important influence can be attributed to the variable thermal properties as well as particle size of the polymer/composite powder [14].

Guo *et al*. 2014 described how it was possible to reduce manufacturing and material costs, including increasing energy efficiency, by adding an environmentally friendly filler material, such as calcium carbonate, into the polymer matrix [14, 15]. However, some drawbacks of the way the filler was added were changes in melt viscosity as well as loss of mechanical properties and interactions with the laser beam. Introducing a functionalised filler with controlled thermal capacity and thermal conductivity should address the potential for further reduction of the current high energy consumption involved in SLS, and this is the motivation

for the work reported here. By increasing the thermal conductivity above that of the polymer matrix alone, the laser power needed to sinter the polymer is reduced. In parallel, the increase in thermal capacity offered by the filler opens the possibility of employing greater total energy density without subsequent material bulk distortion during re-crystallisation. In addition, if a filler that enhances laser radiative absorption can be used, further energy utilisation can be achieved. Calcium carbonate in the form of limestone, can be employed as a functional filler. Its properties can be adjusted to enhance both the melting and crystallisation behaviour.

Calcium carbonate was chosen for this research as it represents a commonly used high brightness filler in polymer applications. Advantages of using natural ground calcium carbonate include the lower resistance to flow offered by isometric granular particles of crystalline calcite, as opposed to anisometric platelets or needle-like structures of high aspect ratio typical of kaolin, talc or mica and precipitated scalenohedral or aragonitic calcium carbonate, respectively. The relatively low hygroscopicity of calcium carbonate - in comparison with, for example, gypsum (calcium sulphate), which exists with thermally unstable crystal water (hemihydrate versus dihydrate) - is a suitably optimal choice among the various mineral calcium salts with respect to maintaining consistent humidity and surface energy as a function of temperature in application with a lipophilic polymer, such as polyamide 12. Another high brightness filler candidate is barium sulphate, which has the frequently cited disadvantage of having a much higher density than calcium carbonate, 4.49 gcm^{-3} versus 2.71 gcm^{-3}, respectively, especially critical in lighter weight applications as typically targeted for polymer use.

1.2 Objectives

The aim was to investigate the ability to beneficially manipulate the thermal properties of a polyamide 12 compound by adjusting the filler level of calcium carbonate with a discrete designed particle size distribution.

Additionally, to understand the effect of an optimised coupling agent on the filler surface on the mechanical properties of a final compound. A common downside of the introduction of a non-flexing mineral filler is the reduction of mechanical properties, such as ductility.

The compounding benefits are exemplified with respect to the improved final properties derived in a twin-screw extruded compound and so are expected to be transferrable for use in an additive manufacturing process.

Chapter two presents a detailed theoretical introduction into the additive manufacturing technology, its limitations and potential research opportunities. The development of a calcium carbonate based functional filler as well important resulting compound properties are described.

Chapter three provides a detailed description of the materials, techniques and equipment used to perform the necessary studies and is divided into six parts:

- Production of mineral filler
- Modification of filler surface
- Compound production
- Formulations used for the experimental programme
- Evaluation of the functional filler
- Analysis of Compound

Chapter four presents and discusses the experimental results. The different sub-chapters separate the different categories, which this study focused on:

- Surface modification of ground calcium carbonate (GCC)
- Adjustment of the particle size distribution of GCC
- Impact of bimodal particle size distribution of GCC
- Combined bimodal particle size distribution and surface modification of GCC
- Comparison of GCC and precipitated calcium carbonate (PCC)

The final findings and potential future research opportunities are concluded and discussed in Chapter five.

2 Background

In this chapter, the theoretical background to the additive manufacturing technology, with a focus on selective laser sintering, will be provided. The production of a calcium carbonate filler as well as the main resulting compound properties are described and explained.

2.1 Additive Manufacturing Technology

In the manufacturing process, products are obtained through their creation out of other materials or by operations made on other/component parts (semi-finished).

According to DIN 8580, the following classifications of manufacturing processes are identified within the general field of manufacturing:

- **Primary shaping:** forming a solid body out of a shapeless material (liquid, powder, plastic)
- **Forming:** body deformation by malleable changes without altering the amount of the material present (e.g., bending, drawing, rolling, stamping etc.)
- **Joining:** previously produced workpieces are converted into one solid compound product (e.g., brazing, welding, gluing)
- **Machining**: changing the shape of a product by a local elimination of the cohesion (usually through grinding or milling)
- **Change of material properties:** conversion by post-treatment (e.g., hardening)

The various additive manufacturing (AM) processes are all classified as ‘primary shaping’ processes. Whereby, powders, liquids or melts are transformed into new products using a variety of energy sources or chemical reactions. The final properties of the developed product arise during the manufacturing process; they are not just determined by the material but from the build parameters as well.

Several different manufacturing technologies have become defined as ‘AM’. The basic principle of each of these processes is: ‘the final part is produced layer by layer’. AM, also known as ‘3D-printing’ or ‘Layer Manufacturing’ can be defined as:

“A process or processes for joining materials to make objects from 3D model data, usually layer upon layer, as opposed to subtractive manufacturing fabrication methodologies” (Schmid 2018: 2) [16]. The model data in this case are almost exclusively derived from computer aided design (CAD).

In contrast to a traditional subtractive method, in AM the material is gradually joined onto the structure only where the CAD image has defined it to build the part. This way, the complexity of a final product, which can be built through AM is much greater than achievable by traditional methods.

AM is already well-established process for the production of detailed prototypes or highly specified functional components in industries such as aerospace, automobile manufacture, architecture, furniture, jewellery and medical technologies [17].

AM methods do not require a tool to provide a certain final part shape. This 'layered tool-less forming' is one of the main driver of these technologies, as it provides significant advantages:

- economical fabrication of small production runs;
- geometric design freedom (cavities, undercuts, free-form surfaces);
- integrated functions (joints, hinges, flexible units);
- product personalisation;
- rapid product customisation;
- reduced material consumption (ecological aspects);
- rapid prototyping.

Several different AM methods have been developed, which can be categorised in three main groups:

- powder-printing/sintering;
- extrusion based printing;
- stereolithography.

The most commonly used construction materials are polymer based, but through the three different main AM groups a variety of materials can be processed, such as metals, gypsum, paper, ceramics, cellulose or resins. In the field of plastics, the material formation can be achieved by chemical reactions, electromagnetic interactions (e.g. UV curing), thermally induced processes (softening, melting) or adhesion of individual particles (usage of suitable binders). Schmid *et al.* broadly illustrated the different classifications of the commonly used polymer based additive processes (**Figure 2-1**) [16].

Final parts should meet industrial standard criteria, such as component precision, mechanical properties, surface quality, thermal and long term stability. Selective laser sintering process (SLS) is considered as being able to cross the border between prototyping and producing industrial functional components.

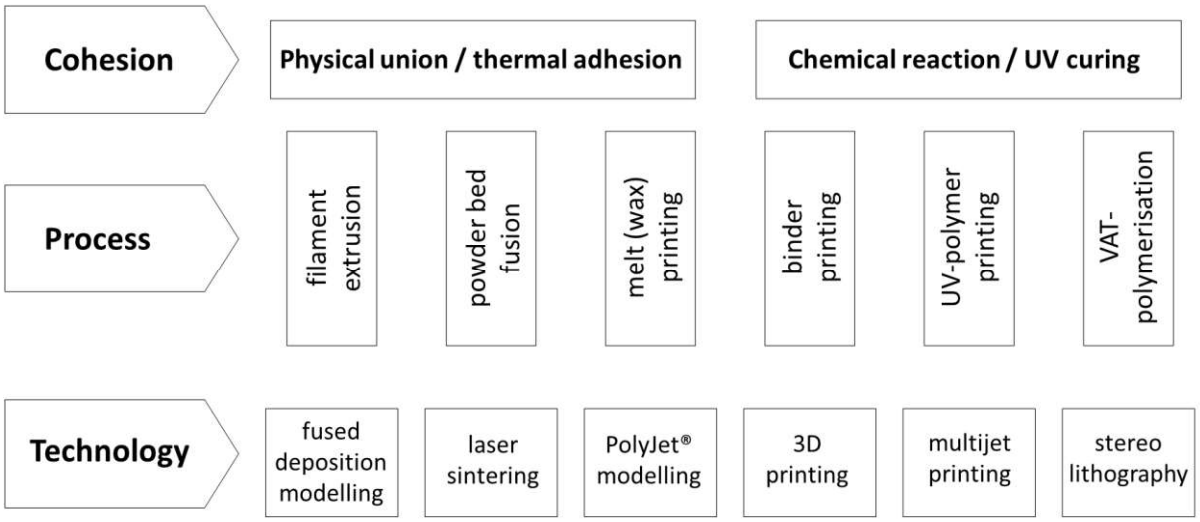

Figure 2-1. *Polymer based AM processes characterisation matrix*

2.1.1 Selective Laser Sintering (SLS)

In selective laser sintering (SLS), the layers of predefined geometry are made by fusing powder together using a laser beam (**Figure 2-2**).

The process follows the sequence: (a) a substrate is lowered to a depth equal to the next applied layer thickness, (b) a powder layer is spread on the substrate and (c) the deposited powder layer is scanned by the laser beam to fuse the powder layer (and create adhesion to the previous layer if present) over the selected pattern area. The sequence (a) through (c) is repeated until the fabrication of the product is completed [18,19]. This printing cycle, as well as a complete overview of the several steps in which the SLS process is split to produce a final part, is shown in the process diagram **Figure 2-3**.

In addition to the powder properties of the composite, the application of a controlled pre-heating stage, an optimised powder preparation procedure, precise laser energy, positioning of the part in the build and a controlled cooling step are just as important in achieving a successful build process [20].

Considering the move from prototype to a full industrial component production, a lot of specific requirements have to be met for this new part production process to be able to compete against traditional and established technologies. All factors within the SLS process chain have to be considered to address requirements, including reproducible quality, process reliability and automation of the production process. The different factors that influence the SLS process can be categorised into four main groups, all presenting their own challenges in the optimisation of the printing process:

- Machine settings
    - calibration status
    - manufacturer
    - powder supply
    - scan head
- Powder
    - powder supplier
    - particle size distribution
    - powder flowability
    - thermal properties
    - optical properties
- Production
    - batch control
    - part orientation
    - process failure
- Finished Part
    - surface properties
    - part density
    - dimension
    - polishing / smoothing

For this study, the objective was to focus on the **SLS powder materials** used in the process, and the potential optimisation of the powder properties of established feed material with the addition of functional filler and the impact on the composite thermal and mechanical properties. This chapter describes the polymeric materials that can be processed by SLS, the required properties imposed on the material, the different ways of powder preparation, suitable for an SLS print, and desired compound properties.

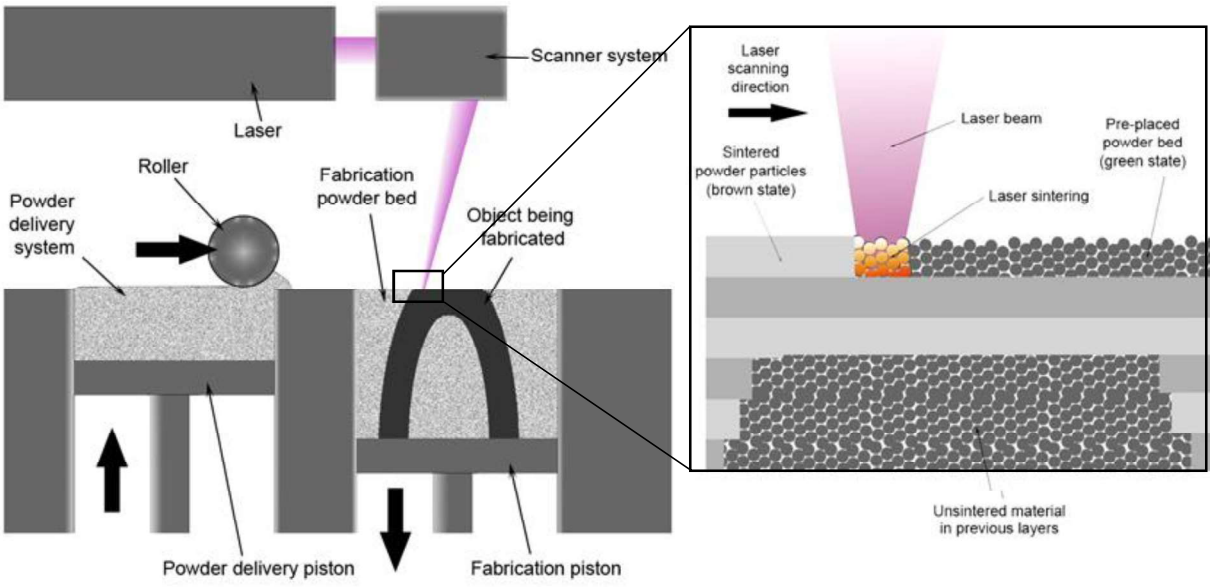

Figure 2-2. *Schematic representation of the SLS process, Image credit: Materialgeeza/Creative Commons; 12.09.2021 [18]*

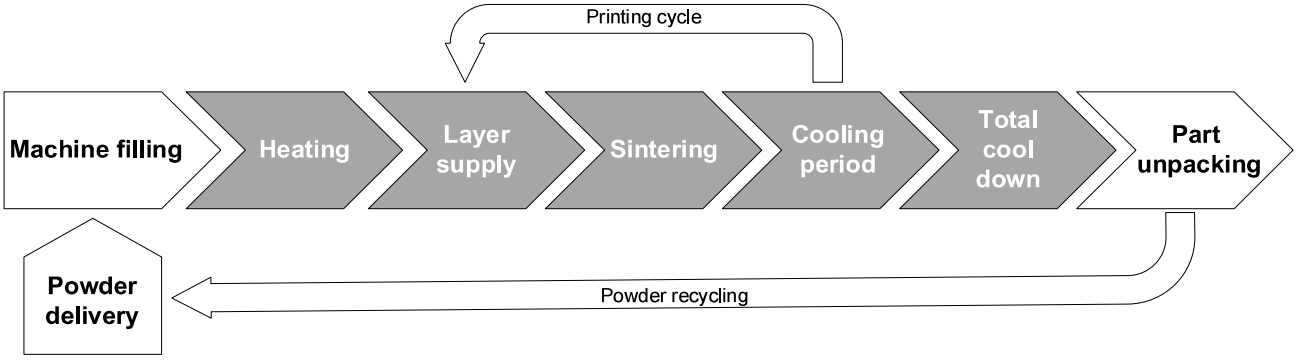

Figure 2-3. *Process diagram for the SLS method*

2.2 SLS Powder Materials

2.2.1 Polymers

Polymer technology distinguishes between a thermoplastic, elastomeric and thermoset polymer [19]. Under the application of a sufficient amount of heat to reach a predefined temperature, thermoplastic systems can be reversibly processed. Elastomers and thermosets on the other hand are elastic (elastomers) or only slightly deformable (thermosets) by heating, whilst retaining their predetermined shape. This is due to the internal cohesion of the polymer chains. Thermoplastic polymeric chains are only interconnected by secondary valence forces, whereas for elastomers and thermosets the chains are linked to each other by chemical bonds. Such chemically formed bonds cannot be easily broken by supplying energy. However, supplying enough thermal energy to thermoplastic chains, connected only by secondary valence forces, the connection is released, and the polymer can behave as a viscous melt.

Thermoplastic systems are most suitable for a laser sintering process. Sufficient energy is supplied by laser irradiation to melt the polymer particles and for them to re-crystallised back to the solid form on cooling.

2.2.2 Comparison of Different Polymer Types

Several thermoplastic resins have been studied and used regularly in the SLS process. In the early work on SLS, amorphous thermoplastics such as acrylonitrile butadiene styrene (ABS), polyvinyl chloride (PVC) or polycarbonate (PC) were used, as well as several waxes. Still in use today are mainly polystyrol (CastForm PS) as well as polymethyl methacrylate (PMMA) and polyacrylate (TrueForm PM). Due to the generally low density of the powder bed, and of the final product, these polymers are mainly used for the production of investment casting forms, whose pattern becomes surrounded (invested) with refractory material to make a casting mould. however, semi-crystalline thermoplastics (mainly polyamide), increase the powder bed density up to 95-98 %, and the final products are rigid enough for functional-prototyping and rapid-manufacturing. The most commonly used semi-crystalline thermoplastics are polyamide 11 and 12, which in 2018 covered almost 90 % of the market share [20].

2.2.3 Production of SLS Powders

A specific powder material in terms of both the particle distribution as well as polymer properties is required depending on the final application. Several methods have been developed, for the production of powders, tailored to the SLS process conditions. The most important and commercially used methods are shown in **Figure 2-4** with their advantages and disadvantages.

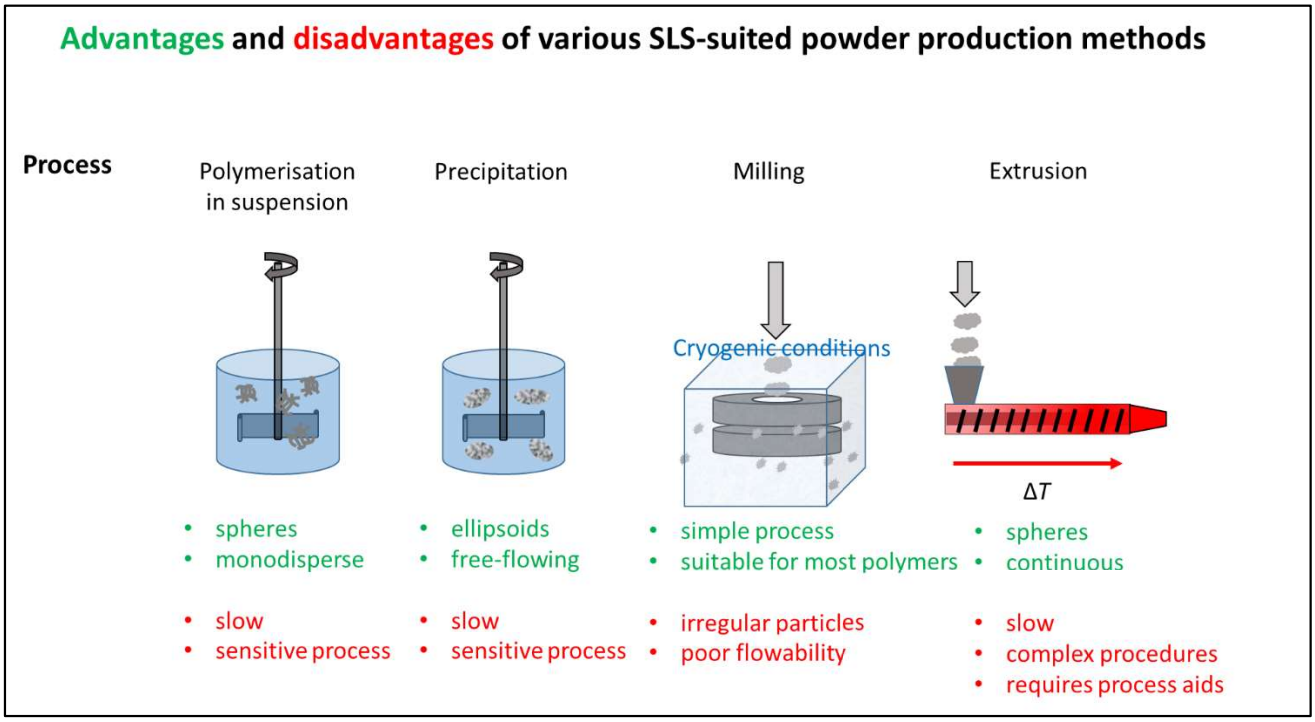

Figure 2-4. *Common methods for the production of SLS polymer powders*

During *polymerisation in suspension*, the particle dimension as well as the resulting average molecular weight of the polymer can be controlled through a precise adjustment of the process parameters and chemical ratios. At the end of the polymerisation process, fine homogeneous powder with good spherical shape is obtained which contributes well to flowability [21, 22].

To produce spherical particles, with high crystallinity and uniform crystal dimension, the polymer can be molten in a non-solvent under high temperature and high pressure. Through a precise cooling and / or pressure reduction, the molten polymer *precipitates* in a droplet-like form with controlled crystal structure [23].

The most available powder production method is the *mechanical milling process*. The high kinetic energy, introduced to the polymer matrix by grinding could lead to a thermo-oxidative damage to the polymer, which is why the milling process of polymers is often carried out using liquid nitrogen. This cryogenic milling results in a broad particle size distribution spectrum, with a significantly high fine particle fraction as well as low sphericity. As a result, powder flowability suffers [24, 25].

In coextrusion, spherical polymer particle powder is produced by dispersing the desired substance within a water-soluble matrix polymer during a precise adjusted coextrusion (usually in a counter-rotated twin-screw extruder) and removing the matrix polymer afterwards by dissolution. The recycling of the matrix polymer, as well as the solvent is a major drawback of the process and needs further optimisation [26, 27].

There are several further production methods, which will not be discussed in more detail, such as 'spray drying', 'drop extrusion', 'melt spinning' or 'rapid expansion of supercritical solution'. They are well-known and described in literature but, so far, have not produced commercially available powder material for the SLS process [28-31].

2.3 Functional Filler Material

According to DIN 55943, a filler material is defined as a substance, insoluble in the application medium, which increases the volume, targets / improves the technical properties and / or affects the optical properties of a final formulation. Not to be mistaken with the terminology of a 'pigment', which is defined as a substance, insoluble in the applied medium, used as colorant or for its anticorrosive, magnetic, electric or electromagnetic properties.

The further improvement and specialisation within polymer development drove the urgency to tailor each polymer for specific applications, while keeping the costs as low as possible, which was managed with the use of specific filler materials and reinforcing agents. This usage of filler material within plastics was already established in the 19th century, where resins were filled with cork- or wood-dust [32-34].

In the past, mineral fillers were used to reduce the overall formulation costs, by replacing expensive polymer with cheaper filler material. **Table 2-1** gives a broad overview of the different possible filler options.

Table 2-1. *Typical filler material used in the past/present polymer industry*

Organic Fillers		**Inorganic Fillers**	
Synthetic	***Natural***	***Synthetic***	***Natural***
carbon black	wood dust	silica gel	natural calcium carbonate
carbon fibre	cellulose fibre	precipitated calcium carbonate	talcum
carbon hollow sphere	starch	precipitated barium sulphate	kaolin
polymer fibre	rice husk	aluminium hydroxide	asbestos
	cork dust	glass sphere	silicates
		metal oxide	barite
			silica dust (present regulatory: respiratory)
			metal powder

The role of a filler within plastic has adapted to bring additional functionality for the final application, and filler, as a result is omnipresent in today's polymer market. Calcium carbonate as a functional filler has gained importance in products such as window profile, cable conduit, blown film, unsaturated polyester resin, tyre inner liner, flooring etc. Approximately 6 million

tonnes (Mt) of natural ground and precipitated calcium carbonate per year are sold into the polymer industry, covering thermosets as well as elastomers.

Calcium carbonate fillers display the following main characteristics, which support the usage within the polymer industry:

- high chemical purity, which prevents negative catalytic influence on the ageing of plastic;
- high brightness and low refractive index;
- low abrasiveness;
- nontoxic, ecological material;
- large particle size spectrum available.

2.3.1 Calcium Carbonate

The formation process of natural calcium carbonate begins with a first step of sedimentation of loose mineral and biological structures and emerges after further steps following one or more of three possible geological transformation routes. Chemical precipitation in fresh water, a biochemical process or an organogenetic sedimentation. The latter two routes are mainly occurring in sea water with a high salt content. The solubility of calcium carbonate in water is dependent on temperature and carbon dioxide content. In warmer sea regions, the dissolved calcium carbonate content is low, as most of it precipitates and builds up underwater structures, such as reefs. In colder regions or the deep sea, the water temperature is much lower, and the dissolved carbon dioxide and the calcium carbonate content is much higher. The depth, in which all existing lime shells are dissolved, depending on degree of latitude, is around 3.5 and 5 km, and is known as the ‘carbonate compensation depth [31]. The most important formation process for natural calcium carbonate is by organogenetic sedimentation. The remains of invertebrates, such as Mollusca, corals, echinoderms or algae form a deposit on the sea floor. Through high water pressure and time, the deposit solidifies to a friable sedimentary rock – chalk [32].

This carbonate sediment is compacted by the layers, which build up on top of it. This leads to a reduction of the porosity of the sediment. With increasing pressure, the still existing pores within the sediment are filled by precipitated calcite in the following ‘cementation’ process. These steps occur over millions of years and are collectively termed ‘diagenesis’ and lead to a stronger material calcium carbonate layer – limestone.

If such a limestone layer is exposed to extreme pressure over 1 000 bar, and temperatures between 200 and 500 °C, the stone melts, and on cooling slowly re-crystallises back to its solid form. Such a metamorphosis increases the crystal structure density of calcite and leads to an increase in calcium carbonate purity – marble.

2.3.1.1 Mineralogy

Calcium carbonate is a polymorphic compound, which exists in three different crystal forms, ‘vaterite’, ‘aragonite’ and ‘calcite’, the latter is the most common occurring form in the earth’s crust.

Calcite is crystallised in the crystallographic rhombohedral system with a rhombohedral cubic prism as an elementary cell. This base form of a cubic rhombohedral is less common in naturally existing calcite, but rather arises as a split shape from most calcite crystals. More common are the hexagonal prismatic and the scalenohedral morphologies. **Figure 2-5** represents the different crystal structures commonly formed during the development of a calcite crystal.

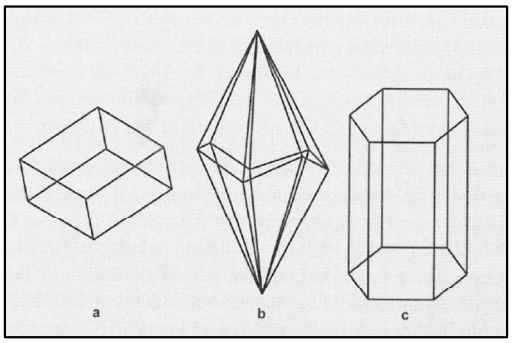

Figure 2-5. *Crystal structure of a calcite - a) Rhombohedral, b) Scalenohedral, c) Prismatic, source: Gysau 2006*

Depending on the nature of carbonate and its crystal modification / structure, the physical properties of calcium carbonate can vary significantly [30]. Depending on the level of compaction, the porosity of calcium carbonate varies between 15-40 % for chalk, 0.1-10 % for a denser limestone and < 1 % for marble. This porosity is also represented in the resulting apparent density of chalk, which lies at 1.5-2.3 gcm^{-3} at 20 °C, where a comparable marble has an apparent density of 2.7 gcm^{-3}. The pure calcite density lies at 2.71 gcm^{-3}, and that of an aragonite crystal modification at 2.93 gcm^{-3}. The hardness and strength of limestone also depend significantly on the geological nature. While the hardness of a pure calcite crystal is at 3 Mohs, tat of naturally occurring chalk lies in the range of 2 Mohs and marble at 4 Mohs, with a respective compressive strength of 10 MPa for chalk and up to 200 MPa for marble.

2.3.2 Production of Natural Ground Calcium Carbonate (GCC)

The predominant industrial production process for calcium carbonate, applicable in the polymer industry, can be scaled in 6 steps, resulting in a ground fine particle size calcium carbonate product (GCC).

In the *prospecting* phase, a geological quality check of a potential mining area is carried out to define a best-suited production site. During the *material recovery*, the raw stone is gathered out of the quarry either in an open cut mining or from deep mining. The stone face is either cut back purely mechanically or with the help of explosives, then gathered and transported for further beneficiation. During *beneficiation*, the raw stones are crushed by a primary breaker, such as a jaw crusher, down to a particle size of approx. 200 mm. After a *sieving and classification step*, the raw material is further split via either a dry or a wet route. For the production of a dry ground product, the raw material is washed and further *ground down*, typically with the use of a media mill, such as a horizontal ball mill, and *classified* to the desired particle size down to approx. 1 µm. If a smaller particle size is required, not easily achievable by dry grinding, the raw material passes a *flotation step*, in which mineral impurities can be separated, and can be *ground down in a dispersed form*, using, for example, an agitator

bead mill, to a desired particle size reaching approx. 20 nm. After a wet grinding process, the product can either be used in the resulting slurry form or pass an additional dewatering step, in which the filler will be dried and pulverised to form the powder product.

2.3.3 Synthetic Precipitation of Calcium Carbonate (PCC)

The production of precipitated calcium carbonate (PCC) is usually carried out through a three-step-process. At a temperature above 900 °C, pure limestone is calcined to calcium oxide, also known as burnt lime or quicklime. The produced burnt lime is afterwards slaked in water to form a milk of lime, predominantly calcium hydroxide. Diluted milk of lime is then transformed back to calcium carbonate by introducing carbon dioxide into the suspension. Depending on the combination of the used additives during the carbonisation, the controlled addition of carbon dioxide, the milk of lime particle size, reaction pressure and temperature, and impurities in the milk of lime, the resulting crystal modification, crystal structure and particle size distribution of the PCC can be adjusted. The final PCC can afterwards be stabilised and used in a dispersed slurry form or pass an additional drying process step.

2.3.4 Surface Modification

Independent of whether natural ground calcium carbonate (GCC) or synthetic precipitated calcium carbonate (PCC), the produced mineral filler exhibits characteristic surface properties, which are not always as desired for the application. Calcium carbonate is hydrophilic by nature without specific strong binding properties with oleophilic polymers. When mixed with polymer, this surface energy incompatibility between inorganic calcium carbonate and organic polymer can lead to a strong tendency for agglomeration in the inorganic phase and a significant loss in the mechanical properties of the resultant composite. This is the reason why most of the mineral fillers commonly used within the polymer industry are surface coated at a late stage, or at the end, of the production process. Fillers are commonly coated with a mono-molecular layer of an organic oleophilic substance, reducing their polar surface energy and increasing the dispersive compatibility with the dominant polymer matrix. In some cases, fillers are also coated with inorganic additives having close to purely dispersive component surface energy [35].

The coating / modification process is either via chemisorption or physisorption, occurring either in a dry or wet step, resulting in a calcium salt conversion degree of the additive from typically 50-70 % up to 90 % for a regularly used surface modifier for polymer application, such as stearic acid [36].

Depending on the chemical nature of the polymer and the targeted compound characteristics, the surface modification step has to be adjusted. For the introduction of calcium carbonate within polyamide, for example, the typically used stearate coated carbonate does not suit the chemical properties of the polymer. The adhesion between the stearate coated filler and the polyamide polymeric material is weakened further than when using simple uncoated filler, due to the poor compatibility of the polymer with the hydrophobic coated filler particle surface. To improve the compatibility between the nitrogen groups within the polyamide chain and the calcium carbonate surface, an optimised adhesion promoter needs to be implemented. As suggested by H. Goodman, a surface coating presenting amino acid groups, for example amino hexanoic acid, results in an improved bonding to the polar groups

within the polymer structure, hence improving the mechanical properties of the compound [37]. As suggested by the literature, the carboxylic acid group of a modifier agent can react with a hydroxyl group on the calcite surface in a condensation reaction, hence, in this case, resulting in free amino groups on the bound molecule at the surface of the mineral filler material [38, 39]. Through such a surface modification, hydrogen bonding to an external material can take place, which improves the adhesion between the filler and the polymer matrix [39]. Kämpfe P. 2011 and Madsen *et al.* 1998 investigated the correlation between the adsorption rate of amino acids on a calcite surface and pH. It was shown that certain amino acids show an improved adsorption at higher pH values (8-10 pH), as the amino acids can react in its deprotonated form with the carbonate surface [40, 41].

2.3.4.1 Amino hexanoic acid

6-aminohexanoic acid (also known as aminocaproic acid) is a derivative of the amino acid lysine and an intermediate in the polymerisation of polyamide 6, in which it is formed by the ring-opening hydrolysis of caprolactam. **Figure 2-6** shows the molecular structure of amino hexanoic acid. Considering its use in the case of a filler surface modifier, the ready access to a free hydroxyl group benefits a surface binding through condensation and provides a plurality of free amine groups which result in a surface modified filler material with improved compatibility with a polymer resin having a polar group.

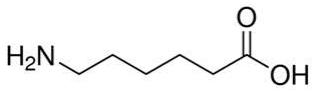

Figure 2-6. *Molecular structure of 6-amino hexanoic acid*

2.4 Compound Properties

Processing a polymer or a compound by SLS imposes specific requirements on the matrix used. **Figure 2-7** presents an overview of the different factors, which all play a role on the printing success. Optimising all parameters is a substantial and complex undertaking. This study is focused on the fundamental requirements for the thermal, rheological and optical properties.

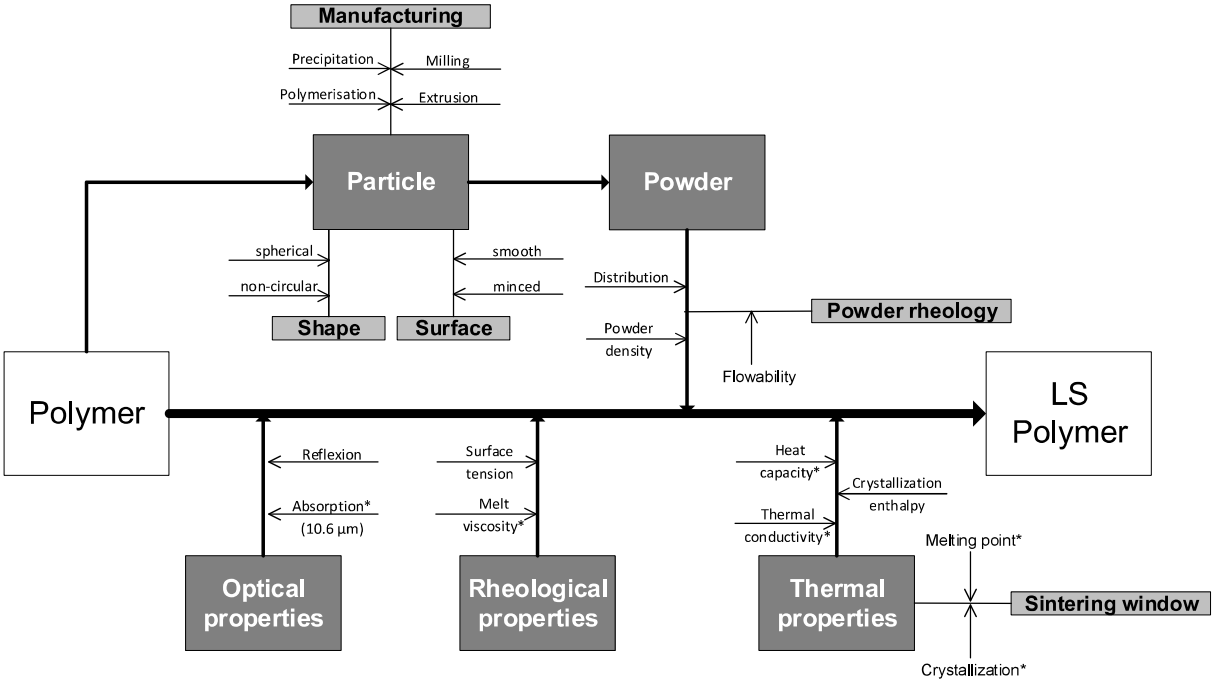

Figure 2-7. *Key properties of SLS polymers in respect to the sintering processing; * focus for this study*

2.4.1 Optical Properties - Surface Temperature and Laser Energy Input

Controlling the temperature on the powder bed surface is another significant factor, which can lead to the need for varying the properties in LS components. To control the entire process, homogeneous temperature conditions (powder bed surface as well as powder cake) must prevail throughout the AM build cavity. This homogeneous temperature distribution is set slightly below the melting point of the polymer / composite to handle the material within the processing sintering window and to avoid issues during the process. At this stabilised temperature, only a small additional energy amount, enough to melt the powder particles, is introduced via laser radiation. Kumar *et al.* 2014 described this laser energy contribution as the laser energy density, also known as the Andrew number (A_n) [43]. During the LS process, the Andrew number, given in Jmm^{-2}, can be calculated through the following components:

- laser power, P_{LS}, in W (= Js^{-1})
- laser beam scan speed, v_{LS}, in mms^{-1}
- laser overlap, d_{LS}, in mm
    - this overlap specifies the extent to which consecutive laser tracks are superimposed, where d_{LS} represents the distance between the middle points of two laser lines (mm)

$$A_n = \frac{P_{LS}}{v_{LS} \times d_{LS}} \tag{3.1}$$

This is a simplified equation, in which the numerical value for the Andrew number can be the same for different P_{LS}, v_{LS} and d_{LS}, but result in different sintering properties. By increasing the scan laser velocity v_{LS} and compensating with an increased laser power P_{LS}, A_n can be

numerically identical but the mechanical strength properties of a printed part are in general lower. This effect cannot be explained by the equation (3.1), since the energy absorption rate is considered constant. The energy absorption of a polymeric compound per unit time is limited, which cannot be easily compensated with a higher laser power. A reduction of the laser power and laser scan speed is considered to be advantageous in terms of the mechanical properties of LS parts. Considering the economics of the LS method, however, the reduction of the time needed per build is desired, without a significant loss in the final part properties. Thus, the challenge becomes one of optimising the thermal response properties of the composite, a major opportunity for the use of suitable filler having the right characteristics.

Another important factor, which the simplified equation for the Andrew number does not take into consideration, is that the laser heat transfer is mostly radiative and needs to be absorbed by the powder particles. The absorbed laser photon energy is converted to heat by molecular excitation. With a wavelength of 10.6 µm for a typical CO_2 laser, the commonly used polyamide powders absorb a significant part of the produced laser power, instead of reflecting off the surface. If the molecular excitation is reduced and the laser energy contribution is kept constant, this will lead to a reduction of the final part quality. In the case of calcium carbonate as a functional filler, Gane *et al*. 2002 studied the use of a 100 % calcium carbonate based filler in a coating formulation for post-print laser marking and the influence of the laser wavelength on the performance with respect to thermal ablation of a previously laid down ink [44]. The absorption spectra of calcite and aragonite have only a very weak absorption in the targeted wavelength range between 10.55 – 10.63 µm, a slightly higher absorption at a wavelength of 9.3 µm and a significantly higher absorption at approx. 11.4 µm. If calcium carbonate is added to a polyamide matrix, the CO_2 laser energy at the common wavelength of 10.6 or 9.3 µm will not be highly absorbed by the filler, which could result in a loss of the enhanced melting and crystallisation behaviour and a worsening of the quality of the final printed part.

One possible solution to overcome this poor radiative absorption by the filler could be to adjust the wavelength of the laser to the absorption spectrum of the filler, which then contributes better by absorbing the energy. By using an isotopic CO_2-laser, $^{13}C^{16}O_2$ instead of the commonly occurring $^{12}C^{16}O_2$, the main wavelength of 10.6 µm is shifted up to around 11.2 µm, which suits the absorption spectrum of calcium carbonate much better. Bollström *et al*. 2016 introduced another idea of improving the absorption rate, by application of an ultrathin layer of nanoclay or nanosilica onto the calcium carbonate, which supported the laser energy absorption in post-print laser marking [45].

2.4.2 Thermal Properties - Sintering Window - Crystallisation and Melting

During the LS process, a thin powder layer of approx. 100 µm is irradiated with the CO_2 laser and melts in the predefined manner. Depending on the chamber size, each build time per layer can typically take around 30 to 40 s. With semi-crystalline polymers, the crystallisation of the polymer starts during the cooling and is always connected with the potential for geometric changes of the part, such as shrinkage or warpage. Therefore, the building chamber temperature needs to be set as high as possible so to suppress the crystallisation during the building process. If the crystallisation occurs prematurely and the adhesion with the underlying previously irradiated layer is insufficient, the final printed part will tend to delaminate and lose mechanical strength. The temperature within the building chamber needs to be above the

crystallisation temperature of the polymer particle, whilst the temperature also needs to be sufficiently below the melting point to avoid powder caking / cake melting within the build cavity. This temperature range between crystallisation and melting of a polymer is frequently called the sintering window of a polymer.

In a simplified way, the sintering window of a polymer can be visualised with a differential scanning calorimeter (DSC) measurement. Thermodynamically, this sintering window is a metastable region, where solid and liquid can coexist. **Figure 2-8** gives an example of a typical DSC curve for a commercially available polyamide 12 powder, in which the area between the onset of the melting point (T_m (onset)) and the onset of the crystallisation point (T_c (onset)) represents the sintering window. For the definition of this sintering window, and the comparison of different polymer types, this measurement curve is used, where the heating and cooling rates are kept constant at 10 Kmin^{-1}, which, however, does not represent an actual temperature change range during a printing process. In reality, the temperature change during heating with a laser occurs within seconds and can jump with a $\Delta T \geq 100$ K, while the cooling rate within the building chamber is typically less than 1 Kmin^{-1} [40].

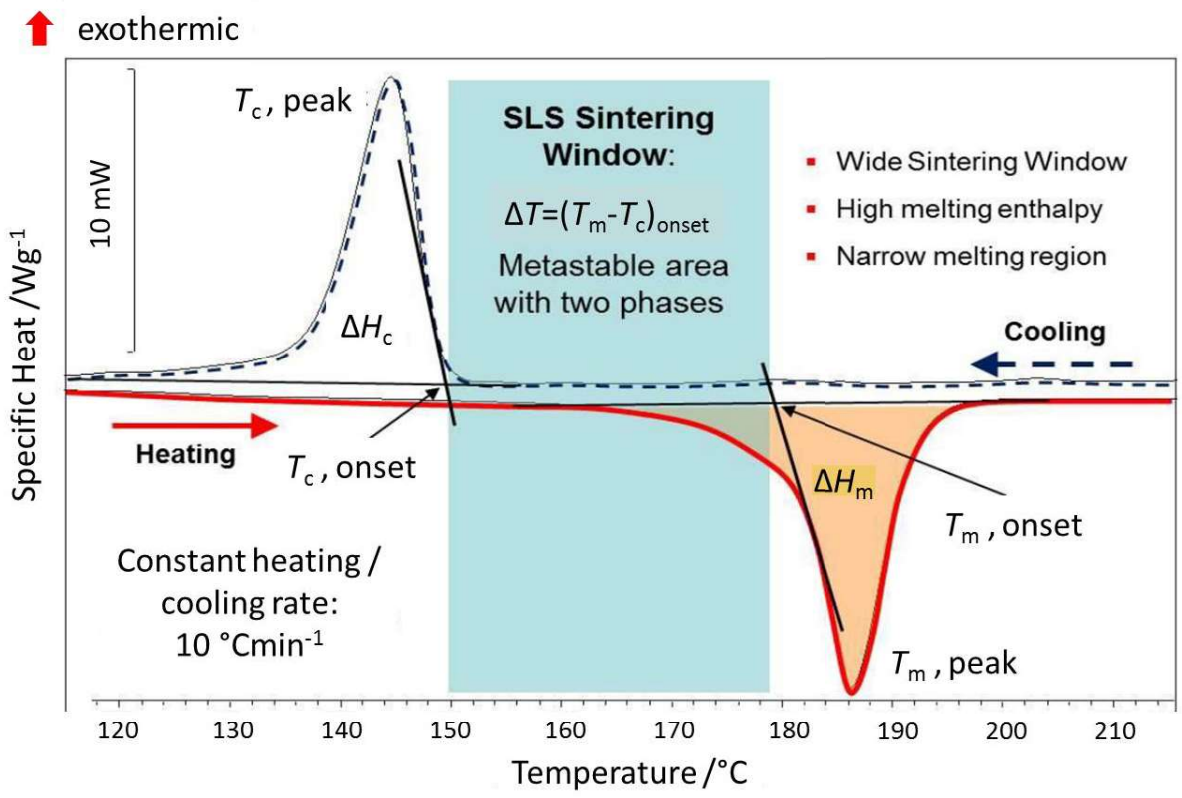

Figure 2-8. *DSC measurement representing the SLS sintering window, lower curve corresponds heating; upper curve the cooling step, source: Schmid 2016: 6* [46]

Ehrenstein *et al*. 2012 described how, for semi-crystalline polymers, the measured crystallisation point through DSC would increase, if the cooling rate during the measurement was decreased [38]. This shifting of T_c (onset) will lead to a narrowing of the actual sintering window, which is why the build temperature within the chamber is often set as close as possible to T_m (onset). Even at a high set building temperature, during and at the end of the LS process,

larger crystal structures occur usually for semi-crystalline polymers. With an approx. average spherulite size of 100 µm and greater, cracks can form at the spherulite boundaries. This leads to a considerable negative effect on the yield stress, tensile and impact strength as well as on the elongation at break of the final printed part. Kleijnen *et al*. 2016 showed how, by disrupting the spherulite growth with additional nucleation points within the system, the compromise in the mechanical properties can be partly alleviated [39].

Different sources have described how a complete melting of semi-crystalline polymers, hence a complete isotropisation of the melt, can take up to several minutes. Such a time span is not practical in an SLS process. Due to the sudden energy supply by the scanning laser beam, the powder surface cannot take up enough energy for all existing crystals to become completely molten. Majewski *et al*. 2008 described how this 'degree of particle melt' (DPM) has a large effect on the mechanical properties of the printed part. By reducing the powder layer thickness or increasing / optimising the laser power during the printing process, the DPM can be reduced and the tensile strength can be enhanced. By increasing the thermal conductivity of the polymeric system, the amount of absorbed laser energy can be improved and the DPM can be reduced as well.

Controlling the heat capacity as well as the thermal conductivity can have a significant influence on the success of the printing process. Low thermal conductivity leads to a low energy absorption, as well as a potential inhomogeneous energy distribution in all spatial directions. In combination with a pronounced heat capacity (ability to store energy), the controlled cooling of the build cavity can be hindered by the polymer within the powder cake layer. If the stored energy of a printed part, within a powder cake bed, cannot be transmitted quickly enough (due to low thermal conductivity / energy absorption), a heat radiation effect can be favoured. This heat build-up at the edge of the parts in the powder cake can lead to a melting / re-melting of the powder surrounding the part, leading to a reduction of the surface quality of the final part. For a successful and sustainable printing process, it is essential that the thermal conductivity is as high as possible, to prevent heat radiation and to be able to control the heat transfer and crystallisation process during the cooling step. One approach in controlling the heat management is the implementation of a suitable filler material.

Comparing the thermal properties of a typical polyamide 12 type used in laser sintering, EOS PA2200, with those of ground calcium carbonate, in **Table 2-2** it can be seen that the energy absorption can be enhanced through the higher thermal conductivity than the polyamide 12 alone, hence reducing potential DPM, whilst the combination, with the lower ability to store the absorbed energy (lower heat capacity), reduces the heat build-up within the powder cake and the resulting heat radiation.

Table 2-2. *Comparison of the thermal properties of PA12 vs $CaCO_3$*

	Omyacarb 10-AV	**PA2200**
Producer / supplier	Omya International AG	EOS e-Manufacturing
Chemical nature	Ground Calcium Carbonate (GCC)	Polyamide 12
Approx. thermal conductivity at 298 K	1.3 Wm^{-1} K^{-1}	0.2 Wm^{-1} K^{-1}
Approx. specific heat capacity	0.8 $kJkg^{-1}$ K^{-1}	2.1 $kJkg^{-1}$ K^{-1}

2.4.3 Rheological Properties – Polymer Melt Flow Viscosity

To achieve the highest possible melt flowability without additional shear forces during the sintering process is of a major importance. Only with a low melt flow viscosity, a complete coalescence of the powder particles can occur during the short time in which the powder particles exist in the molten state.

Various authors such as Liang 2002, Zoukrami *et al.* 2012 and Hristov *et al.* 2008 have shown how the introduction of a solid filler material within a polymeric melt results in an increase of the melt flow viscosity [47-49]. Such an increase will result in a reduction of the final part density, due to the loss of sufficient merging of the different molten powder layers. Therefore, it is of importance to adjust filler particle introduction in a way in which the resulting melt flow viscosity is not significantly increased.

2.5 Research Opportunity

This Chapter discussed the mineralogical difference between a mineral filler consisting of GCC versus PCC. One objective of this study was to focus on the influence of size and shape of the mineral filler on the resulting compound properties.

Introducing a functional filler with controlled thermal capacity and conductivity addresses the potential for further reduction of the current high energy consumption involved in SLS. By increasing the thermal conductivity above that of the polymer matrix alone, the laser power needed to sinter the polymer is reduced. In parallel, the increase in thermal capacity offered by the filler opens the possibility of employing greater total energy density without subsequent material bulk distortion during re-crystallisation. In addition, if a filler can be used that enhances laser radiative absorption, further energy utilisation could be achieved. Calcium carbonate in the form of limestone, can be employed as a functional filler. Its properties can be adjusted to enhance both the melting and crystallisation behaviour.

A common downside of the introduction of a non-flexing mineral filler is the reduction of the mechanical properties, such as ductility. Introducing an optimised coupling agent on top of a functional filler counteracts this drawback in ductility.

The principle of adjusting the absorption spectrum of the functional filler to be better suited for an energy absorption at 10.6 µm was used in this study with the idea, that by surface treating the filler with a suitable modifying agent, the absorption spectrum of a calcium carbonate can be adjusted to suit better the usage in a CO2-laser system.

The following objectives were defined in order to address the research opportunities identified by the literature survey:

- Investigate the ability to manipulate the thermal properties of a polyamide 12 compound beneficially with calcium carbonate;
- Optimize the application performance by adjusting the mineral filler level, designing a discrete size combination and shape;
- Understand the effect of an optimised coupling agent attached to the filler surface on the mechanical properties of the final compound

3 Materials and Methods

This chapter provides a detailed description of the materials, techniques and equipment used to perform the necessary studies. It is divided into six parts:

- Mineral filler production;
- Filler surface modification;
- Compound production;
- Formulations used for the experimental programme;
- Evaluation of the functional filler;
- Compound analysis.

3.1 Filler Production

The different mineral fillers used in this study, were produced by the techniques described below.

3.1.1 Ground Calcium Carbonate

The particle size of the GCC-feed was adjusted to form the controlled variation in particle size distribution by dispersing the starting product in demineralised water to a solids content of 25 w/w% and grinding the suspension in an agitator bead mill (Dyno®-Mill ECM AP-05 from Willy A. Bachofen AG Maschinenfabrik, 4132 Muttenz, Switzerland, (**Figure 3-1**)) employing a grinding medium consisting of ~1 mm diameter high intensity grinding beads. No dispersing aid was used during the grinding to avoid any negative influence on the subsequent surface treatment, the homogenised suspension was circulated by a peristaltic pump (E-2) through the agitator bead mill (E-3), back into a stirred container (E-1) until the desired particle size distribution was achieved (**Figure 3-2**).

As feed material for all GCC based mineral filler productions, a marble-derived ground calcium carbonate was used, provided by Omya International AG (Baslerstrasse 42, 4665 Oftringen, Switzerland). General material specifications for the used GCC feed are listed in

Table 3-1.

Table 3-1. *Feed Material Specification*

	Omyacarb 10-AV
producer/supplier	Omya International AG
volume-based median particle size, d_{v50}	9 µm
particle shape	irregular
approx. thermal conductivity at 298 K	1.3 $Wm^{-1}\ K^{-1}$
approx. specific heat	0.8 $kJkg^{-1}\ K^{-1}$

Figure 3-1. *D Dyno®-Mill ECM AP-05 agitator bead mill, source: wab-group.com*

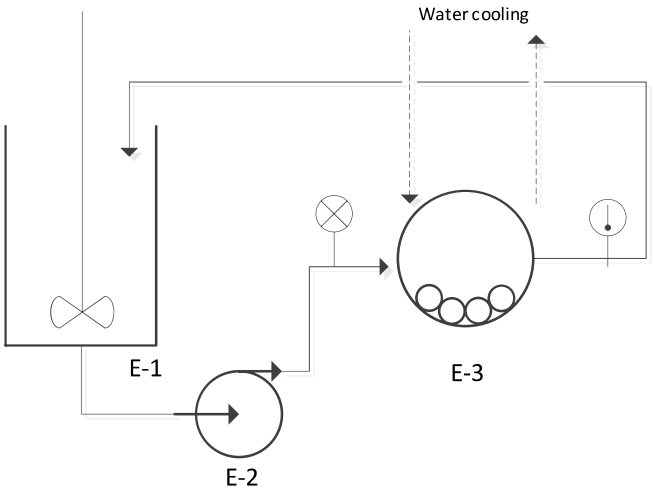

Figure 3-2. *Schematic of laboratory wet grinding process, E 1: stirred container, E-2: peristaltic pump, E-3: agitator bead mill*

3.1.2 Precipitated Calcium Carbonate

The particle size as well as particle shape of the individual PCC products were achieved through a controlled slaking and carbonation process. Two PCC production conditions were used to distinguish between two different PCC types: a fine scalenohedral PCC (sc-PCC) and a coarser prismatic PCC (pr-PCC).

The sc-PCC was produced by slaking calcium oxide in warm water for 30 min with an addition of 0.1 % (active / dry CaO) sucrose to the slaking water. After screening the produced milk of lime through a 200 µm sieve, the carbonation was initiated with a constant flow of 20 % carbon dioxide gas at 200 $Nm^3\,h^{-1}$ (1 Normal cubic metre Nm^3 refers to the volume of gas occupying 1 m^3 at normal (standard) temperature and pressure). As soon as the conductivity started to

decrease, a continuous stream of fresh milk of lime was added, to keep the conductivity at a constant level of approx. 3 500 µS cm^{-1}. As soon as the reactant reached the target volume, the addition of fresh milk of lime was stopped and the carbonation was finalised after reaching the minimum conductivity [50].

The pr-PCC was produced by slaking calcium oxide in warm water for 30 min with an addition of 0.05 % (active / dry CaO) sucrose to the slaking water. After screening the produced milk of lime through a 200 µm sieve, the carbonation was initiated by pre-gassing water for 5 min with a constant flow of 20 % carbon dioxide gas at 200 $Nm^3\ h^{-1}$. After the pre-gassing step, a continuous stream of fresh milk of lime was added, to keep the pH at a constant level between 7 – 7.5. As soon as the reactant reached the target volume, the addition of fresh milk of lime was stopped and the product was sieved through a 45 µm sieve [51].

3.1.3 Drying Process

After all desired filler product specifications were achieved, each carbonate suspension was dewatered via a chamber filter press and subsequently spray dried using a 'GEA Niro MOBILE MINOR® nozzle spray dryer (GEA Group, Peter-Müller-Strasse 12, 40468 Düsseldorf, Germany) as illustrated in **Figure *3-3***. The atomization pressure in the dryer was kept constant at 3 bar, with an inlet temperature of 200 °C and an outlet temperature of 90 °C.

Figure 3-3. *GEA Niro MOBILE MINOR® nozzle spray dryer, source: gea.com*

The concentrated feed entering the drying chamber was atomized by co-current nozzles placed in the drying air duct (**Figure 3-4**). The air entered the spray dryer vertically through the air disperser at high velocity, ensuring optimal mixing of the atomized droplets with the drying air. Evaporation instantaneous took place during the vertical passage down the drying chamber [52].

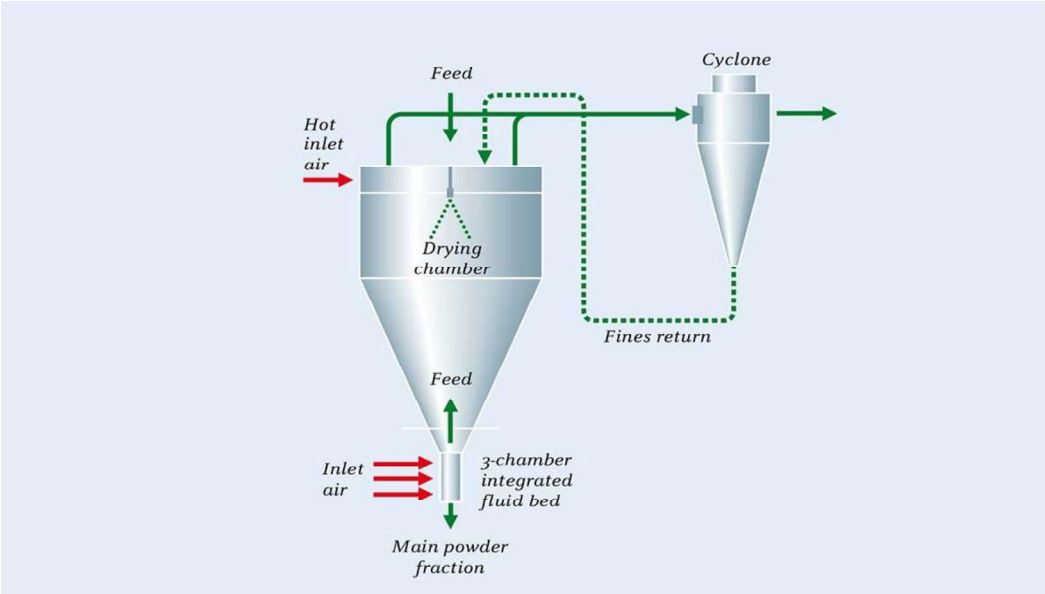

Figure 3-4. *Schematic diagram of spray drying process, source: gea.com*

3.2 Filler Surface Modification

A precise adhesion promoter will produce an improved compatibility between the nitrogen groups within the polyamide 12 chain and the calcium carbonate surface.

A selection of various amino-containing acids was chosen to improve the compatibility of the mineral filler material with the polar group in the polymer structure. The defined amino acids were chosen to be able to determine a difference in the polymer interactional compatibility of end- against side-chained amino groups. The molecular structure of each amino acid surface modifier is shown in **Figure 3-5**.

As a benchmark, stearic acid, a typical surface modifier for calcium carbonate in polyolefin applications, was used [53]. General material specifications for the surface modifiers used are listed in **Table 3-2**.

The modifications of all the raw filler material were made using a dry pigment surface modification process. To develop a homogeneous treatment, a batch coater (MP-LB mixer from Somakon Verfahrenstechnik UG, 44536 Lünen, Germany, (**Figure 3-6**)) was used, in which the mineral filler was pre-heated up to 120 °C with a stirring speed of 500 min^{-1} (rpm). The coating agent was distributed under conditions of uniform heating and homogeneous mixing for 10 min maintaining the temperature at 120 °C.

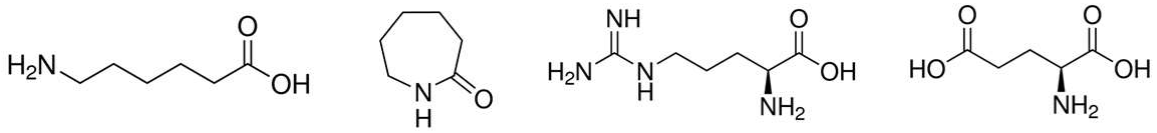

(**A**) (**B**) (**C**) (**D**)

***Figure 3-5**. Molecular structure of (**A**) 6-amino hexanoic acid; (**B**) ε-caprolactam; (**C**) L-arginine and (**D**) glutamic acid*

***Table 3-2**. Material specification of surface modification agents*

	Stearic acid	**Amino hexanoic acid**	**ε-Caprolactam**	**L-Arginine**	**Glutamic acid**
producer/supplier	Wilfar	Sigma Aldrich	Sigma Aldrich	Sigma Aldrich	Sigma Aldrich
CAS Number	57-11-4	60-32-2	105-60-20	74-79-3	56-86-0
Linear Formula	$C_{18}H_{36}O_2$	$C_6H_{12}NO_2$	$C_6H_{11}NO$	$C_6H_{14}N_4O_2$	$C_5H_9NO_4$
Molecular weight	284.5 g mol^{-1}	131.17 g mol^{-1}	113.2 g mol^{-1}	174.2 g mol^{-1}	147.1 g mol^{-1}

***Figure 3-6.** Somakon MP-LB batch coater, source: biomation.de*

3.3 Compound Production

To demonstrate the possible use of optimised calcium carbonate as a functional filler in additive manufacturing, which could potentially be transferred into the selective laser sintering process, the produced functional filler materials were compression moulded through a twin-screw extruder system and conjunct with polyamide 12. For this study, SLS-approved polyamide 12 (PA2200) powder, obtained from EOS e-Manufacturing Solutions (Electro Optical Systems, Robert-Stirling-Ring 1, 82152 Krailling, Germany), was used. General material specifications of this material are listed in **Table 3-3**.

***Table 3-3**. Raw polyamide 12 specification*

	PA2200
producer/supplier	EOS e-Manufacturing
volume-based median particle size	60 µm
particle shape	spherical
approx. thermal conductivity at 298 K	0.2 Wm^{-1} K^{-1}
approx. specific heat	2.1 $kJkg^{-1}$ K^{-1}

The solid polyamide 12 powder was homogeneously premixed with the specific weight-defined amount of surface-coated functional filler to achieve the desired filler loading. This powder processing resulted in a homogeneously mixed powder blend, for use directly in compression moulding.

Since the filler-polymer interaction occurs at the interface between the filler and the polymer, throughout the whole study, the surface area was used to describe the functional loading effect of the filler per given mass of polymer.

Compounds were extruded via a twin-screw extruder system (Extruder ZE 12 from Three-Tec GmbH, 5703 Seon, Switzerland) as illustrated in **Figure 3-7**. The extruder barrel-length was 25 cm and the conveying twin-screws had a diameter of 12 mm with a flank pitch of 12 mm. The barrel temperature profile was split in three parts along its length, with an inlet temperature of 160 °C, a compounding zone at 200 °C and an outlet temperature of 170 °C. The twin-screw rotation speed was kept constant for all trials at 90 min^{-1} (rpm), resulting in a compound residence time of approximately 30 s. The compound was formed through a filament nozzle with a diameter of 2 mm and granulated into cylindrical pellets with a length ≈ 1 mm.

In addition to the pellets, approx. 1-mm-thick sample plates with a width of 3 cm were produced. The compound was formed through a plate nozzle (**Figure 3-8**) with a thickness of 2 mm and a width of 2 cm, passed through a calender press and pulled by an extract roller. The calender was set to a thickness of 1 mm and a roller speed adjusted to the extruder. **Figure 3-9** shows a schematic of the calender system used. The resulting plates were punched to normalised tensile test ‘dog bones’ for further analysis (**Figure 3-10**).

The compounded samples were stored at a constant relative humidity of 50 % at a temperature of 22 °C for at least 24 h before analysis.

***Figure 3-7**. Three-Tec twin-screw extruder ZE 12, source: three-tec.ch*

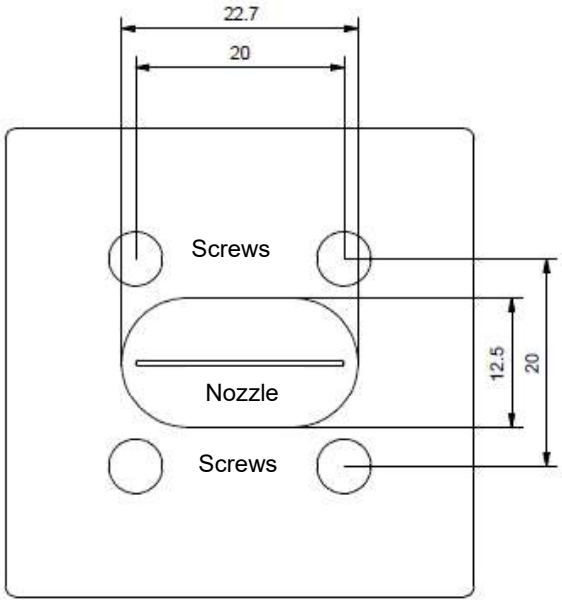

***Figure 3-8**. Plate nozzle used for plate extrusion (dimensions in mm)*

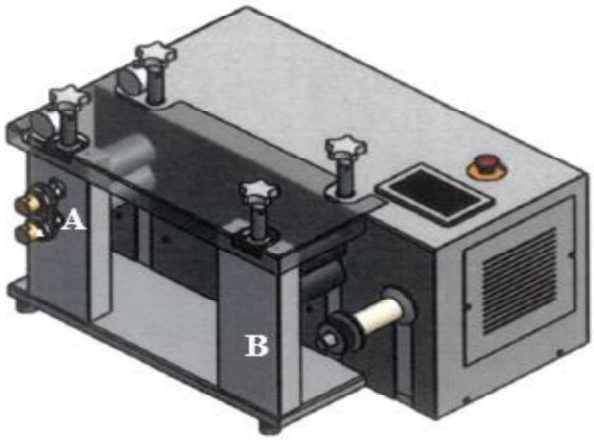

Figure 3-9. *Schematic diagram of used calender system with the (A) calender press and the (B) extraction roller*

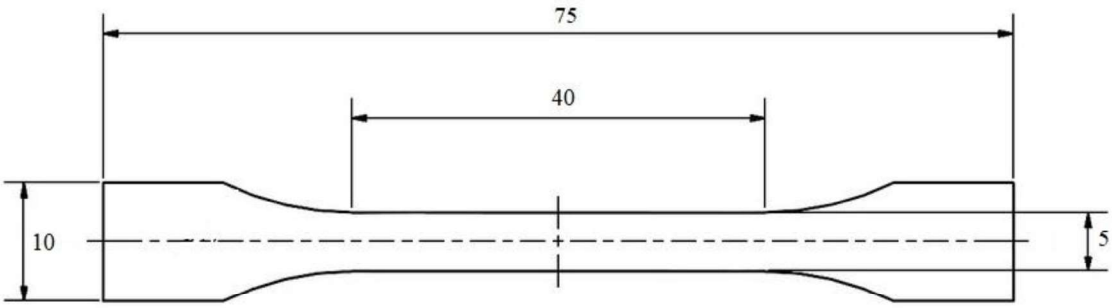

Figure 3-10*. "Dog bones" used for tensile tests (dimensions in mm)*

3.4 Formulation Used for the Experimental Program

This study investigated two different perspectives of manipulating a calcium carbonate based filler and their influence in a polyamide 12 composite.

1. Influence of size and shape of the mineral filler
2. Influence of the surface modification of calcium carbonate

In addition to these two main topics, the combination of the findings resulted in five individual parts, each consisting of a specific set of formulations used for the experimental programme:

- surface modification of GCC
- adjustment of the particle size distribution of GCC
- impact of bimodal particle size distribution of GCC
- combined bimodal particle size and surface modification of GCC
- comparison of GCC and PCC

The following sections present the formulations used, for each of the five investigated parts.

3.4.1 Surface Modification of GCC

To determine the beneficial role of the surface modification agent, bound on a calcium carbonate based mineral filler, the size and shape of the mineral filler was kept constant throughout the whole investigation. The feed material was ground to medium size with an approx. volume-based median particle size of 2 µm and a specific surface area of 3.7 m^2g^{-1} (m-G). The main filler data as well as particle size distribution are shown in **Table 3-4** and **Figure 3-11**.

The mineral filler was surface modified with the selection of various amino-containing acids: namely (A) 6-amino hexanoic acid; (B) ε-caprolactam; (C) L-arginine and (D) glutamic acid. As a reference, (R) stearic acid was chosen. **Table 3-5** shows an overview of all filler surface modifications carried out and the modifier used. A regular surface modifier amount of average 1 w/w% was determined for the investigation. For amino hexanoic acid a broader surface modifier range was covered to observe the effect of an over- or underdosage. The actual achieved coating thickness of each surface modification was not within the scope of the project and was not determined.

For the compound production, a constant filler load of 10 w/w% mineral filler in PA2200 was used. Considering the surface area of the filler, in this case, the introduced surface area of filler per given mass of polymer at the designed loading of 10 w/w% was 41 m^2 filler / 100 g PA12.

***Table 3-4**. Single component filler data*

Filler nomenclature	Filler type	d_{v10} / µm	d_{v50} / µm	d_{v90} / µm	SSA / m^2g^{-1}
m-G	medium sized GCC	1 ± 0.5	2 ± 0.5	5 ± 0.5	4 ± 0.5

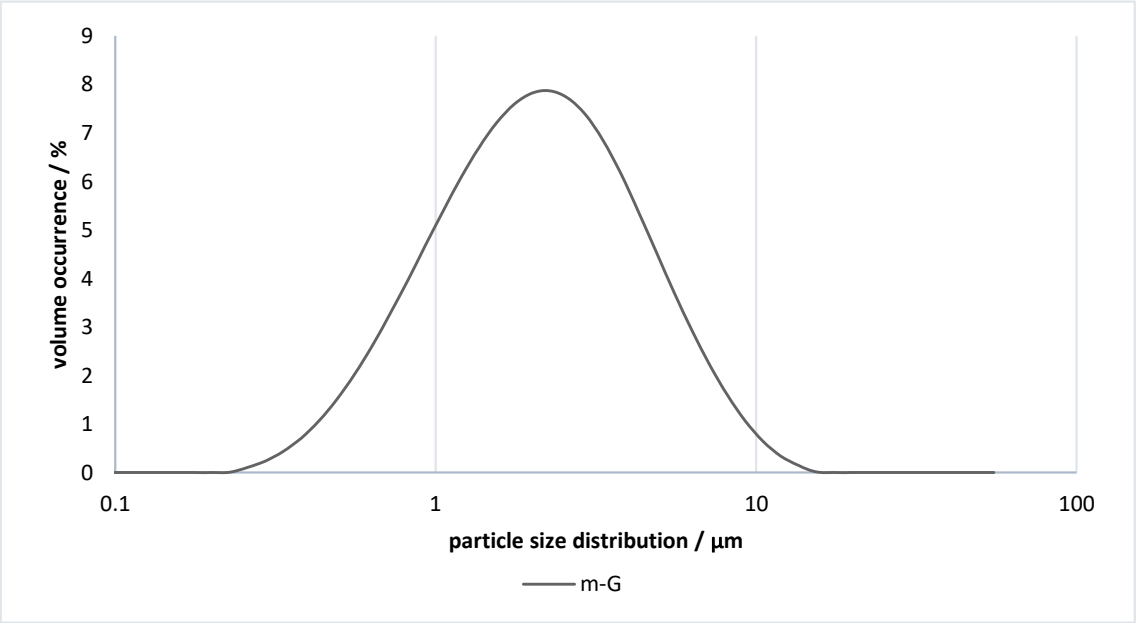

***Figure 3-11.** Particle size distribution of medium sized single component GCC filler*

***Table 3-5**. Functional filler data resulting after surface modification*

Filler Definition	Surface modifier	Additive amount/% by weight (w/w%)
R	Stearic acid	1.0 ± 0.1
A.1	Amino hexanoic acid	0.5 ± 0.1
A.2	Amino hexanoic acid	1.0 ± 0.1
A.3	Amino hexanoic acid	1.5 ± 0.1
A.4	Amino hexanoic acid	2.0 ± 0.1
B	ε-Caprolactam	1.0 ± 0.1
C	L-Arginine	1.0 ± 0.1
D	Glutamic acid	1.0 ± 0.1

3.4.2 Adjustment of the Particle Size Distribution of Ground Calcium Carbonate

The introduced surface of mineral filler within a polymeric matrix showed a significant influence on the thermal response behaviour of the resulting composite. To determine the effect that a change in particle size, as well as filler amount of the chosen mineral filler may have in a PA12 composite, different particle sized GCC-based mineral fillers were produced.

Figure 3-12 shows the grinding efficiency of the wet grinding process for the used GCC feed sample. With increasing grinding time, the volume median particle size decreases and the specific surface area of the particles increases. Although the volume-based median particle size d_{v50}, tends toward a plateau fine value after extended grinding time, the specific surface area continues to rise exponentially. The particle size distribution broadens extensively during the grinding process, generating high levels of very fine particles, which, although they do not contribute to a high-volume fraction as d_{v50} tends slowly toward a fine constant, contribute to a rapid increase in the surface area.

Table 3-6 gives an overview of the resulting properties of the processed mineral fillers after the drying step as well as the achieved particle size distribution.

As it interestingly can be observed, the product of the median volume particle size multiplied by the specific surface area is approximately constant as these values change. To a rough approximation, this can be explained, since the volume median particle size will scale inversely with the specific surface area. With the assumption that the particle is a sphere, the surface area of the median volume sized particle of diameter d_{v50} is $\pi * d_{v50}^2$.

The specific surface area (SSA) in m^2g^{-1} for this representative particle is therefore,

SSA = $((\pi * d_{v50}^2)/(\pi * d_{v50}^3/6)) / \rho$, where ρ is the constant material density. Thus,

SSA * d_{v50} * ρ = 6, which is indeed a constant.

Of course, taking the volume median size is an approximation limited by the particles size distribution, however, mechanical fracture during grinding of crystalline mineral calcium carbonate follows quite closely a log-normal particle size distribution and, as such, using a single parameter size does form a reasonable proportional representation.

For the compound production, a variation in filler load was defined. As shown in **Table 3-7**, depending on the mineral filler used, the filler load varied between 0.2 to 40 w/w%. **Figure 3-13** shows an overview of the pigment surface area in ratio to 100 g of polymer in the compound matrix as a function of d_{v50} and increasing filler loading level.

With the chosen filler loading level, it was possible to cover the range of up to approx. 150 m^2 of filler material per 100 g of polymer with all given particle size distributions, without influencing the brittleness of the resulting extruded compound. At a filler surface introduction above ~ 200 m^2 per 100 g polymer, the compound started to lose its elasticity and was, therefore, not included in this study. An increased amount of a very coarse GCC filler 'vc-G', greater than 20 w/w%, was also not included due to a significant increase in the compound melt viscosity resulting from the introduction of such a large amount of coarse filler particles.

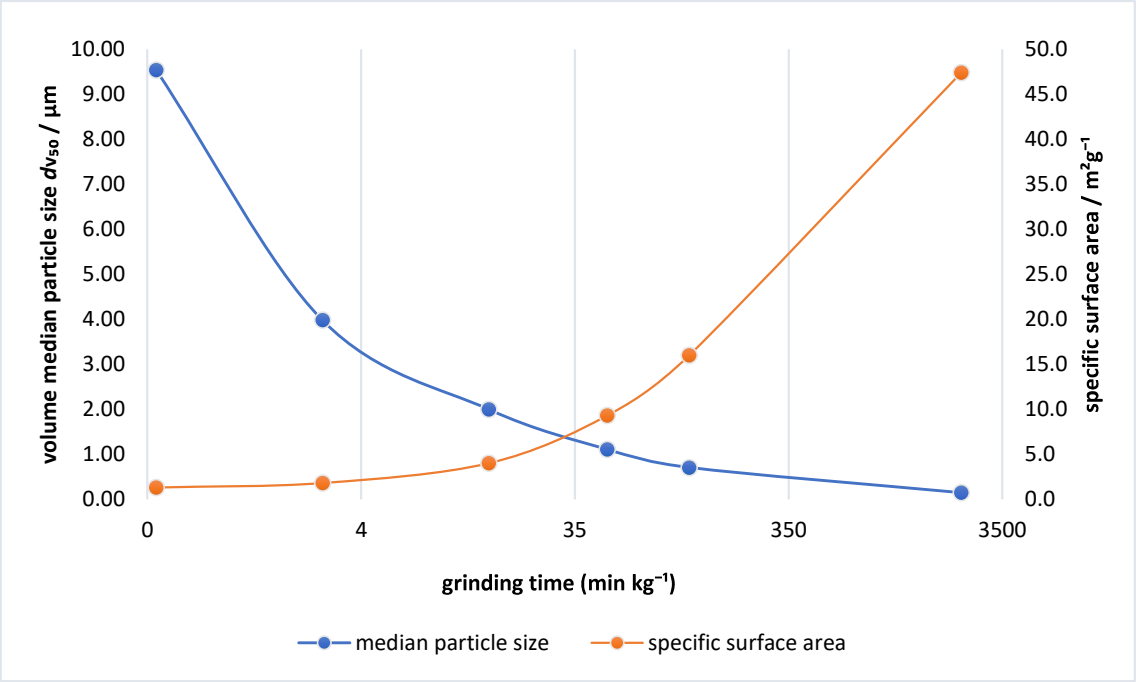

***Figure 3-12**. Wet grinding efficiency of calcium carbonate: comparison of the volume median particle size d_{v50} and the specific surface area in dependency of the grinding time*

***Table 3-6**. Mineral filler data after drying step*

Filler nomenclature	Filler type	d_{v10} / µm	d_{v50} / µm	d_{v90} / µm	SSA / m^2g^{-1}
vc-G	very coarse sized GCC	1 ± 0.5	10 ± 1.5	35 ± 5.0	1 ± 0.3
c-G	coarse sized GCC	1 ± 0.5	5 ± 1.5	17 ± 2.0	2 ± 0.2
m-G	medium sized GCC	1 ± 0.5	2 ± 0.5	5 ± 0.5	4 ± 0.5
vs-G	very small sized GCC		1 ± 0.1		16 ± 1.0
us-G	Ultra-small sized GCC		0.2 ± 0.05		50 ± 3.0

***Table 3-7**. Overview of the produced compounds at different filler levels as well as the resulting filler surface introduced*

Compound nomenclature	Filler used	Filler amount / w/w%	Total carbonate surface per 100 g polyamide 12 / m²
vc-G_2.5	vc-G	2.5	3.3 ± 0.1
vc-G_5		5.0	6.8 ± 0.5
vc-G_10		10.0	14.4 ± 1.0
vc-G_20		20.0	32.5 ± 2.0
c-G_5	c-G	5.0	9.5 ± 0.5
c-G_10		10.0	20.0 ± 1.0
c-G_20		20.0	45.0 ± 2.0
c-G_40		40.0	120.0 ± 5.0
m-G_2.5	m-G	2.5	10.3 ± 0.5
m-G_5		5.0	21.1 ± 1.0
m-G_10		10.0	44.4 ± 2.0
m-G_20		20.0	100.0 ± 5.0
vs-G_2.5	vs-G	2.5	41.0 ± 2.0
vs-G_5		5.0	84.2 ± 5.0
vs-G_10		10.0	177.8 ± 5.0
vs-G_20		20.0	400.0 ± 10.0
us-G_0.2	us-G	0.2	9.0 ± 0.5
us-G_0.5		0.5	24.0 ± 1.0
us-G_1		1.0	48.0 ± 2.0
us-G_2.5		2.5	122.0 ± 5.0

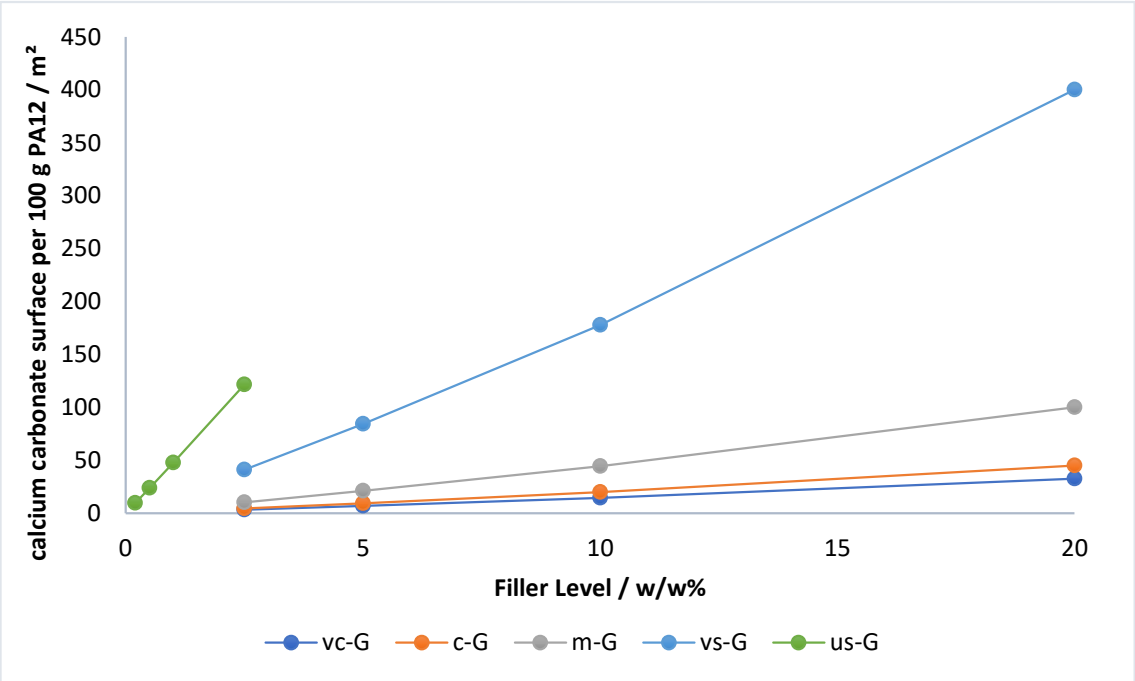

***Figure 3-13**. Resulting filler surface in the compounded polymer matrix dependent on the median particle size of the filler material*

3.4.3 Bimodal Particle Size Distribution of Ground Calcium Carbonate

The particle size distribution of calcium carbonate as a functional filler is designed to be adjusted so that the melting, as well as crystallisation behaviour of a PA12 compound can be studied. To further control the thermal response properties of a filling compound for improved properties in additive manufacturing processing through selective laser sintering, the possibility to combine precisely defined particle size distributions was studied, thereby combining the benefits that each particle size range within the chosen material size distribution contributes to the matrix. To achieve this, combinations of materials were used to generate bimodal size distributions.

To be able to design the combinations, two functional fillers were produced. **Table 3-8** shows an overview of the resulting particle size distribution and specific surface area properties of the processed functional filler particle after drying. **Table 3-9** gives an overview of all tested ratios, as well as the resulting carbonate surface. **Figure 3-14** shows the individual particle size distribution of each of the final combined functional fillers. The precise mixture of the two monomodal mineral filler results in a controlled bimodal particle size distribution.

It is enlightening to consider the particle size distributions, **Figure 3-14**, in a little more detail. Taking note of the logarithmic size scale, the extra small sized GCC, ‘es-G’, displays a close to perfect Gaussian (bell-shaped) curve, which indicates a log-normal distribution, and the volume median d_{v50} size equals the mode, or most commonly present particle volume size. The nature of calcium carbonate when ground in water leads to a dynamic dissolution and re-precipitation of ultrafine particles, and, in addition, the grinding process itself creates fines from the desired larger particles in the coarse sized GCC, ‘c-G’. This leads to a distinctive skew of the distribution, such that not only the desired coarse material is obtained, but also at least 10 v/v% of the sample consists of particles that cover the range of the distribution for the fine ‘es-G’. The overlap in fines is advantageous since the process requires a number of properties that benefit from a broad size distribution, such as filler particle powder flowability, sufficient surface area even of the coarse fraction to provide composite homogeneity and to support controlled polymer crystallisation nucleation. The presence of fines in the coarse fraction also supports a mid-range particle size continuity in the bimodal mix of coarse and fine particles, which supports the uniformity of compounding and acts against settling and demixing. Furthermore, the volume median dv_{50} lies away from the mode volume size for the coarse fraction, such that the volume capacity, and, therefore, heat capacity is represented by particles considerably larger than the median. Conversely, the majority of the surface area of the coarse fraction, ‘c-G’, is contributed by the fines it contains.

For the compound production, a constant filler load of 10 w/w% mineral filler in PA2200 was used for the four filler mixtures. As a single component reference, 5 w/w% of either ‘c-G’ or ‘es-G’ was compounded additionally, which represent the theoretical implemented surface area of either ‘c-G’ or ‘es-G’ in the developed blends. **Table 3-10** gives an overview of all produced compounds and the introduced filler surface area in ratio to 100 g of PA12 in the compound matrix.

Table 3-8. *Filler particle data after drying step*

Filler nomenclature	Filler type	d_{v10} / µm	d_{v50} / µm	d_{v90} / µm	SSA / m^2g^{-1}
c-G	coarse sized GCC	1 ± 0.5	5 ± 1.5	17 ± 2.0	2 ± 0.2
es-G	extra small sized GCC	0.2 ± 0.05	0.5 ± 0.1	1 ± 0.2	23 ± 2.0

Table 3-9. *Filler particle data after forming filler mixtures*

Mixed filler nomenclature	Mix proportions		Specific surface area / m^2g^{-1}
	Amount of c-G / w/w%	Amount of es-G / w/w%	
50/50_c/es-G	50	50	12.2
70/30_c/es-G	70	30	7.8
30/70_c/es-G	30	70	21.8
33/66_c/es-G	33	66	21.6

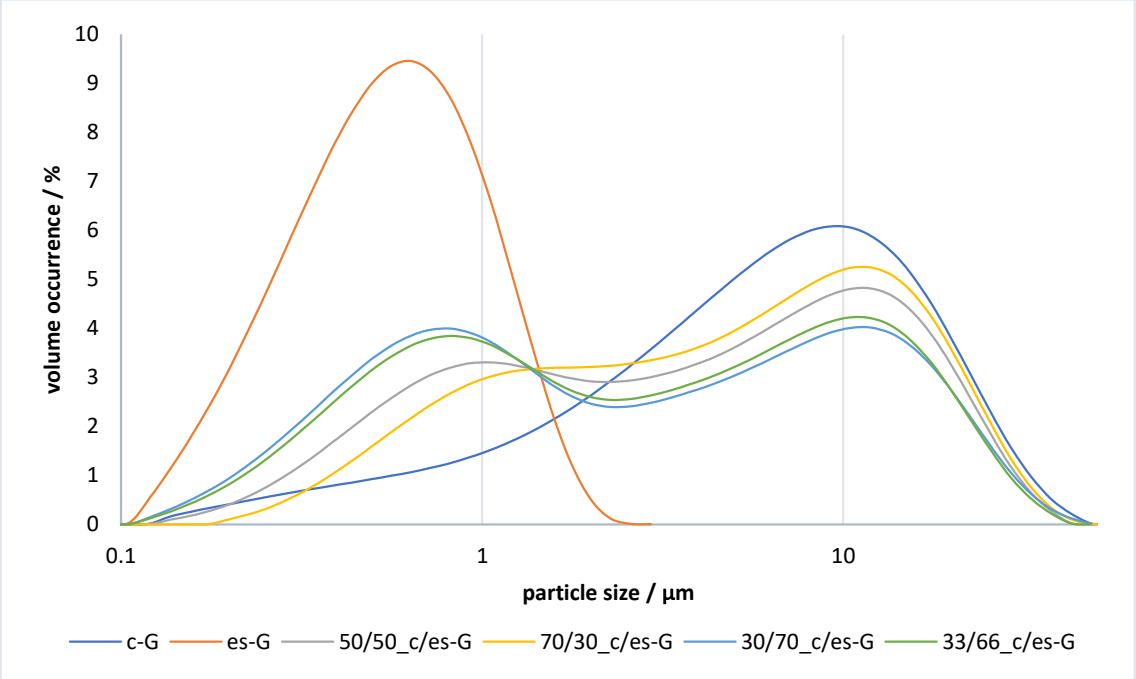

Figure 3-14. *Particle size distribution of developed GCC-fillers*

***Table 3-10**. Tested filler loadings and introduced surface area of filler per 100 g PA12*

Compound nomenclature	Filler used	Filler amount /w/w%	Total carbonate surface per 100 g Polyamide 12 /m²	c-G surface per 100 g PA12 /m²	es-G surface per 100 g PA12 /m²
c-G_5	c-G	5	10	10	0
es-G_5	es-G	5	120	0	120
50/50_c/es-G_10	50/50_c/es-G	10	141	11	130
70/30_c/es-G_10	70/30_c/es-G	10	95	15	80
30/70_c/es-G_10	30/70_c/es-G	10	187	6	181
33/66_c/es-G_15	33/66_c/es-G	15	286	11	275

3.4.4 Combination of Bimodal Particle Size and Surface Modification of Ground Calcium Carbonate

A further part of the study, set out to establish the influence of combining the spectrum of findings depending on particle size distribution, specific surface area and the findings on the surface modification, with the end effect of controlling heating and the mechanical properties of the compounded polyamide 12. To optimise the ratio between a fine calcium carbonate and a previous used broader size distribution ground calcium carbonate filler, different functional fillers were produced. **Table 3-11** shows an overview of the resulting particle size distribution and specific surface area properties of the used single component functional filler particle after the drying step. **Table 3-12** gives an overview of all tested filler mix ratios, and hence the discrete particle size distribution ratios as well as the resulting total carbonate specific surface. **Figure 3-15** and **Figure 3-16** show the particle size distribution of each of the used functional fillers and blends. The precise mixtures result in a specifically controlled bimodal particle size distribution.

To determine the influence of the surface modifier amount on thermal properties, two modifier levels were considered and tested, series 1 and 2, respectively, where series 1 employed a high level of surface treatment (~3 mmol per 100 m^2) applied to all single component fillers before mixing into the designed blends as shown in **Table 3-12**, and series 2 the reduced amount (~2 mmol per 100 m^2) applied to selected examples of the single components and thus used in a second series of blends. **Table 3-13** gives an overview of the resulting single component functional fillers and their modifier amount for series 1 and 2, in which the higher amount of modification and lower modification levels were used, respectively.

Additionally, a third series was constructed, in which only the fine filler fraction was surface modified at the lower level (~2 mmol per 100 m^2), to prevent the modification agent from interfering with the thermal transfer between the coarse filler fraction and the polymer matrix. **Table 3-14** gives an overview of the tested ratios from series 2 and 3, showing the differences between the untreated and treated fractions.

As control samples, the same filler blends and ratios were tested in which the mineral filler was not surface modified at all, having the properties as shown previously in **Table 3-11** and **Table 3-12**. This enabled the evaluation of the effect that the calcium carbonate alone gave to the system and the effect that the surface modification had on the thermal and mechanical properties.

Table 3-15 shows the used filler loadings as well as the resulting surface area of filler introduced per given mass of polymer, after compounding process.

***Table 3-11**. Single component GCC-mineral filler data*

Filler nomenclature	Filler type	d_{v10} / µm	d_{v50} / µm	d_{v90} / µm	SSA / m^2g^{-1}
c-G	coarse sized GCC	1 ± 0.5	5 ± 1.5	17 ± 2.0	2 ± 0.2
m-G	medium sized GCC	1 ± 0.5	2 ± 0.5	5 ± 0.5	4 ± 0.5
s-G	small sized GCC	0.5 ± 0.1	1 ± 0.5	3 ± 0.5	8 ± 0.5

***Table 3-12.** Mineral GCC-filler data after filler mixing*

Mixed filler nomenclature	Single components		Mix proportions		Specific surface area / m^2g^{-1}
	Coarse Filler	Fine Filler	Amount Coarse Filler / w/w%	Amount Fine Filler / w/w%	
70/30_c/s-G	c-G	s-G	70	30	3.6
33/66_c/s-G	c-G	s-G	33	66	5.7
50/50_c/m-G	c-G	m-G	50	50	2.7

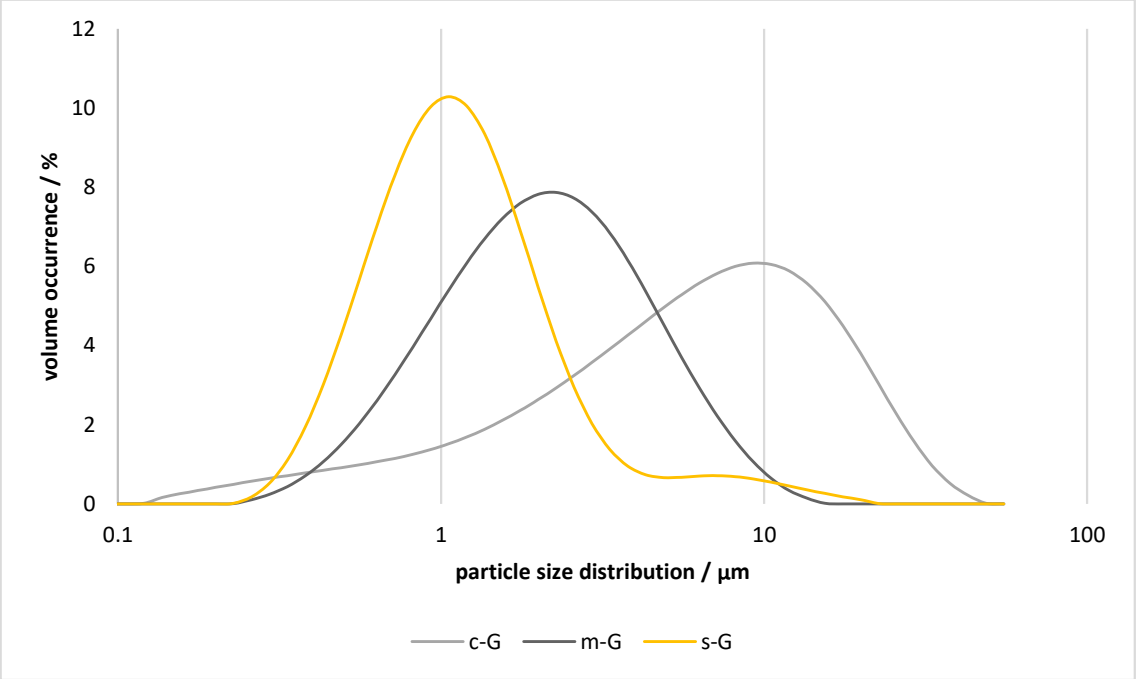

***Figure 3-15.** Particle size distribution of developed single component mineral GCC-filler*

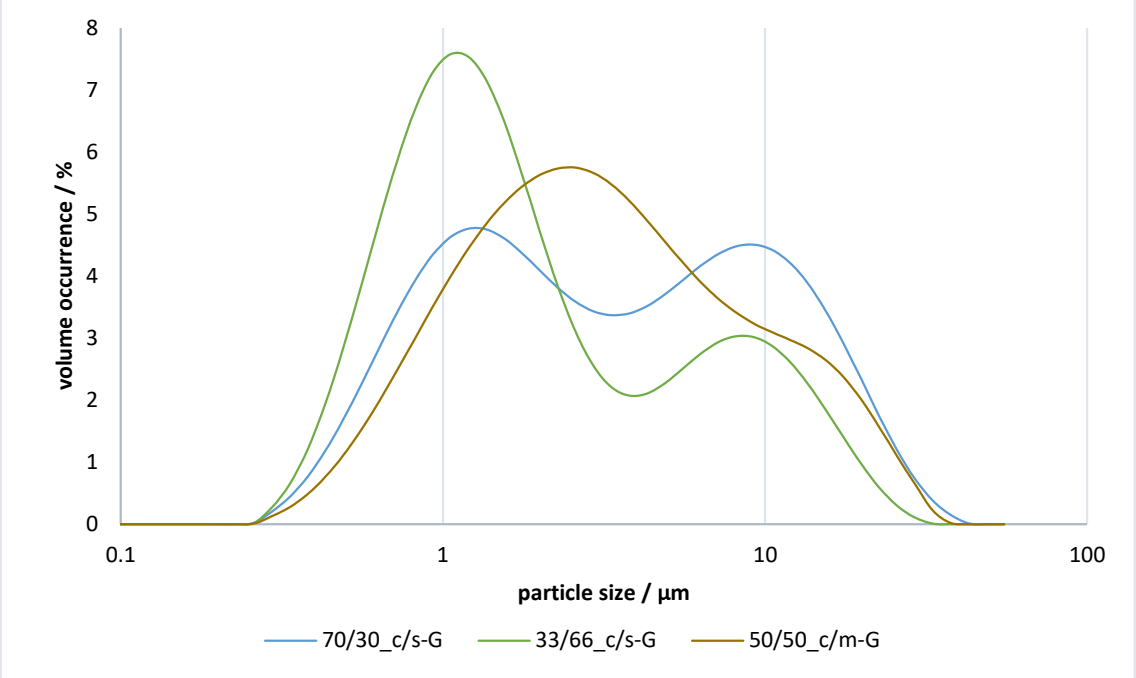

Figure 3-16. *Particle size distribution of developed mineral GCC-filler blends*

Table 3-13*. Single component functional GCC-filler data resulting after surface modification – series 1 and 2*

Treated Filler nomenclature	Modifier surface concentration / mmol per 100 m^2 filler	Modifier amount / w/w%
c-G.1	3.05	0.7
m-G.1	3.05	1.5
s-G.1	3.05	3.1
c-G.2	2.30	0.5
s-G.2	2.30	2.3

Table 3-14*. Functional GCC-filler data resulting after filler mixing – blends arising comparing series 2 and series 3*

Filler nomenclature	Coarse Filler	Fine Filler	Amount Coarse Filler / w/w%	Amount Fine Filler / w/w%	Amount untreated Coarse Filler / w/w%
70/30_c/s-G.2	c-G.2	s-G.2	70	30	0
70/30_c/s-G.3	c-G	s-G.2	0	30	70

***Table 3-15**. Tested GCC-filler loadings and introduced surface area of filler per given 100 g mass of polyamide 12*

Compound nomenclature	Filler used	Filler amount / w/w%	Total carbonate surface per 100 g polyamide 12 / m^2	Coarse Filler surface per 100 g polyamide 12 / m^2	Fine Filler surface per 100 g polyamide 12 / m^2
70/30_c/s-G_12	70/30_c/s-G	12	49	17	32
70/30_c/s-G_15	70/30_c/s-G	15	63	22	41
33/66_c/s-G_15	33/66_c/s-G	15	101	11	90
50/50_c/m-G_15	50/50_c/m-G	15	48	16	32
70/30_c/s-G.1_12	70/30_c/s-G.1	12	49	17	32
70/30_c/s-G.1_15	70/30_c/s-G.1	15	63	22	41
33/66_c/s-G.1_15	33/66_c/s-G.1	15	101	11	90
50/50_c/m-G.1_15	50/50_c/m-G.1	15	48	16	32
70/30_c/s-G.2_12	70/30_c/s-G.2	12	49	17	32
70/30_c/s-G.2_15	70/30_c/s-G.2	15	63	22	41
70/30_c/s-G.3_12	70/30_c/s-G.3	12	49	17	32
70/30_c/s-G.3_15	70/30_c/s-G.3	15	63	22	41

3.4.5 Particle Size and Surface Area of GCC and PCC as Functional Filler

The morphology of the mineral filler was also investigated, by a controlled synthesis of precipitated calcium carbonate. The crystal structure, particle size distribution as well as morphology of the final filler product was adjusted, to achieve a fine scalenohedral PCC (sc-PCC) and a coarser prismatic PCC (pr-PCC). **Table 3-16** shows the resulting particle size distribution and specific surface area properties of the used single component functional filler particle after drying. **Figure 3-17** compares the particle size distribution of the developed PCC fillers against the used GCC fillers, used in 3.4.4.

The amount of surface modifier was kept identical to the materials produced in the previous section. This resulted in different functional PCC-fillers, listed in **Table 3-17** and different blends (**Table 3-18** and **Table 3-19**).

Figure 3-18 shows the particle size distribution of the resulting PCC-blends. The filler amount in the PA12 compound was kept constant at 15 weight% and can be overviewed in **Table 3-20**.

***Table 3-16.** Single component filler data of synthesised PCC*

Filler nomenclature	Filler type	d_{v10} / µm	d_{v50} / µm	d_{v90} / µm	SSA / m^2g^{-1}
pr-P	coarse sized PCC	1 ± 0.5	5 ± 0.5	9 ± 0.5	1 ± 0.3
sc-P	small sized PCC	0.5 ± 0.1	2 ± 0.5	4 ± 0.5	6 ± 0.5

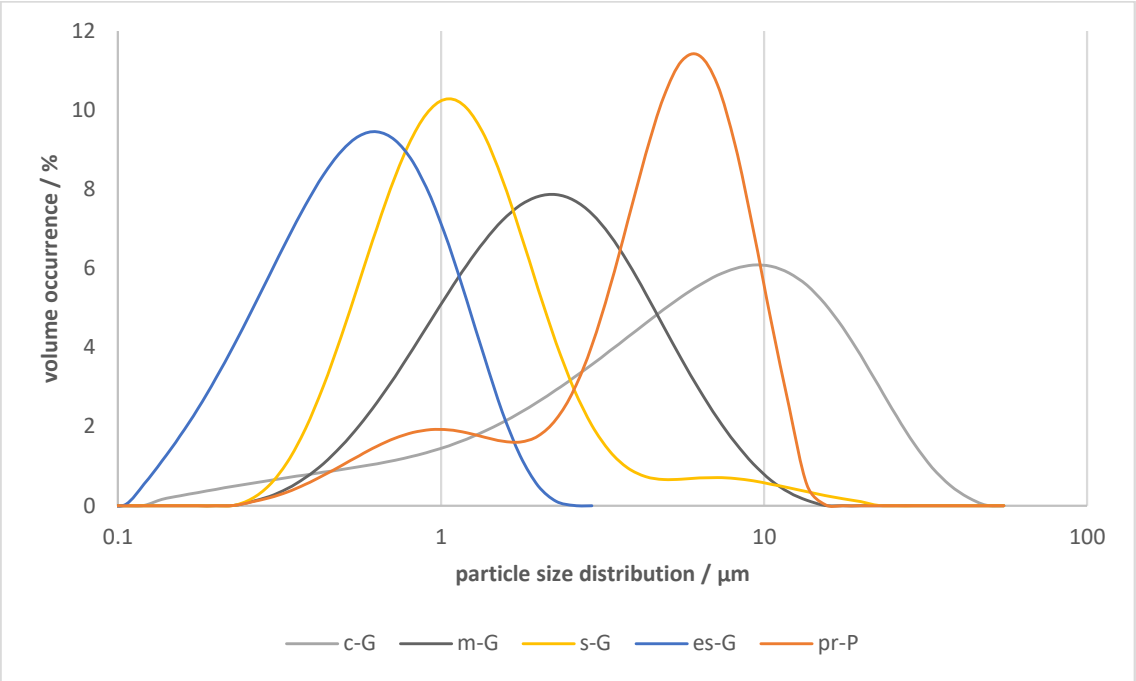

Figure 3-17. *Particle size distribution of developed single component mineral GCC- and PCC-fillers*

Table 3-17. Single component functional PCC-filler data resulting after surface modification – series 1 and 2

Treated Filler nomenclature	**Modifier surface concentration / mmol per 100 m^2 filler**	**Modifier amount / w/w%**
pr-P.1	3.05	0.5
sc-P.1	3.05	2.6
pr-P.2	2.30	0.4
sc-P.2	2.30	1.9

Table 3-18. *Resulting mineral PCC-filler data after filler mixing*

Mixed filler nomenclature	Single components		Mix proportions		Specific surface area / m^2g^{-1}
	Coarse Filler	Fine Filler	Amount Coarse Filler / w/w%	Amount Fine Filler / w/w%	
30/70_pr/sc-P	pr-P	sc-P	30	70	4.9
70/30_pr/sc-P	pr-P	sc-P	70	30	2.8

Table 3-19*. Functional PCC-filler data resulting after filler mixing – blends arising comparing series 2 and series 3*

Filler nomenclature	Coarse Filler	Fine Filler	Amount Coarse Filler / w/w%	Amount Fine Filler / w/w%	Amount untreated Coarse Filler / w/w%
70/30_pr/sc-P.2	pr-P.2	sc-P.2	70	30	0
70/30_pr/sc-P.3	pr-P	sc-P.2	0	30	70

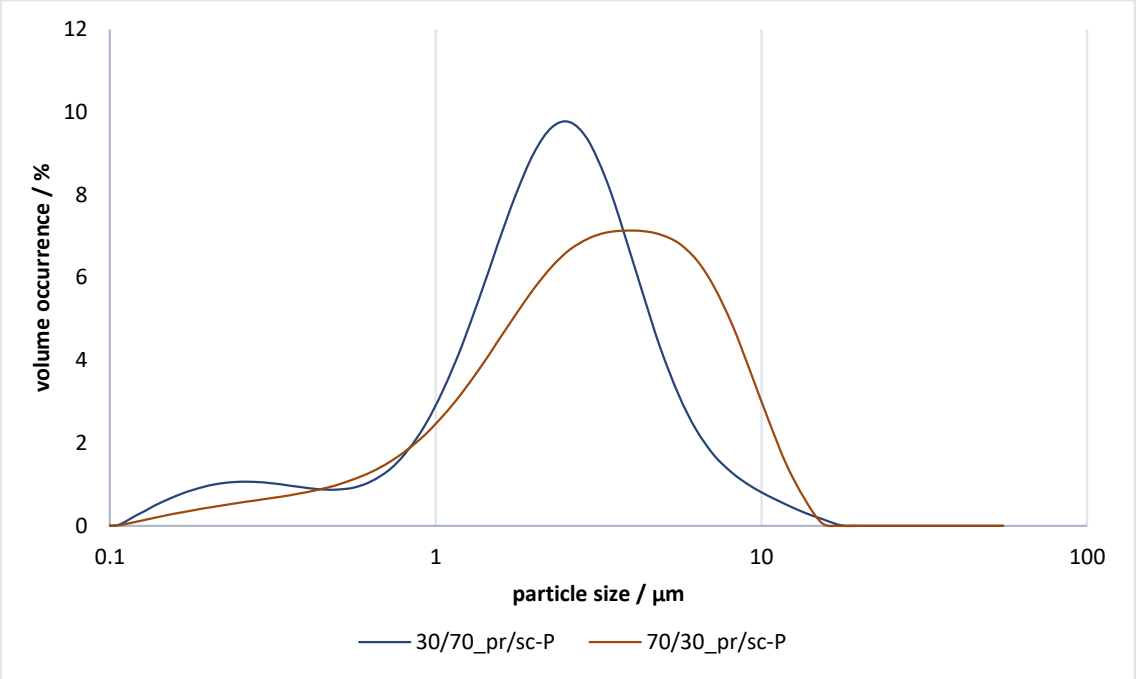

Figure 3-18. *Particle size distribution of developed mineral PCC-filler blends*

Table 3-20. *Tested PCC-filler loadings and introduced surface area of filler per given 100 g mass of polyamide 12*

Compound nomenclature	Filler used	Filler amount / w/w%	Total carbonate surface per 100 g polyamide 12 / m^2	Coarse Filler surface per 100 g polyamide 12 / m^2	Fine Filler surface per 100 g polyamide 12 / m^2
30/70_pr/sc-P_15	30/70_pr/sc-P	15	86	7	79
70/30_pr/sc-P_15	70/30_pr/sc-P	15	50	16	34
30/70_pr/sc-P.1_15	30/70_pr/sc-P.1	15	86	7	79
70/30_pr/sc-P.1_15	70/30_pr/sc-P.1	15	50	16	34
70/30_pr/sc-P.2_15	70/30_pr/sc-P.2	15	50	16	34
70/30_pr/sc-P.3_15	70/30_pr/sc-P.3	15	50	16	34

3.5 Evaluation of the Functional Filler

The main focus was the comparison of different particle size distributions and morphological structures of the different developed mineral fillers and their effect in the final polymeric compound. The analytical methods used, to determine these differences are described below.

3.5.1 Particle Shape and Powder Distribution

The volume defined particle size distribution of all products was determined using dynamic laser light scattering (Malvern Instruments Mastersizer 3000, Malvern Panalytical Ltd., Enigma Business Park, Grovewood Road, Malvern WR14 1XZ, United Kingdom), adopting the Fraunhofer particle scattering cross-section model [54, 55]. All samples were stabilized in aqueous suspension in advance of measurement by adding approx. 500 ppm of a polyacrylate based dispersing agent.

3.5.2 Specific Surface Area

The specific surface area (SSA) was determined via the nitrogen gas adsorption method (BET-Method) [56] (ASAP 2460 Surface Area and Porosity Analyzer, Micromeritics®, 4356 Communications Drive, Norcross, GA 30093-2901, USA).

3.5.3 Morphological Structure

The morphology of each developed functional filler was recorded using a field emission scanning electron microscope (FESEM) (Zeiss Sigma VP, Carl-Zeiss-Strasse 22, 73447 Oberkochen, Germany). The samples were Au-coated and analysed using a secondary electron detector (SE) which clearly revealed the particle shape of each filler type.

3.6 Compound Analysis

After the functional filler development and twin-screw compounding, within a PA12 matrix, the analysis of the resulting composites was structured in three sections:

- visual homogeneity of filler distribution
- thermal response analysis
    - degradation temperature through TGA
    - temperature-related material transitions through DSC
    - viscoelastic behaviour through TMA
    - melt flow viscosity through MFI
- ductility through mechanical tensile test

3.6.1 Filler Distribution Homogeneity

The resulting compound structure and homogeneity of the polymer/filler matrix were visually observed using scanning electron microscopy (SEM) (Zeiss Sigma VP, Carl-Zeiss-Strasse 22, 73447 Oberkochen, Germany).

The compound samples were embedded in epoxy resin and SEM specimens were prepared by cutting down the surface with a diamond knife (20 µm and 15 µm) and polishing with corundum (0.05 µm). The specimens were studied with a backscatter detector in variable pressure mode (50 Pa) at 20 kV and a 60 µm cover.

3.6.2 Thermogravimetry (TGA)

The degradation temperature of the compounds was analysed by thermogravimetric analysis (TGA). The technique enables changes in the physical and chemical properties of materials to be determined as a function of increasing temperature. It is regularly used in this context to measure thermal degradation occurring in filled organic materials. In addition, it is possible in turn to determine approximate values of sample humidity, the content of low-molecular auxiliary agents and the total organic material content each revealed as temperature rises. Depending on the measuring method, the thermal degradation of all likely components can be determined up to 1 000 °C as a summation (cumulative loss of mass).

TGA curves were generated using a Mettler-Toledo TGA/DSC 1-LF apparatus (Im Hackacker 15, 8902 Urdorf, Switzerland), applying a continuous flow of nitrogen gas (50 cm^3 min^{-1}). The samples (~150 mg) were initially heated to 100 °C, kept at this constant temperature for 2 min and then heated up to 700 °C at a rate of 10 °C min^{-1}. The onset temperature of the main gravimetric weight loss of the compound during temperature increase from 100 °C to 600 °C was determined.

Successful laser sintering depends on the material's heat conductivity, thermal capacity and melt flow properties. Therefore, the phase change behaviour in response to thermal energy input revealed by TGA provides a crucial assessment of suitability for SLS [57].

3.6.3 Thermal Mechanical Analysis (TMA)

When polymers in their stationary state are subjected to a high mechanical load (strain), they tend to yield when a critical static stress is reached prior to flow. At its viscoelastic state, the elastic structure may harden as strain increases until the viscous flow dominates after the dynamic yield stress point is reached. Thermal Mechanical Analysis (TMA) provides a

technique to study the viscoelastic nature of polymers/compounds at their melting temperature [58, 59].

Through TMA analysis the liquefaction rate of a compound can be determined at its melting point as a function of energy input rate, related to the latent heat of the phase change. The thermal melting inflection slope (Tism) shows the percentage force drop that occurs at the temperature increase of 1 °C during the melting process of the compound.

A Mettler-Toledo (Im Hackacker 15, 8902 Urdorf, Switzerland) TMA/SDTA 840 apparatus was used to monitor the liquefaction rate of the compounds under a continuous nitrogen flow of 10 $cm^3 min^{-1}$. The samples were heated from 100 °C up to 200 °C at a rate of 10 $°C min^{-1}$ under a constant sample deformation of 0.01 N.

3.6.4 Differential Scanning Calorimetry (DSC)

The temperature transitions and melting range of polymers can be observed by recording a differential scanning calorimetry (DSC) plot. DSC is a thermo-analytical technique where the heat difference between a sample and the reference is measured as a function of temperature. The reference and the sample are heated at a specific heating rate above the melting temperature of the sample and afterwards cooled at a specific heating rate to below the crystallisation point. The difference in the heat-curve gives information of the different phase transitions. At a specific temperature, the sample undergoes a physical transformation (phase transition), in which more or less heat is needed than the reference to maintain both at the same temperature [60].

Due to the absorption of heat by the sample (endothermic phase transition), more heat is required during the melting process to increase the sample temperature at the same rate as the reference. During the cooling step, the sample crystallises back to the solid state and less heat is required to keep the temperature at the reference level due to the exothermic phase transition from liquid to solid [61].

DSC curves were recorded on a Mettler-Toledo DSC 823 apparatus under a continuous nitrogen flow of 50 cm^3 min^{-1}. An approx. 7 mg sample was heated to 100 °C, kept constant for 2 min, heated up to 200 °C at a rate of 5 °C min^{-1} and then kept at a constant temperature for an additional 2 min. To determine the crystallisation properties, the melt was cooled down to 100 °C at a rate of 5 °C min^{-1}. **Figure 3-19** shows the schematic temperature program used for the melting and crystallisation temperature determination measurements. **Figure 3-20** represents a typical DSC curve, obtained with this method, showing the main thermal properties which can be detected through such an analysis. The resulting absorption curves were precise and repeatable so, the standard deviation of the double measurements is not shown in the following results.

For a detailed investigation of the crystallisation kinetics, the crystallisation time was measured at a constant temperature to provide a record of the material's isothermal response [62]. The samples (≈ 7 mg) were heated to 100 °C, kept constant for 2 min, heated up to 200 °C at a rate of 20 °C min^{-1}, cooled down with a cooling rate of 40 °C min^{-1} and finally kept at the measuring temperature of 172 °C, until the sample was completely recrystallised. **Figure 3-21**

shows the schematic temperature program used for the crystallisation time determination measurements.

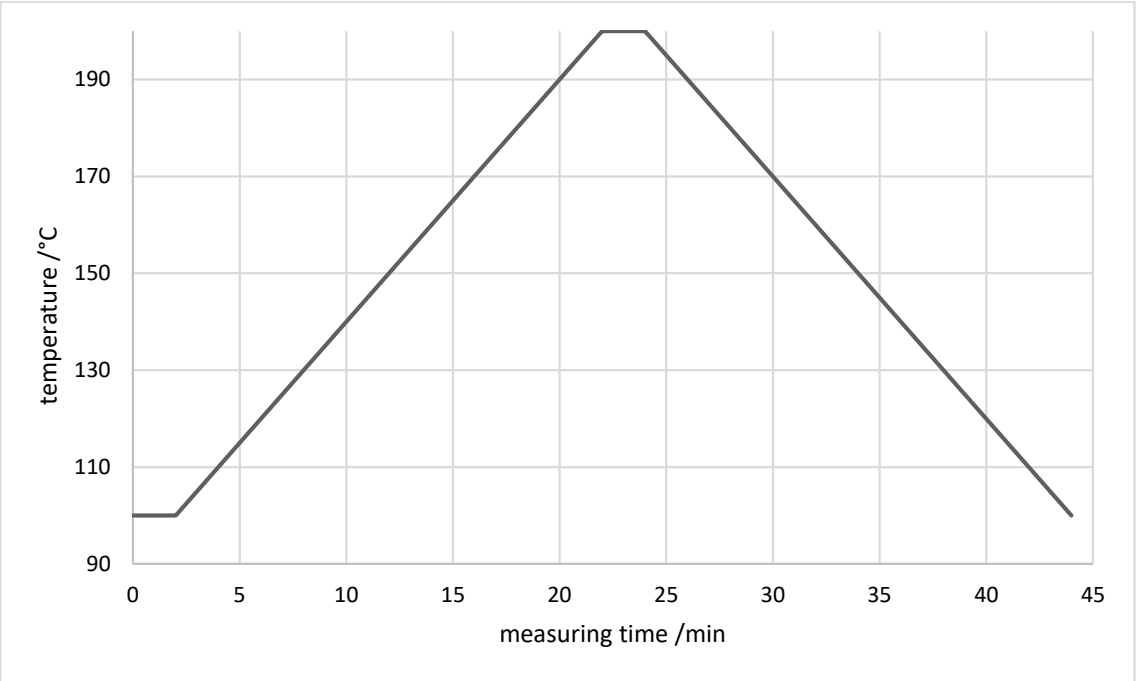

Figure 3-19. *Schematic temperature profile program used in differential scanning calorimetry measurements for melting and crystallisation behaviour; intersection point at 90°C, close to the initial temperature*

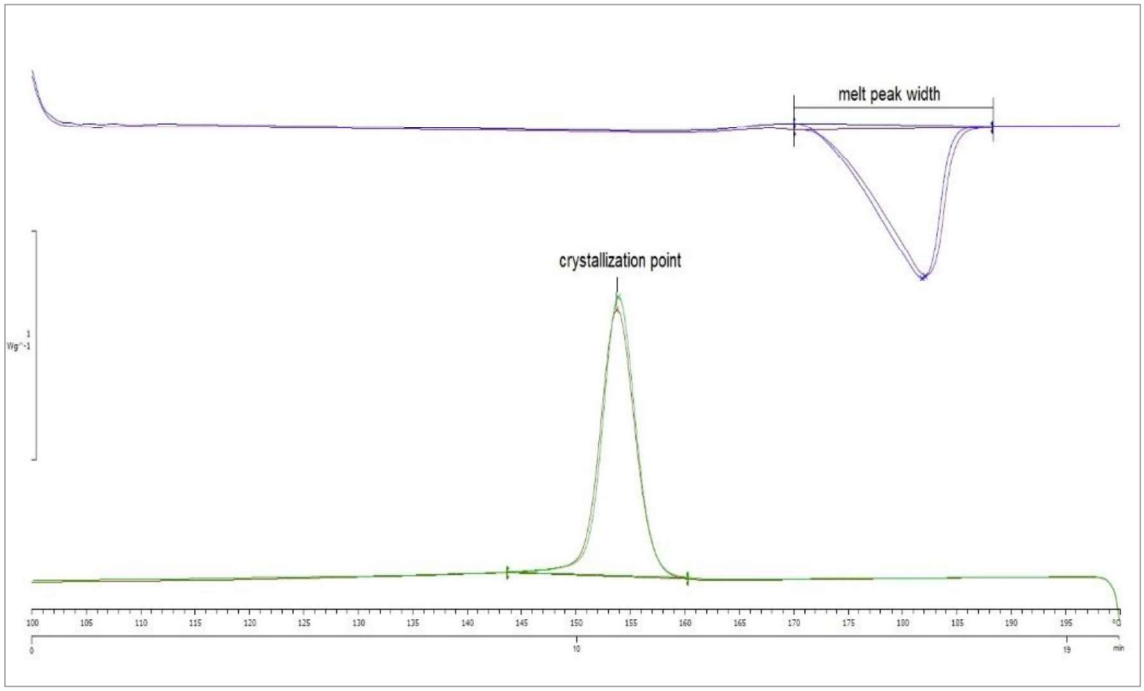

***Figure 3-20**. Example for measured DSC curve - DSC curve of EOS PA 2200*

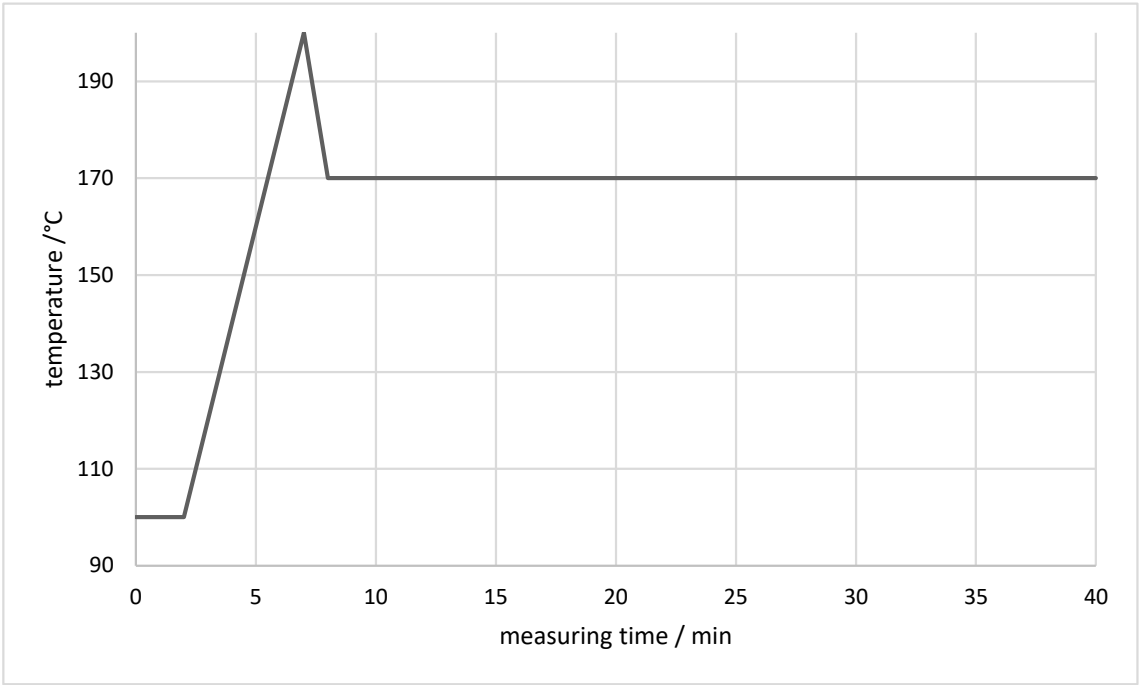

***Figure 3-21.** Schematic temperature program used in differential scanning calorimetry measurements for crystallisation time behaviour; intersection point at 90°C, close to the initial temperature*

3.6.5 Melt Viscosity – Melt Flow Index (MFI)

As an alternative to the more precise but complex measurement method of a cone-plate rheometer, which requires a heating stage and evaporative casing to capture the melt phase data, the melt flow index using an enclosed cylinder-die method provides an easier access to basic rheological data, which is commonly used in the plastics industry [16]. The melt flow index is the flow in grams that occurs within 10 min through a standard die, when a fixed pressure is applied to the melt via a piston at a temperature above the melt temperature of the polymer. At the used conditions of the test, the MFI is an inverse measure of the process melt flow viscosity [57]. The resulting viscosity value for a measured material is only valid at the given applied force and temperature under the conditions of die extrusion.

The MFI was determined with the use of a 'CEAST Melt Flow Index Tester Model 702700' according to the 'DIN EN ISO 1133' guidelines. Thus, the compound was pre-heated in the barrel for 5 min without load at 190 °C. Afterwards, a constant pressure exerted by a force of 2.16 kgf, or 21.2 Newton, was applied to the compound which pressed the compound through a die with a diameter of 2.095 mm. The measuring length was kept constant at 20.00 mm.

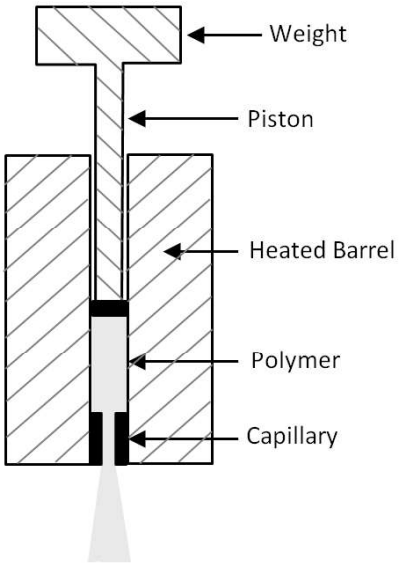

Figure 3-22. *Schematics of the melt flow index measurement, source: polymerdatabase.com*

3.6.6 Mechanical Properties – Short-Term Load: Tensile Test

The mechanical properties of each compounded sample were evaluated with a Zwick/Roell ProLine table-top testing machine (ZwickRoell GmbH & C. KG, August-Nagel-Strasse 11, 89079 Ulm, Germany) according to the European Norm ISO 527-1 guidelines. Ten tensile test dog bones of each compound were measured adopting a tensile extension rate of 1 mm min^{-1} providing a determination between 0.05 % and 0.25 % extension. Afterwards, the yield stress was measured under an extensional rate of 50 mm min^{-1}, with a force threshold of 60 % of the maximum force and a sensitivity of 0.5 %.

4 Results and Discussion

In this chapter, the experimental results will be presented and discussed in five parts:

- Surface modification of GCC
- Adjustment of the particle size distribution of GCC
- Impact of bimodal particle size distribution of GCC
- Combined bimodal particle size distribution and surface modification of GCC
- Comparison of GCC and PCC

To facilitate the discussion, the key tables from chapter 3 will be presented again in the specific sections to repeat the used acronyms and different developed samples.

4.1 Optimised Surface Modification of Ground Calcium Carbonate in a Polyamide 12 Compound

Different functional filler materials were produced (section 3.4.1) to investigate the beneficial impact of a precise surface modification on the mechanical properties of a PA12 compound.

***Table 4-1**. Functional filler data resulting after surface modification*

Filler Definition	Surface modifier	Additive amount/% by weight (w/w%)
R	Stearic acid	1.0 ± 0.1
A.1	Amino hexanoic acid	0.5 ± 0.1
A.2	Amino hexanoic acid	1.0 ± 0.1
A.3	Amino hexanoic acid	1.5 ± 0.1
A.4	Amino hexanoic acid	2.0 ± 0.1
B	ε-Caprolactam	1.0 ± 0.1
C	L-Arginine	1.0 ± 0.1
D	Glutamic acid	1.0 ± 0.1

A selection of amino-containing acids were chosen as the surface modification agent to improve the compatibility of the mineral filler material with the polar group in the polymer structure. The defined amino acids were chosen to determine a difference in the polymer interactional compatibility of end- versus side-chained amino groups.

4.1.1 Homogeneity of the Filler Distribution

The SEM pictures in **Figure 4-1** show the elemental contrast within the sample, where the filler materials reflect more electrons and appear brighter (white spots on the image) than the polymer matrix, which constitutes the black (electron-absorbing) background. The degree of the compounding homogeneity at the loading level of 10 w/w% filler can be seen across the different filler surface modifications with the different amino acids (A) amino hexanoic acid, (B) ε-caprolactam, (C) L-arginine and (D) glutamic acid.

The filler material is homogeneously distributed throughout the polymer matrix as exemplified in all four cases. The change of the surface modification agent showed no significant influence on filler particle–particle interaction, i.e. not worsening the agglomeration behaviour.

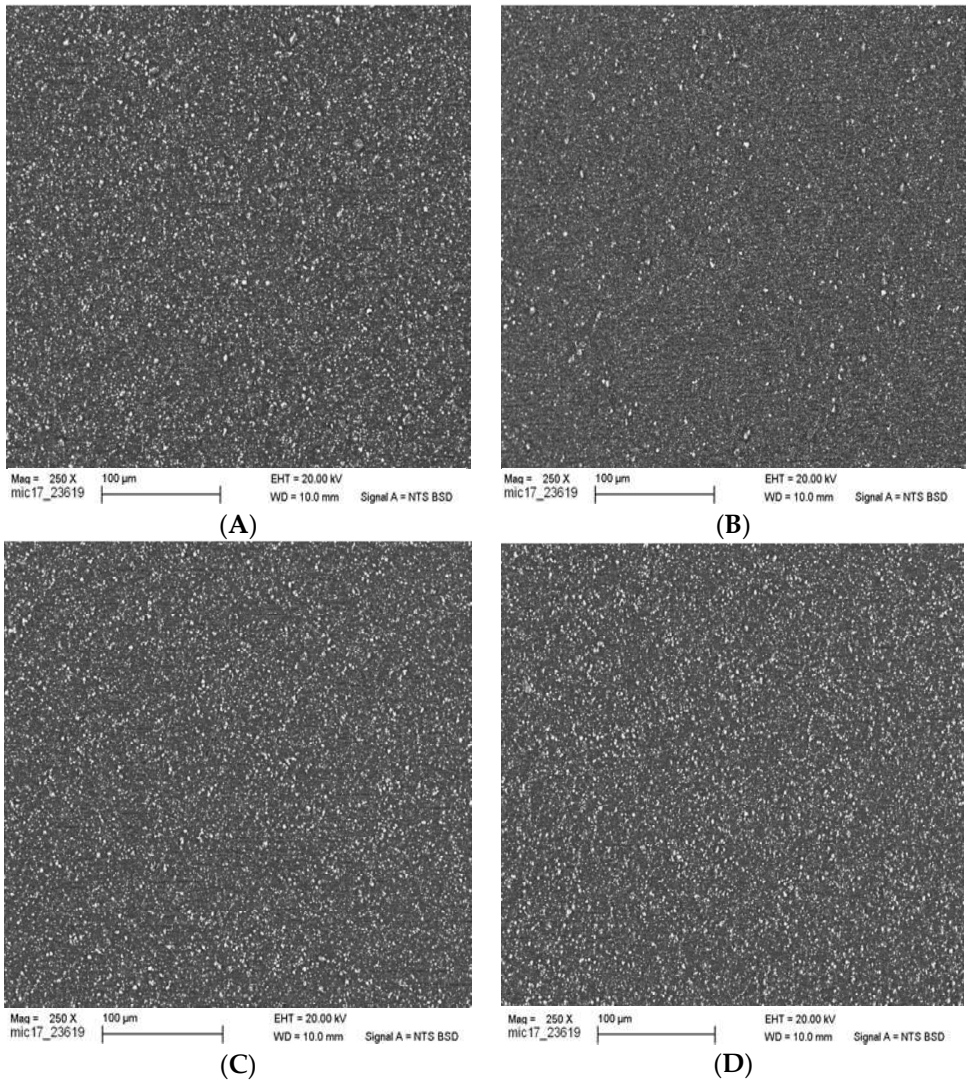

***Figure 4-1**. SEM images of morphology of PA-$CaCO_3$ composites: (A) 1 % amino hexanoic acid treated; (B) 1% ε-caprolactam treated; (C) L-arginine treated; (D) glutamic acid treated*

4.1.2 Influence on Stiffness / Tensile Modulus

As indicated by Y.W. Leong *et al*., the implementation of a solid filler in a polymer matrix results in an increase of the tensile modulus, due to increase in stiffness (rigidity) and the restriction of the mobility and deformability of the matrix [63].

The tensile modulus can be increased by approximately 30 % with the introduction of the ~ 40 m^2 filler/100 g PA12 (**Figure 4-2**). The tensile modulus is measured before any significant plastic deformation takes place, so is not influenced by the surface flow-related interaction between the filler and the polymer matrix [63]. Therefore, this increase in pre-flow stiffness

remains unaffected by the surface modification of the mineral filler with the different amino acids, as long as the filler amount is consistent.

The measured deviation between the 10 tested “dog bones” of each sample is quite high. This is a result of the experimental set up, used for these investigations. Due to the direct plate extrusion of the compound via a twin-screw extruder and a calender system, the outer layer of the plates shows a slight inhomogeneity. This effect can be seen in **Figure 4-3** and is the same throughout all produced samples. Since the punched out “dog bones” are quite thin and small, this effect and the resulting deviation in the modulus is significantly higher than it is on properties after plastic deformation takes place.

This increased deviation could be reduced by injection moulding larger and thicker tensile test pieces, instead of a direct plate extrusion process.

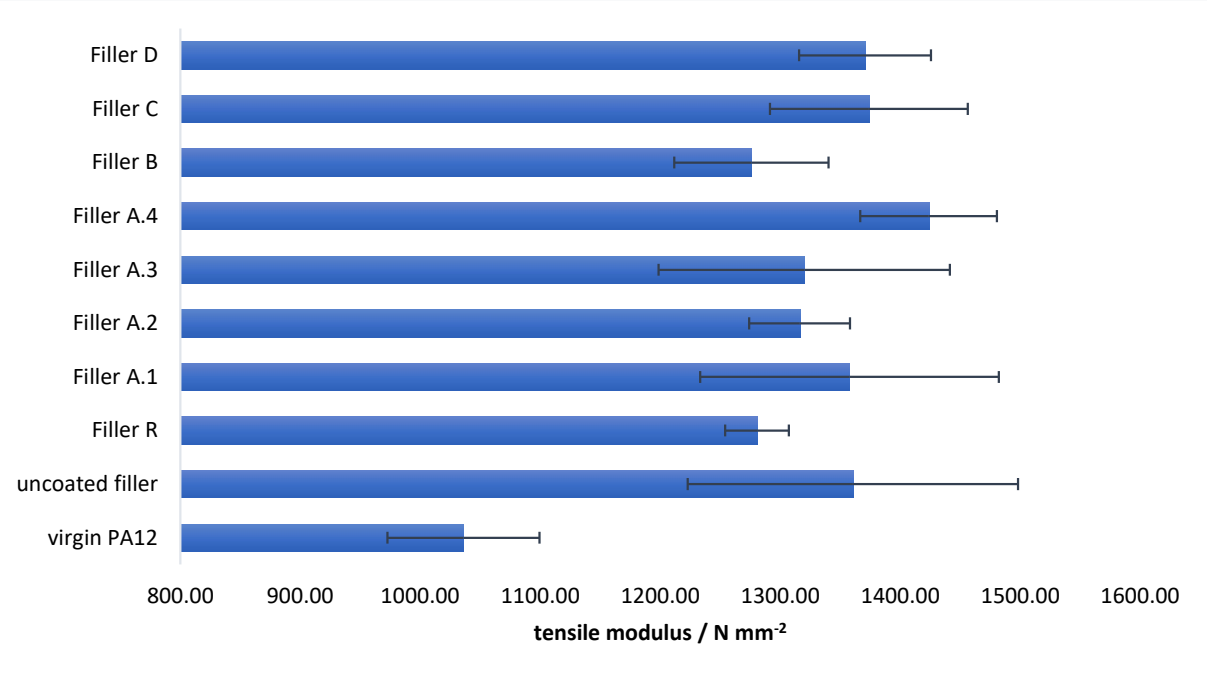

***Figure 4-2**. Effect of the amount of surface modifier on the tensile modulus of treated $CaCO_3$-filled PA12 composites; (R) stearic acid, (A) amino hexanoic acid (1: 0.5%; 2: 1.0%; 3: 1.5%; 4: 2.0%); (B) ε-caprolactam; (C) L-arginine; (D) glutamic acid*

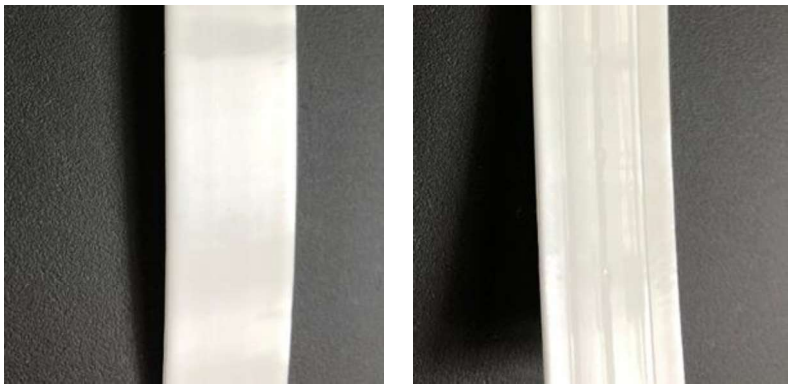

(A) (B)

***Figure 4-3**. Extruded plate with (A) smooth front side and (B) back side with slight inhomogeneity*

4.1.3 Influence on Ductility and Toughness

4.1.3.1 Effect of Surface Modifier Chemistry

The influence of the modifier chemistry on the mechanical properties was compared to prove that by the implementation of free amino groups, bound on the surface of the mineral filler material, hydrogen bonding can take place, hence improving the adhesion between the filler and the polymer matrix. **Figure 4-4** compares the increase in the elongation at break of an unsuited surface modifier, namely stearic acid, with the effect of the same amount of amino hexanoic acid. By optimizing the surface modification, hence increasing the intermolecular forces between the filler material and the polymer, the elongation at break can be improved from 440 % up to 530 %. This results in a regain of 50% of the lost ductility arising from originally implementing a solid mineral filler (Regain of EaB (%)). The use of stearic acid as a surface modifier nonetheless results in a regain of 20 % of the lost properties, due to the plasticising effect of stearic acid embedded into the polymer matrix, rather than a filler surface-polymer interface interaction [36].

$$Regain\ of\ EaB\ (\%) = \frac{EaB_{modified\ filler} - EaB_{not\ modified\ filler}}{EaB_{PA12} - EaB_{not\ modified\ filler}} x100 \qquad (4.1)$$

Figure 4-5 and **Figure 4-6** compare the different amino acid types. The surface modification with the same amount of amino hexanoic acid and ε-caprolactam showed similar behaviour with regards to elongation at break. The cyclic structure of caprolactam breaks open and the carboxylic acid group binds the same way on the calcium carbonate surface as amino hexanoic acid. Although L-arginine has more free nitrogen groups, which could increase the hydrogen bonding forces between filler and polymer matrix, the increased regain of elongation at break, in comparison with 6-Amino hexanoic acid, is negligible. This can be explained by comparing the influence of side-chained amino groups on the elongation at break. With a surface modification with glutamic acid, which only possesses a side-chained amino group, the regain of force at break drops below 20 %, as for L-arginine, which consists of an end-chained as well as side-chained amino groups, the regain is at 50 %. The same regain of force at break counts for a corresponding amount of 6-amino hexanoic acid, which only offers an end-chained amino group, indicating that the hydrogen bonding forces of side-chained amino groups are too weak to result in an increase of the ductility, if used as surface modifier for mineral fillers in a PA12 matrix.

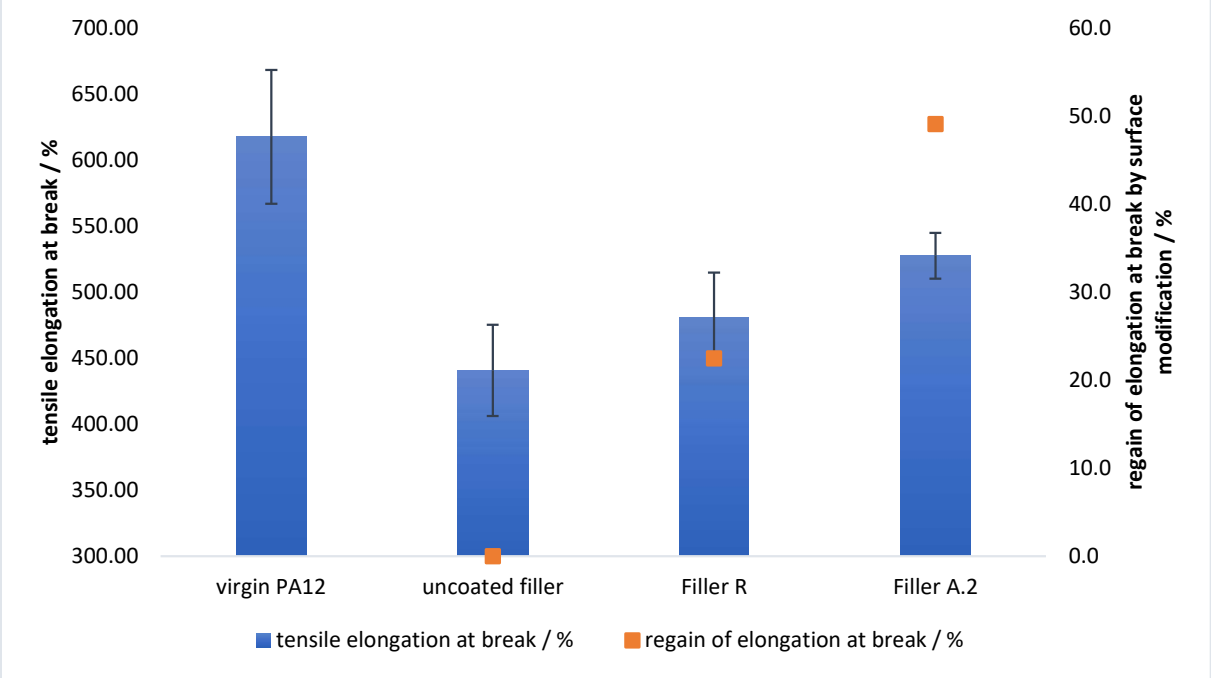

Figure 4-4. *Effect of the surface modifier chemistry on the elongation at break of (R) stearic acid and (A) amino hexanoic acid treated $CaCO_3$-filled PA12 composites*

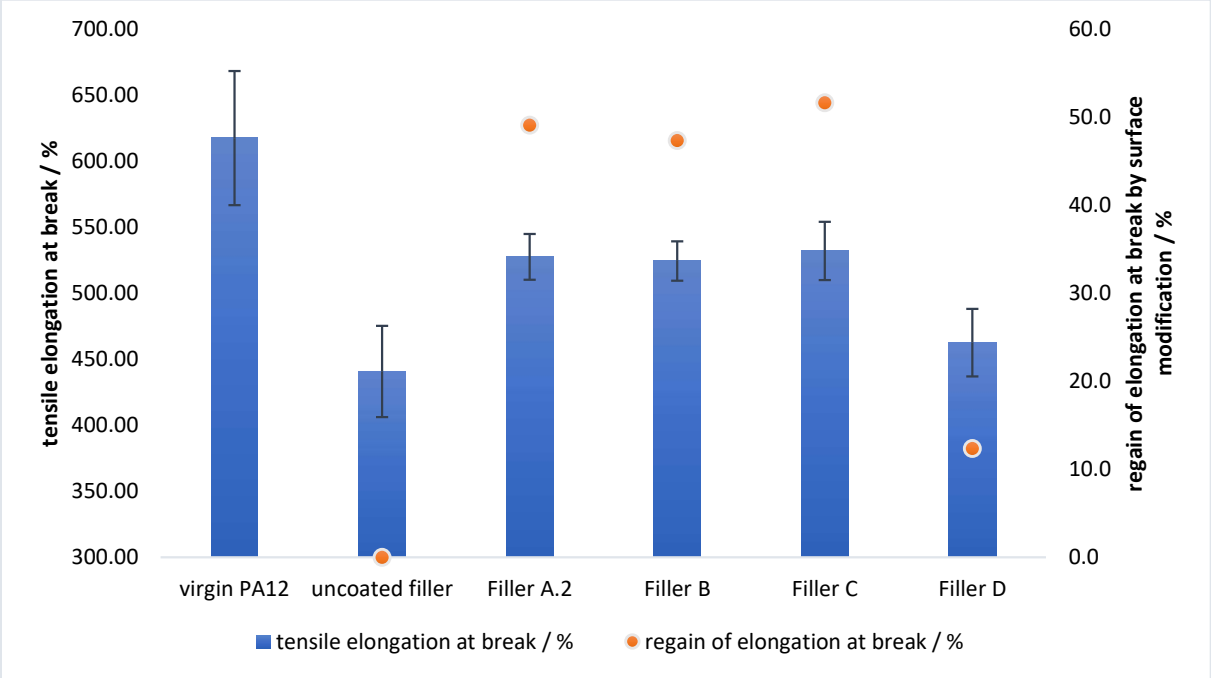

Figure 4-5. *Effect of the surface modifier chemistry on the elongation at break of (A) amino hexanoic acid; (B) ε-caprolactam; (C) L-arginine; (D) glutamic acid treated $CaCO_3$-filled PA12 composites*

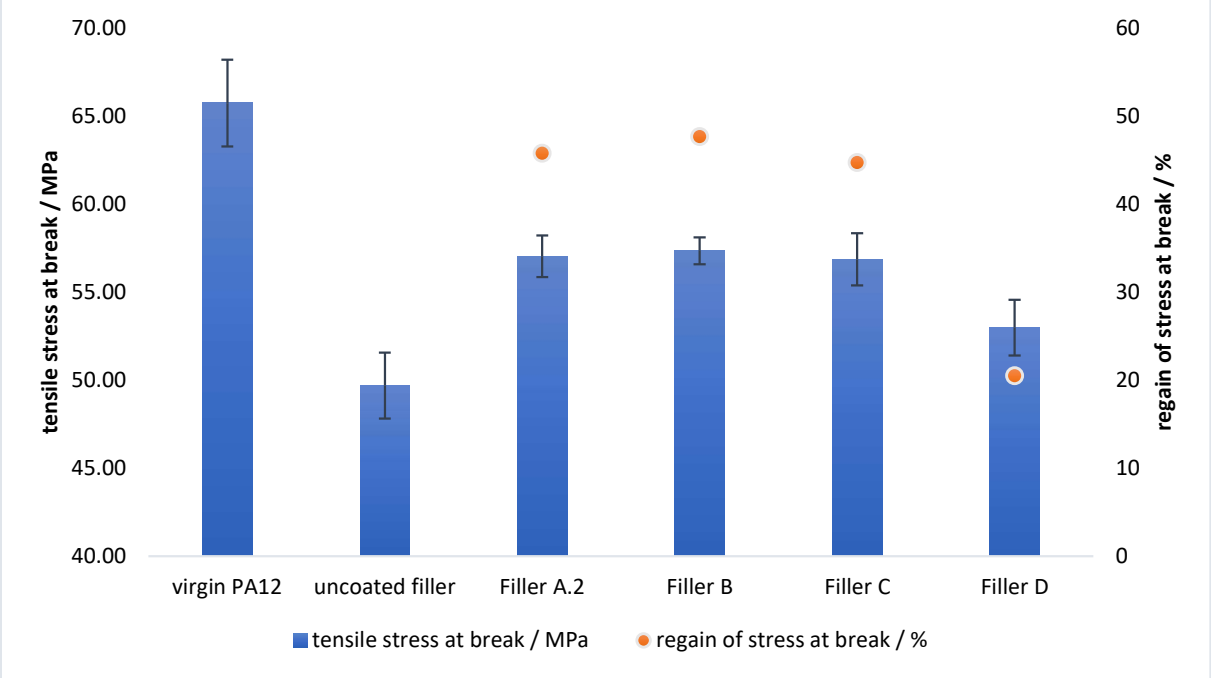

Figure 4-6. *Effect of the surface modifier chemistry on the tensile stress at break of (R) stearic acid, (A) amino hexanoic acid; (B) ε-caprolactam; (C) L-arginine; (D) glutamic acid treated $CaCO_3$-filled PA12 composites*

4.1.3.2 Effect of Amount of Surface Modifier

Determination of the ductility and toughness as a function of the amount of filler surface modifier indicates a clear dependency of the achievable regain of the reduced properties.

Figure 4-7 shows how the elongation at break is reduced by approx. 30 % by the implementation of the given amount of calcium carbonate as mineral filler. With increased treatment amount of 6-amino hexanoic acid, hence increased polar bonding groups on the filler surface, the ductility can be regained up to approx. 60 % of the filler-free value. The difference plateaus between 1.5 and 2.0 w/w% of surface modifier on the mineral filler, suggesting that the optimum amount of 6-amino hexanoic acid as the surface modifier is between 1.0 and 1.5 w/w%.

A similar effect can be seen in **Figure 4-8** with respect to the tensile force at break. With up to 1.5 w/w% of amino hexanoic acid as filler surface modifier, the loss in tensile toughness can be regained up to approximately 60 % in comparison with using an uncoated filler.

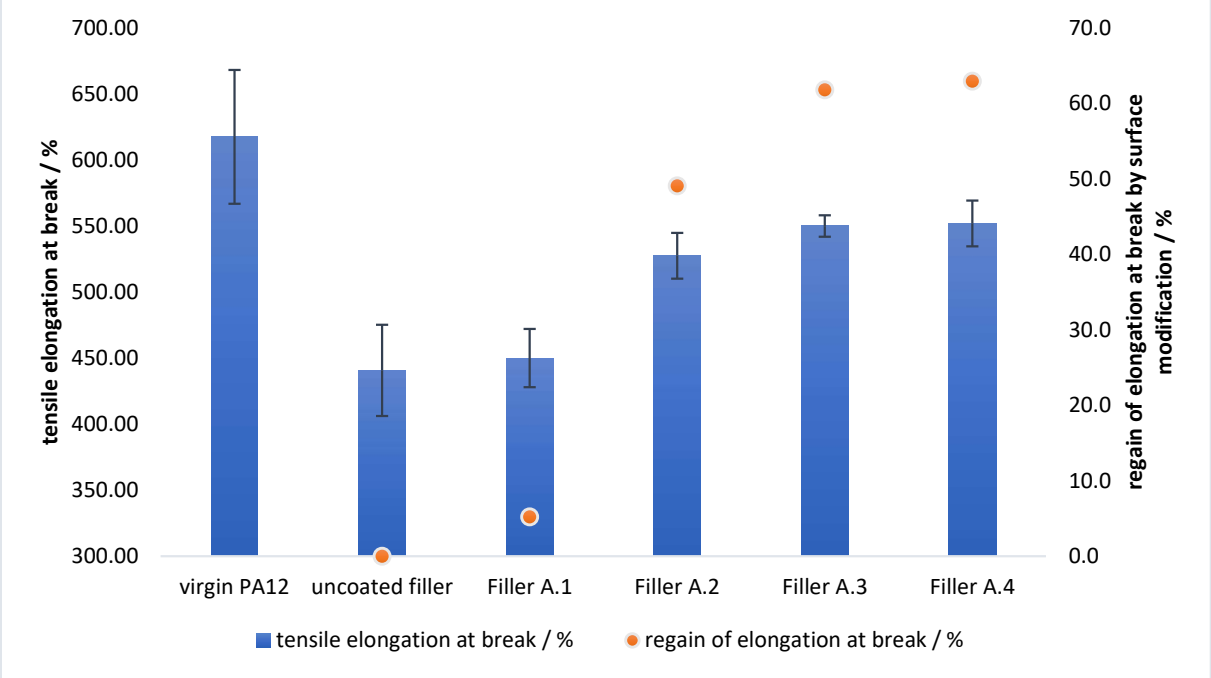

Figure 4-7. *Effect of the amount of surface modifier on the tensile elongation at the break of amino hexanoic acid-treated $CaCO_3$-filled PA12 composites*

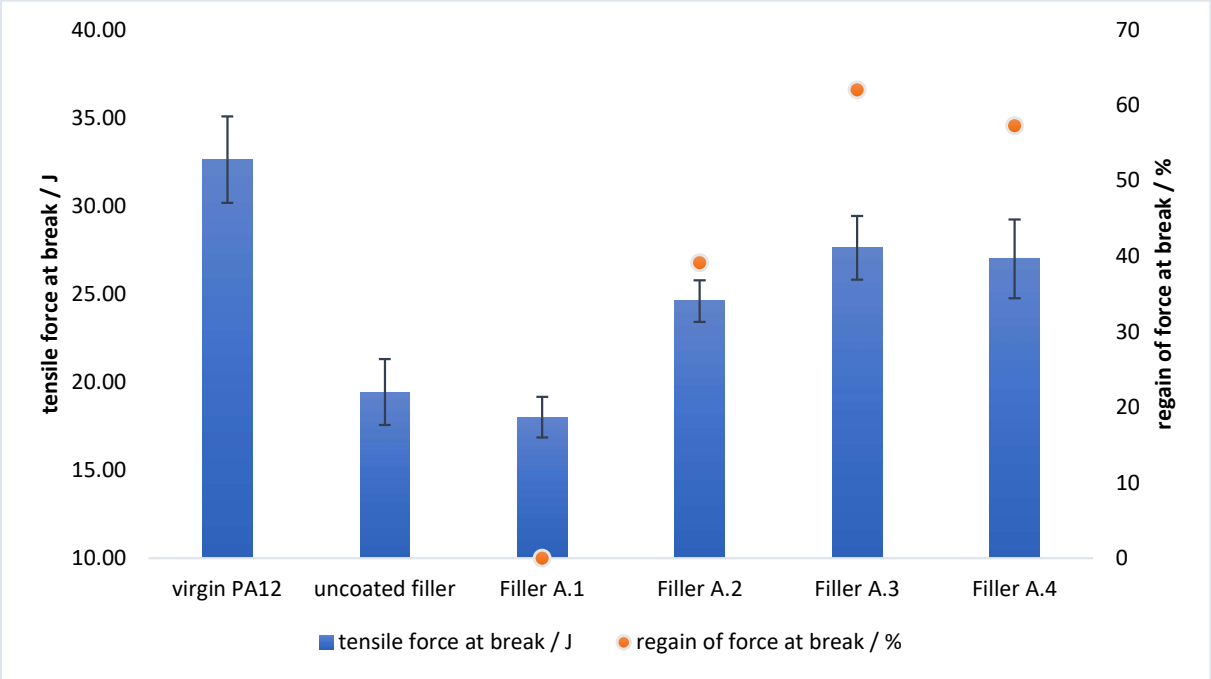

Figure 4-8. *Effect of the amount of surface modifier on the tensile force at break of amino hexanoic acid treated $CaCO_3$-filled PA12 composites*

The ductility as well as tensile strength showed a clear improvement if the filler is surface modified with an appropriate amino acid instead of stearic acid. The greatest improvements were obtained with amino acids, which consist of free amino groups at the end of the carboxylic

chain, instead of only as side chains. To have an optimised filler/coated adhesion promoter ratio, between 1.0 and 1.5 w/w% of surface modifier with respect to calcium carbonate is needed. With the tested filler grade, this results in an approx. optimum of 2.5 to 3.0 mmol of treatment agent per 100 m^2 $CaCO_3$.

Up to 60 % of the loss of ductility of a PA12 matrix, following from the introduction of a non-flexible mineral filler, can potentially be regained with appropriate surface modification of the filler.

4.2 Particle Size Adjustment of Ground Calcium Carbonate

Various GCC-based mineral fillers having different particle size distributions were developed as defined in Section 3.4.2. These were used to determine the effect that the mineral filler surface, within the PA12 matrix, has on the thermal properties of the resulting compound.

***Table 4-2**. Mineral filler data after drying step*

Filler nomenclature	**Filler type**	**d_{v10} / µm**	**d_{v50} / µm**	**d_{v90} / µm**	**SSA / m^2g^{-1}**
vc-G	very coarse sized GCC	1 ± 0.5	10 ± 1.5	35 ± 5.0	1 ± 0.3
c-G	coarse sized GCC	1 ± 0.5	5 ± 1.5	17 ± 2.0	2 ± 0.2
m-G	medium sized GCC	1 ± 0.5	2 ± 0.5	5 ± 0.5	4 ± 0.5
vs-G	very small sized GCC		1 ± 0.1		16 ± 1.0
us-G	Ultra-small sized GCC		0.2 ± 0.05		50 ± 3.0

4.2.1 Melt Flow Viscosity through MFI

The melt flow viscosity showed a clear dependency on the filler particle size as well as the processing-induced surface in the compound matrix. To express this effect of particle size, independently of surface area, an analysis was made loading to a level that provided equal surface area within the matrix across the various filler samples. The coarse filler particles show a greater influence on the resulting melt viscosity at 190 °C than the addition of the equivalent surface amount of fine calcium carbonate particles (**Figure 4-9**).

A rapid and homogeneous melt distribution during the laser sintering process is key to efficient and reliable structure forming [62, 64], plus sufficient flow and molecular diffusion to intersperse the newly applied layer with the previous one during AM. A large increase in the melt viscosity arising from the addition of filler would be detrimental. It was found that the use of fine filler particles in the polymer matrix can increase the filler material surface-polymer interface by up to 100 m^2 per 100 g PA12 without influencing the melt viscosity. Using finer filler particles with a smaller single-particle volume than that of coarser filler particles results in a better melt flowability, and hence has less influence on the melt viscosity in comparison with the implementation of coarser calcium carbonate particles.

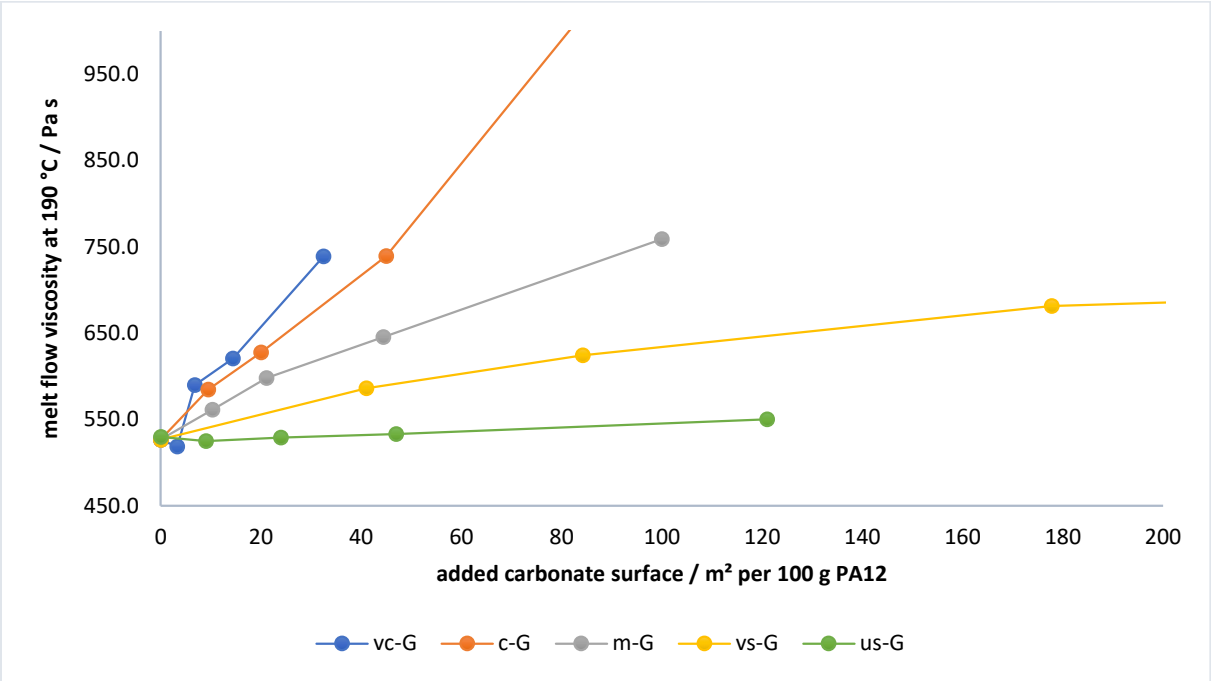

Figure 4-9. *Melt flow viscosity at 190 °C, 2.16 kgf against added filler surface in correlation with the different mineral fillers used; intersection point at 450 Pa*s, closer to the melt flow viscosity of the reference*

4.2.2 Viscoelastic Behaviour through TMA

The melting speed was determined by thermal mechanical analysis. A lower Tism-value indicates a quicker melting process. The influence on the melting inflection slope shows a clear filler particle size dependency, as well as filler surface area dependency. **Figure 4-10** shows how the melting speed can be increased with the implementation of a low amount of larger filler particles in the polymer matrix. With a reduction of the filler particle size, the influence on the melting speed is reduced.

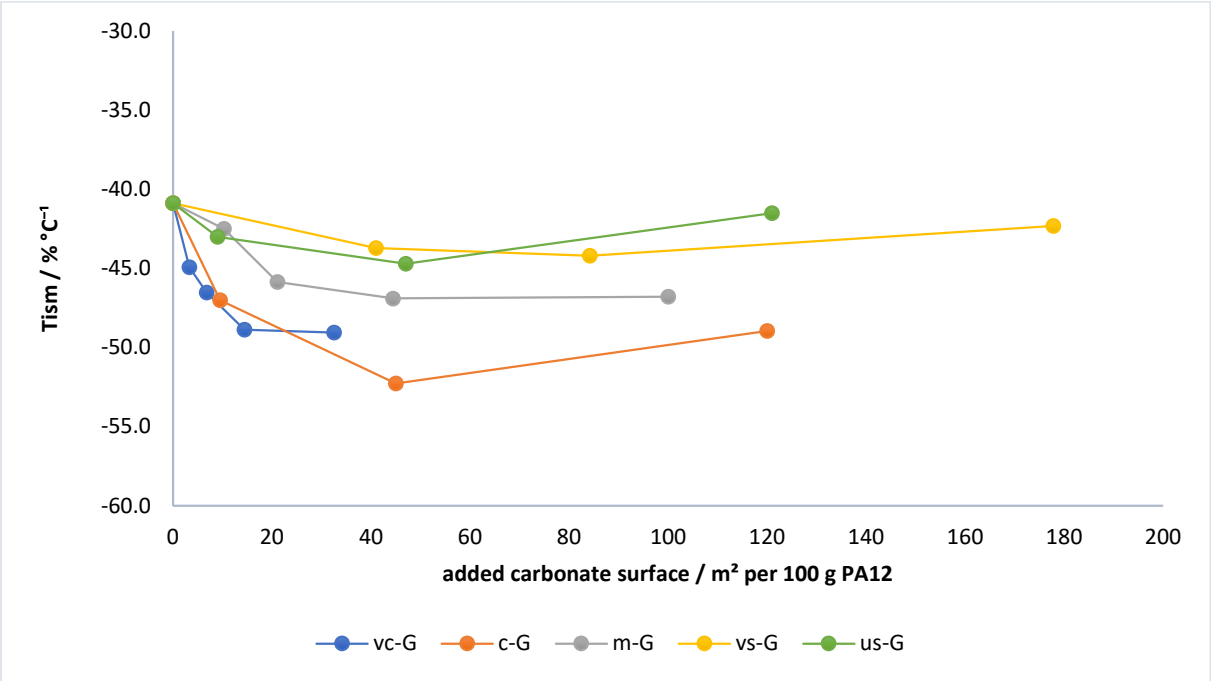

Figure 4-10. *Melting inflection slope against added filler surface in correlation with the different used mineral fillers; intersection point at -60 %*°C^{-1}, closer to the melt behaviour of the reference*

4.2.3 Temperature-related Material Transition through DSC

A similar effect can be seen in the DSC determination of the melting point as well as the broadening of the melting transition region. The melting point can be lowered with a low amount of coarser filler particles, and the transition narrowed significantly, compared with the implementation of finer filler particles. **Figure 4-11** shows this influence of the particle size as well as filler surface area in the polymer matrix on the melting point and **Figure 4-12** the additional melting transition breadth behaviour, given by the peak width of the total time over which the transition occurs. Both figures show an optimum point for the introduction of very coarse and coarse particles and a slight increase in the melting behaviour afterwards. This phenomenon is explained through the significant increase of filler volume with a higher amount of coarser particles, which, through their increased contribution to heat conductivity, take up and store energy from the surrounding, without giving enough time for re-distribution within the timescale used in the testing method. At a reduced temperature rate of 1 °C min^{-1}, instead of 10 °C min^{-1}, re-increase no longer occurs.

Finer particles lead to less disturbance of the overall thermal response properties of the polymer, whereas the inclusion of larger particles increases the melt rate and sharpens the transition response, but in doing so raises the melt viscosity. These thermal effects result from the higher thermal conductivity and lower specific heat of calcium carbonate versus PA12. Less thermal energy is stored and released more rapidly to the surrounding polymer by the filler particles than the PA12 particles. More thermal energy can be transmitted in comparison with a multitude of single fine filler particles due to a higher single-particle volume of the coarser calcium carbonate particles. This results in a greater influence on the melting behaviour of the compound with the input of a few coarse instead of many fine calcium carbonate filler particles.

With an increased melting speed and a reduction of the melting point as well as melting transition breadth, the polymer melt can be distributed quicker in the current layer, resulting in an increased final part density as well as a possible increase in printing speed [64].

Figure 4-13 reveals the influence of the filler particles on the crystallisation point of the polymer compound, detected during cooling in DSC. The influence on the crystallisation point shows a dependency on added filler surface down to a filler volume median particle size d_{v50} of 1 µm. With an increased filler surface area in the polymer matrix, independent of the volume median particle size, the crystallisation point of the compound can be raised significantly. With the use of sub-micrometre calcium carbonate particles, the influence on the crystallisation point can be increased above that of the effect with coarser filler particles. This can be attributed to the increased filler particle number in the compound at a given mass loading following the inclusion of sub-micrometre/ultrafine calcium carbonate particles in the polymer matrix. The amount of nucleation points for a crystallisation to occur during the temperature reduction is greater and more homogeneously distributed due to the reduced single-particle volume of fine filler particles, resulting in a larger impact on the crystallisation point.

A more detailed analysis of the crystallisation kinetics through the determination of the crystallisation time at a certain temperature, shows a clear dependence on the added filler surface area. The crystallisation time on cooling to 170 °C can be manipulated with a given amount of calcium carbonate particles in the PA12 matrix, independent of the volume median particle size of the filler (**Figure 4-14**). This supports the hypothesis that the crystallisation point is dependent on particle number, i.e. nucleation points.

By only cooling to 172 °C, a more precise investigation was made regarding crystallisation time. A small amount of coarser filler particles has a greater influence on the crystallisation time than the equivalent surface area comprising finer particles. A limited amount of < 20 m^2 surface area per 100 g PA12 consisting of coarse filler particles, having a volume-based median particle size d_{v50} > 5 µm, produces a larger reduction of the crystallisation time than the equivalent surface area consisting of finer calcium carbonate particles (**Figure 4-15**). In the isothermal state of the measurement, the higher single-particle-volume of the coarser filler particles results in thermal energy being taken out of the polymer matrix at a faster rate than with the same number of associated finer particles. Through this effect, the surrounding polyamide matrix can be cooled down more effectively and, therefore, results in a shorter crystallisation time, even though the amount of nucleation points is reduced with the smaller number of coarser filler particles. Thus, similarly to the melt-comparison, the implementation of finer particles leads to a change in crystallisation point, but the use of larger particles reduces the time over which that crystallisation occurs.

The speed of the laser sintering additive cycle during part formation is limited by the crystallisation time of each layer before the next powder layer can be spread on the previous one. Several different authors have described the influence on the final part density arising from the precise relationship between powder bed temperature, energy density and time between layers [65-70]. If the powder bed temperature is reduced too much and hence the laser energy input is increased, the risk increases of curling and shrinking due to a high temperature shock and a rapid cooling rate. If the powder bed temperature is set too high, the printing time for each layer will increase and/or the separate layers won't crystallize properly resulting in a printing failure. With a controlled reduction of the crystallisation time for the

printing compound, the laser energy input as well as the printing time can be reduced. The well-known property advantages, with respect to material stiffness and controlled impact resistance, on adding calcium carbonate in a polymer matrix can be expected to provide additional resistance to the shrinking and curling behaviour [71]. In addition, parts displaying enhanced brightness and opacity can be constructed.

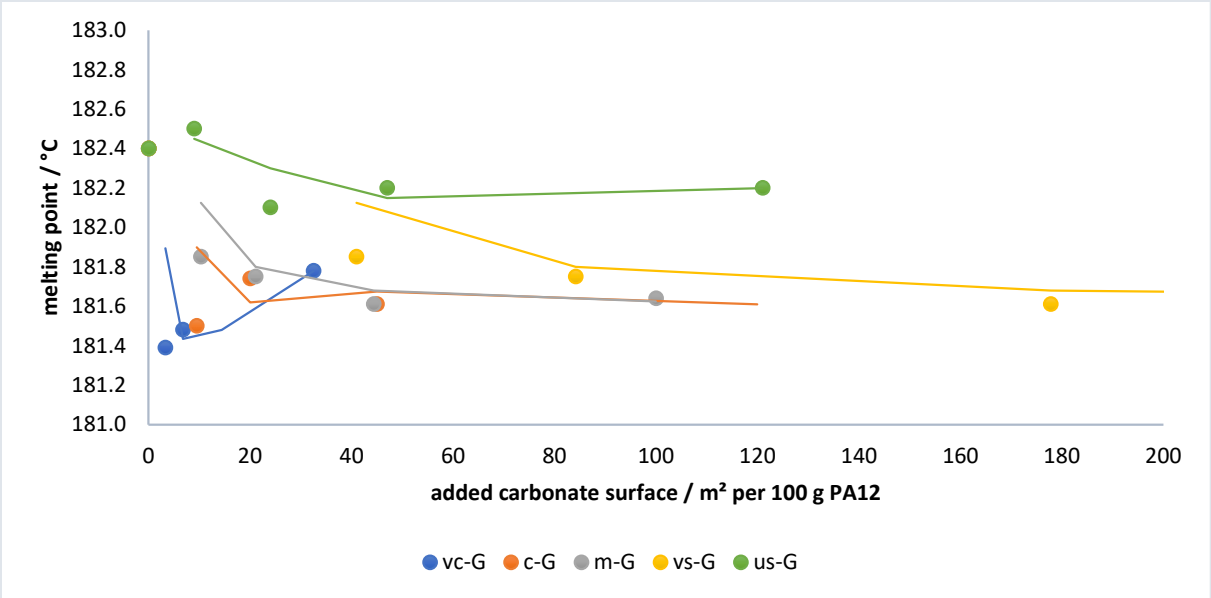

Figure 4-11. *Melting point against added filler surface in correlation with the different mineral fillers used; intersection point at 181°C, closer to the melting point of the reference*

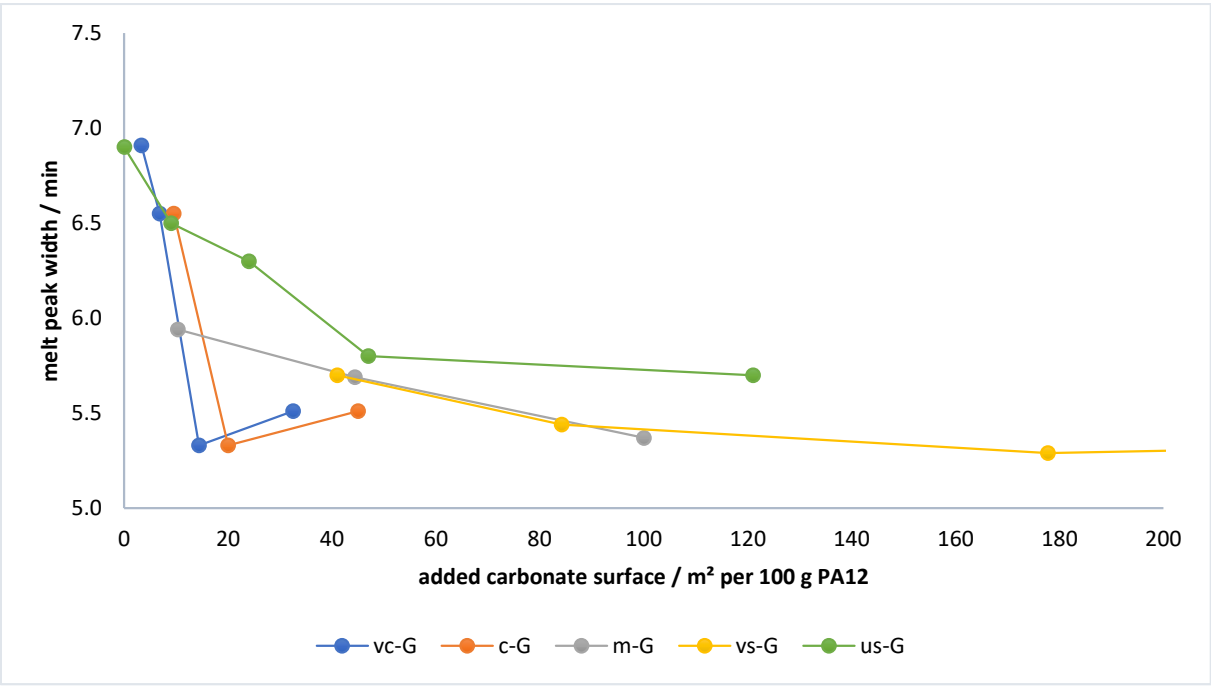

Figure 4-12. *Melting peak width as a function of added filler surface in correlation with the different mineral fillers used; intersection point at 5.0 min, closer to the melt peak width of the reference*

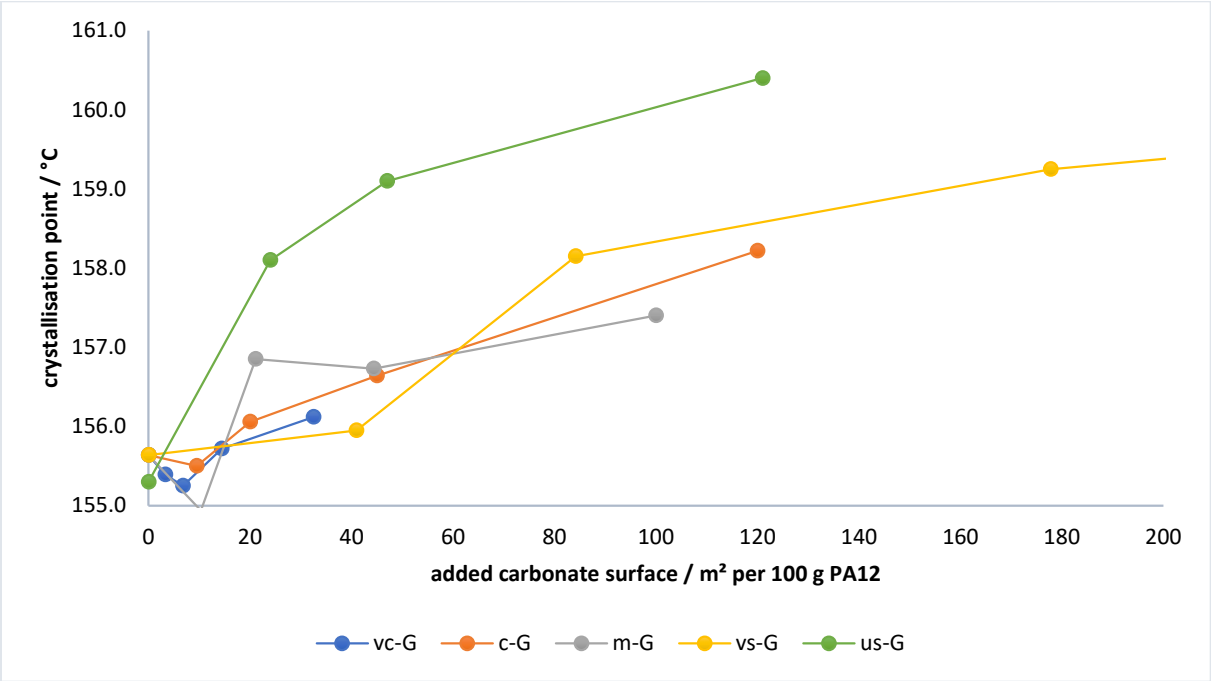

Figure 4-13. *Crystallisation point as a function of added filler surface in correlation with the different mineral fillers used; intersection point at 155°C, closer to the crystallisation point of the reference*

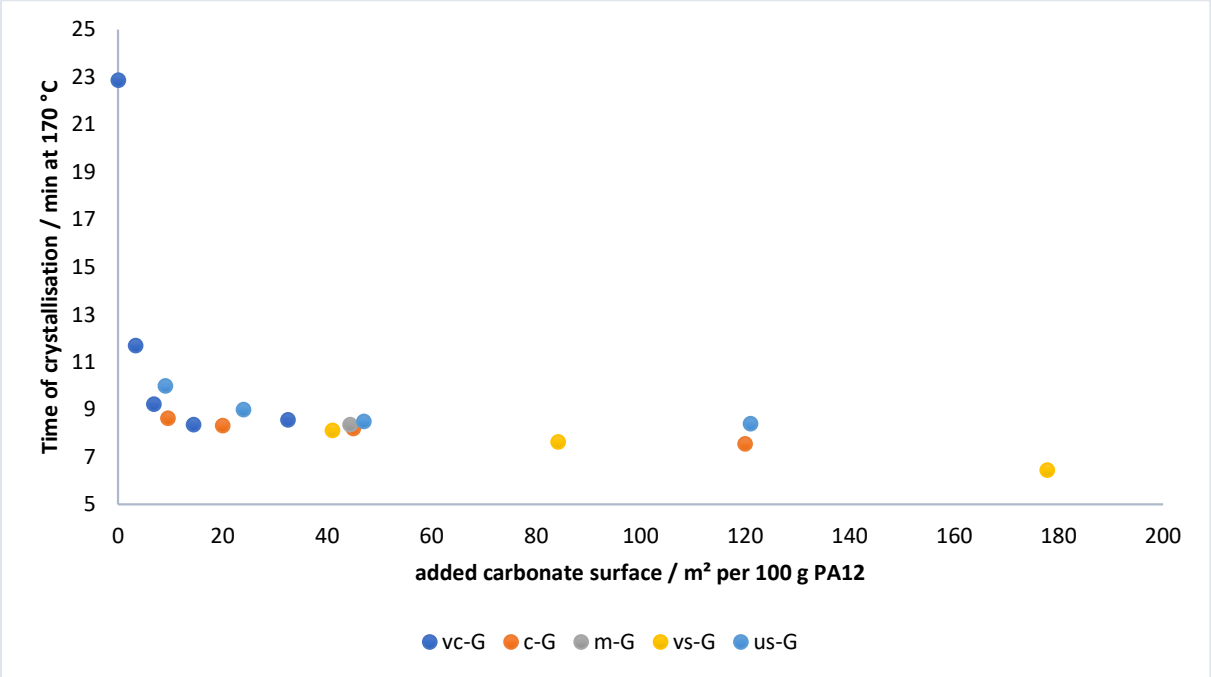

Figure 4-14. *Crystallisation time at 170 °C against added filler surface in correlation with the different mineral fillers used; intersection point at 5 min, closer to the lowest crystallisation time of all samples*

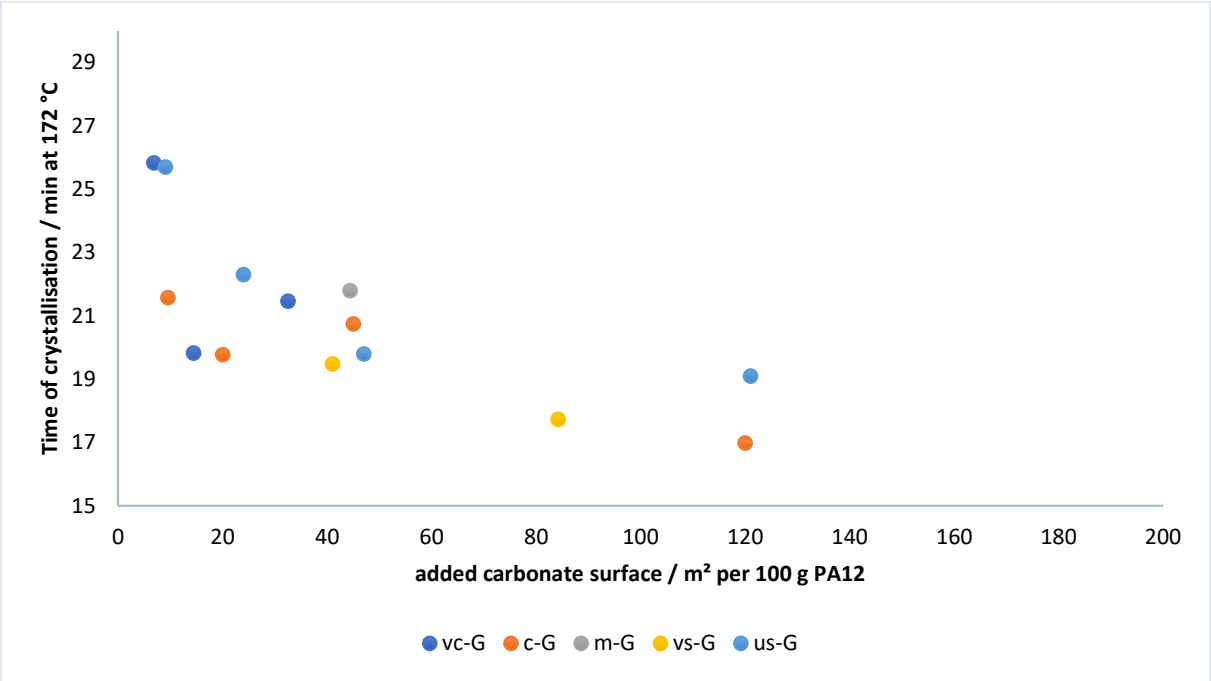

Figure 4-15. *Crystallisation time at 172 °C against added filler surface in correlation with the different mineral fillers used; intersection point at 15 min, closer to the lowest crystallisation time of all samples*

4.3 Optimised Particle Size Ratio – Impact of Bimodal Particle Size Distribution Ratio of Ground Calcium Carbonate

In the previous section, it was shown that the melting, as well as crystallisation behaviour of PA12, could be manipulated by adjusting the particle size distribution of calcium carbonate as a functional filler. The melt properties of this compound show a significant dependency on the filler volume-based particle size. As the calcium carbonate particles in the polymer matrix become finer and narrower, the filler has less influence on the melting properties, influencing the melt flow less significantly than the same surface amount of broad size distribution coarse calcium carbonate filler particles. However, the crystallisation behaviour on cooling showed a markedly more rapid onset in the case of fine sub-micrometre filler particle size due to increased nucleation. To further control and optimise the thermal response properties of a filling compound for improved properties in additive manufacturing processing through selective laser sintering, the possibility to combine precisely defined particle size distributions has been studied, thereby combining the benefits of each particle size range within the chosen material size distribution contributes to the matrix. The thermal response of the developed samples, as defined in section 3.4.3, was determined.

Table 4-3. *Filler particle data after drying step*

Filler nomenclature	**Filler type**	**d_{v10} / µm**	**d_{v50} / µm**	**d_{v90} / µm**	**SSA / m^2g^{-1}**
c-G	coarse sized GCC	1 ± 0.5	5 ± 1.5	17 ± 2.0	2 ± 0.2
es-G	extra small sized GCC	0.2 ± 0.05	0.5 ± 0.1	1 ± 0.2	23 ± 2.0

***Table 4-4**. Tested filler loadings and introduced surface area of filler per 100 g PA12*

Compound nomenclature	Filler used	Filler amount /w/w%	Total carbonate surface per 100 g Polyamide 12 /m²	c-G surface per 100 g PA12 /m²	es-G surface per 100 g PA12 /m²
c-G_5	c-G	5	10	10	0
es-G_5	es-G	5	120	0	120
50/50_c/es-G_10	50/50_c/es-G	10	141	11	130
70/30_c/es-G_10	70/30_c/es-G	10	95	15	80
30/70_c/es-G_10	30/70_c/es-G	10	187	6	181
33/66_c/es-G_15	33/66_c/es-G	15	286	11	275

4.3.1 Degradation temperature through TGA

The degradation temperature of the compound can be increased by adjusting the mineral filler (**Figure 4-16**). The overall degradation temperature can be increased up to 6 % with the correct amount of coarse particles, with a higher single-particle volume, and fine filler particles. If the coarse filler fraction is reduced or the fine filler fraction increased significantly, the effect on the degradation temperature is reduced. This increase in the degradation temperature can be explained by the higher thermal conductivity of calcium carbonate. The surrounding energy input is taken up quicker by the filler particles, but less is stored due to their lower thermal capacity than the PA12.

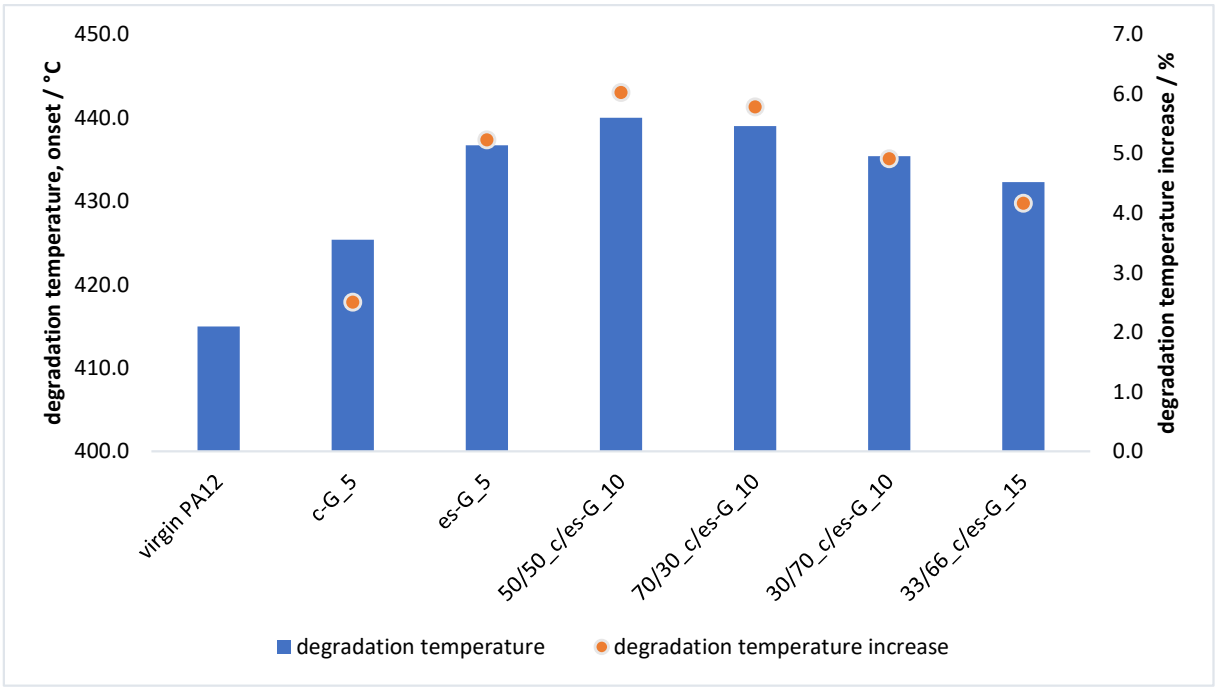

***Figure 4-16.** Degradation temperature in comparison with the tested GCC blends*

4.3.2 Melt Flow Viscosity through MFI

The previous section presented how the increase in the melt flow, due to the introduction of a solid mineral filler, shows a significant dependency on the filler particle size as well as the processing-induced filler surface in the compound matrix. The melt flow increased more

significantly if only 10 m^2 of coarse mineral filler is included in 100 g of PA12 instead of finer mineral filler (**Figure 4-17**). Blending the same amount of coarse filler material with a finer fraction showed no significant increase in the melt flow. Therefore, the overall increase can be reduced by approx. 50 %. Filler '33/66_c/es-G' shows how the melt flow increases up to 20 % if the fine mineral filler fraction exceeds the optimum range. This effect was shown by using finer filler particles with a smaller single-particle volume than that of coarser filler particles. This results in a better melt flow in comparison with the implementation of only coarser calcium carbonate particles. This can result in a comparable better melt flow during a selective laser sintering print, hence higher final part density.

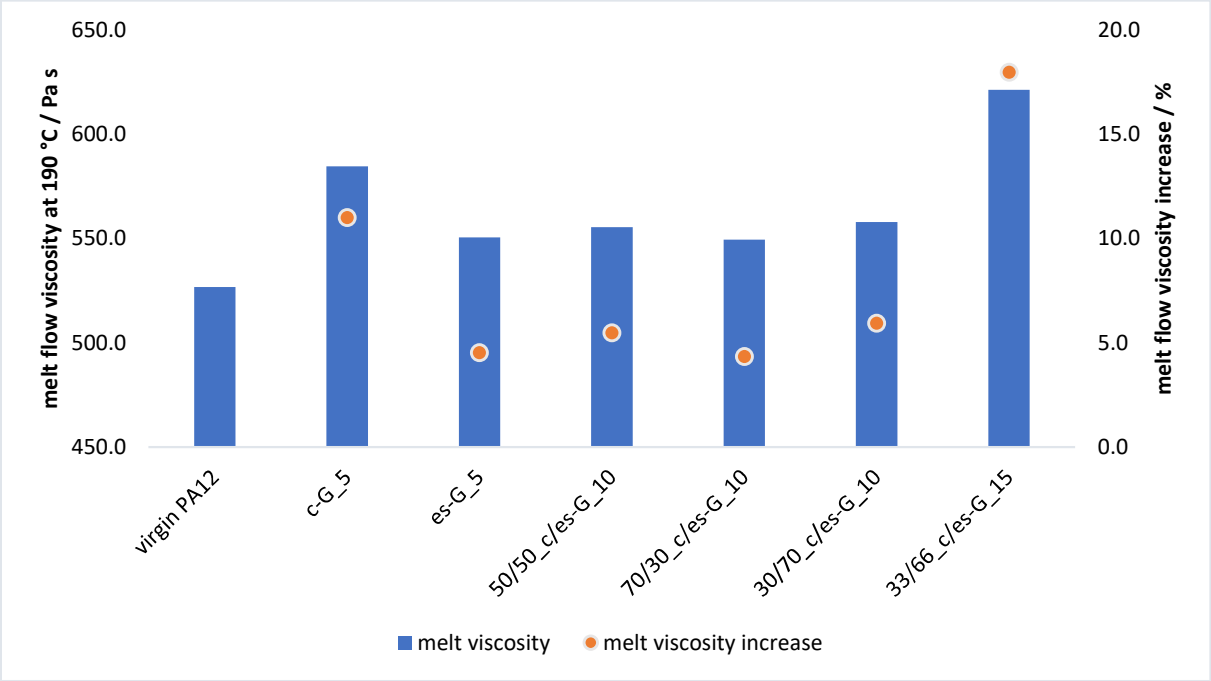

Figure 4-17. *Melt flow viscosity at 190 °C, 2.16 kgf in comparison of the tested GCC blends*

4.3.3 Temperature-related Material Transition Observed through DSC

The melting point can be manipulated with the introduction of a precise amount of coarse mineral filler into the polymer matrix (**Figure 4-18**). A significant possible melt-point reduction of approx. 1 °C with the implementation of 10 m^2 of coarse mineral filler (c-G_5) can also be achieved with fillers '50/50_c/es-G', '70/30_c/es-G', as well as '33/66_c/es-G'. All three filler combinations introduced approx. 10 m^2 of coarse filler material, where the finer filler fraction varied and did not show any significant effect on the melt point manipulation. Referring to the particle size distribution of the coarse fraction in **Figure 3-14**, the sensitivity of melting point to the use of a small amount of coarse filler 'c-G' in the blend relates to particles significantly larger than the volume median size, d_{v50}, which control the thermal properties more strongly. Filler '30/70_c/es-G' showed how the melting point is not affected if the coarser mineral filler fraction is reduced below the optimum range of 10 m^2 per 100 g polymer matrix. The same effect can be seen in **Figure 4-19**, which shows the melting transition width behaviour, given by the peak width of the total time over which the melt transition occurs. The melt peak width can be reduced by up to 25 % if the compound is filled with 10 m^2 of coarse filler material within 100 g of PA12. Filler '30/70_c/es-G' and '33/66_c/es-G' showed how an extensive amount of

the fine filler fraction masks the benefits of the coarser fractions. Considering the difference in the thermal properties between the functional filler and the polymer matrix (higher thermal conductivity and lower specific heat of calcium carbonate), the energy is taken up quickly by the filler material and released more rapidly to the PA12, surrounding the filler particle. More thermal energy can be transmitted due to the greater single-particle volume of the coarser calcium carbonate particles, in comparison with a multitude of single fine filler particles. This results in a greater influence on the melting behaviour of the compound with the inclusion of a few coarse instead of many fine calcium carbonate filler particles. The extensive number of fine filler particles take up all the energy and therefore hinder the more ready distribution of the stored energy by the coarser fraction. This results in the loss of the melt energy efficiency given by the coarse calcium carbonate filler particles.

Figure 4-20 reveals how the increase of the crystallisation point can be achieved if an optimised amount of fine calcium carbonate filler particles is present in the blend. Filler ‘c-G’ shows that the purely coarse fraction, implemented into the polymer matrix, does not influence the crystallisation point. It is the greater single-particle number and homogeneous distribution of fine filler particles, when present within the polymer matrix, that promotes more frequent points of nucleation for crystallisation to occur during the temperature reduction phase, resulting in a larger and more rapid onset at the point of crystallisation.

Figure 4-21 reflects the results in the previous section. With the addition of an increased surface area of calcium carbonate filler material within the polymer matrix, the crystallisation kinetics exhibit a filler surface area dependency. Even a low, coarse filler loading, as with the low addition level of Filler ‘c-G’, the crystallisation time at a constant 170 °C can be reduced by approx. 60 %. This manipulation of faster crystallisation rate remains supported even when large numbers of fine filler particles are added. These findings support the hypothesis that the crystallisation point is dependent on particle number, i.e. available nucleation points.

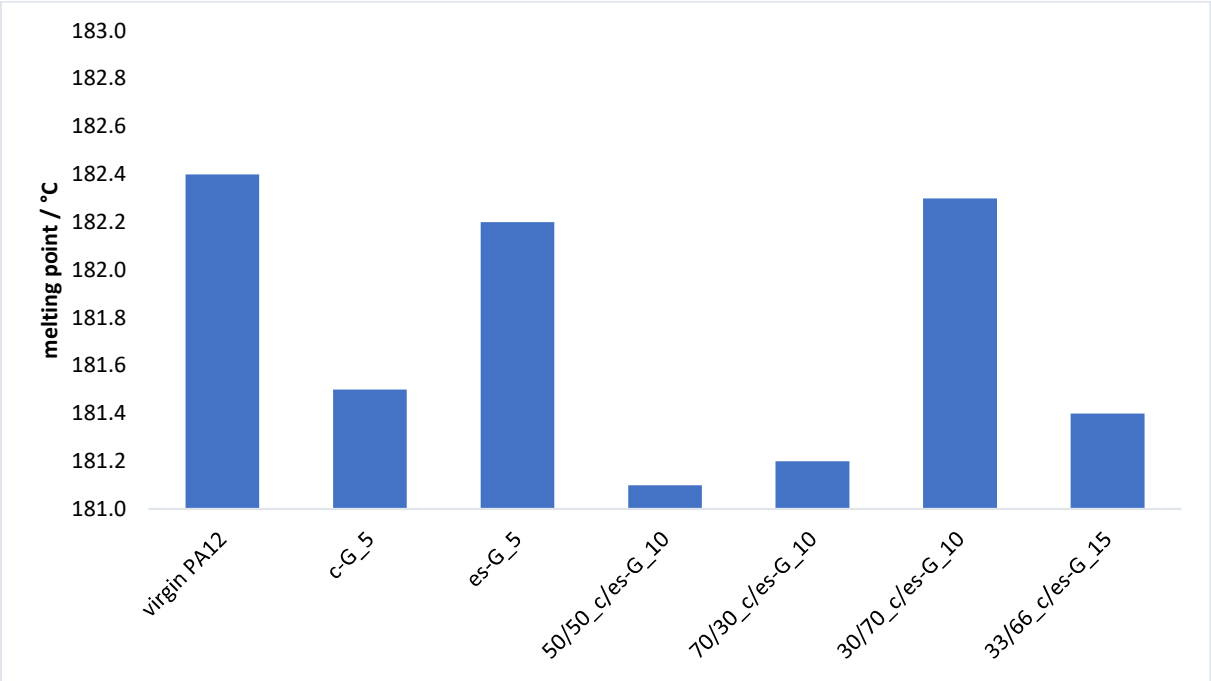

Figure 4-18. *Influence of the tested functional filler blends on the melting point at 5 °C min^{-1}*

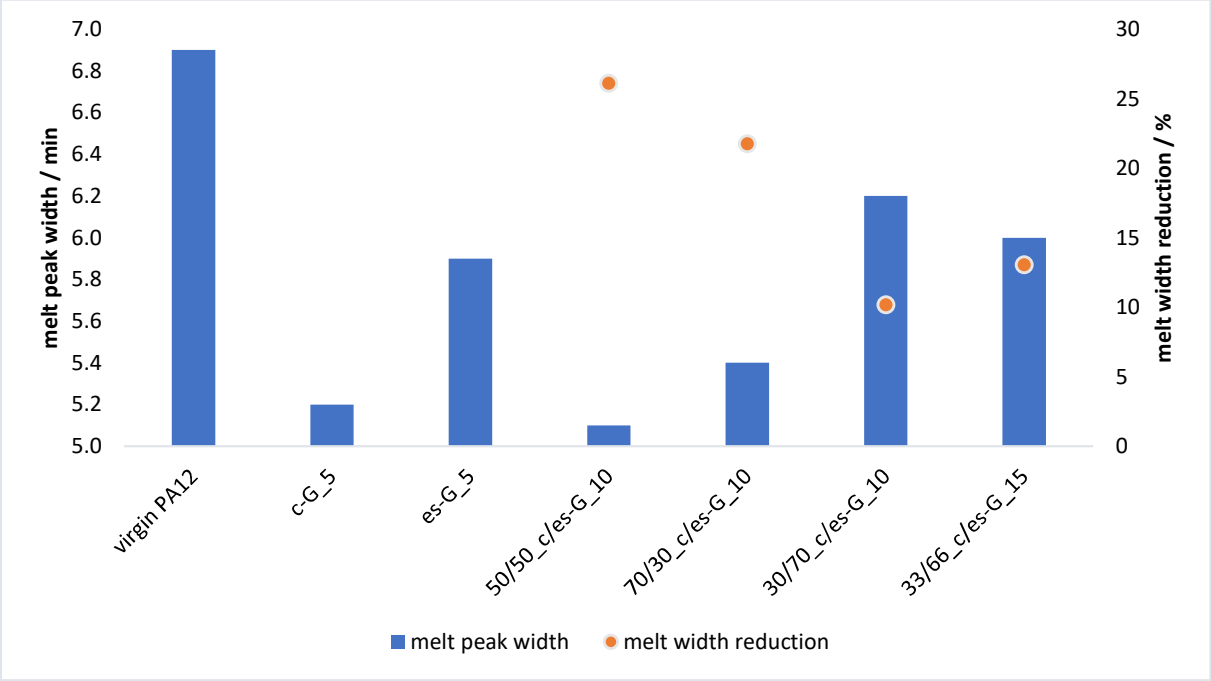

Figure 4-19. *Influence of the tested functional filler blends on the melt peak width at 5 °C min^{-1}*

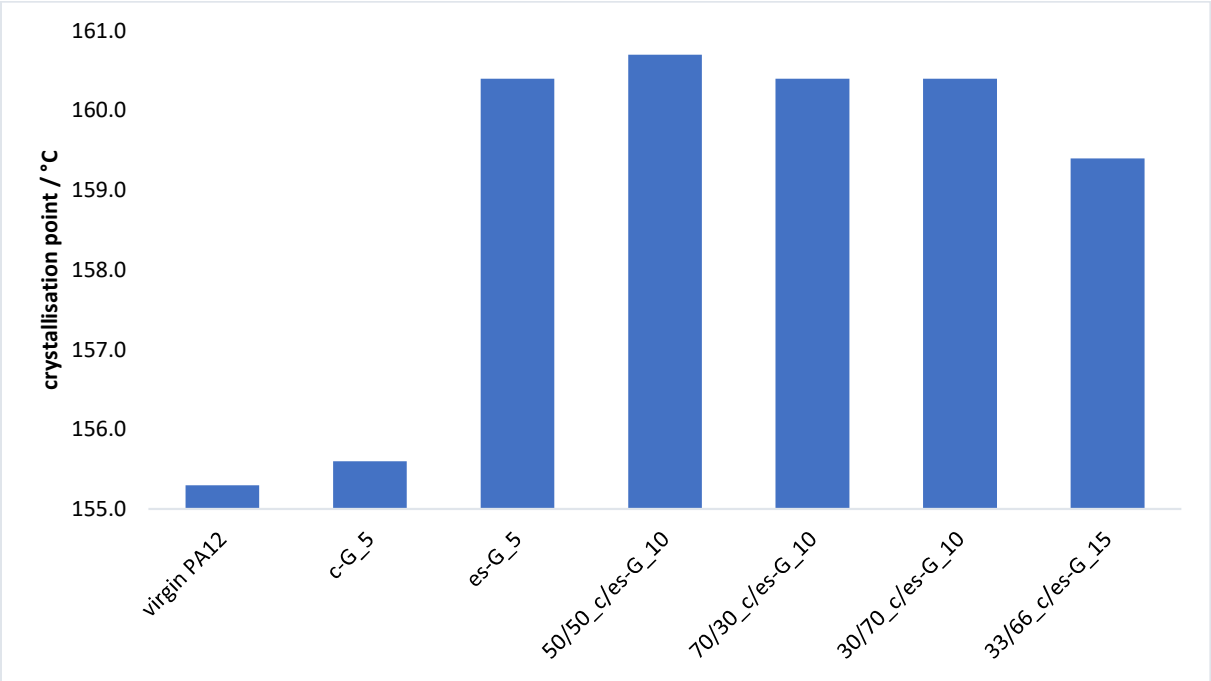

Figure 4-20. *Influence of the tested functional filler blends on the crystallisation point at 5 °C min^{-1}*

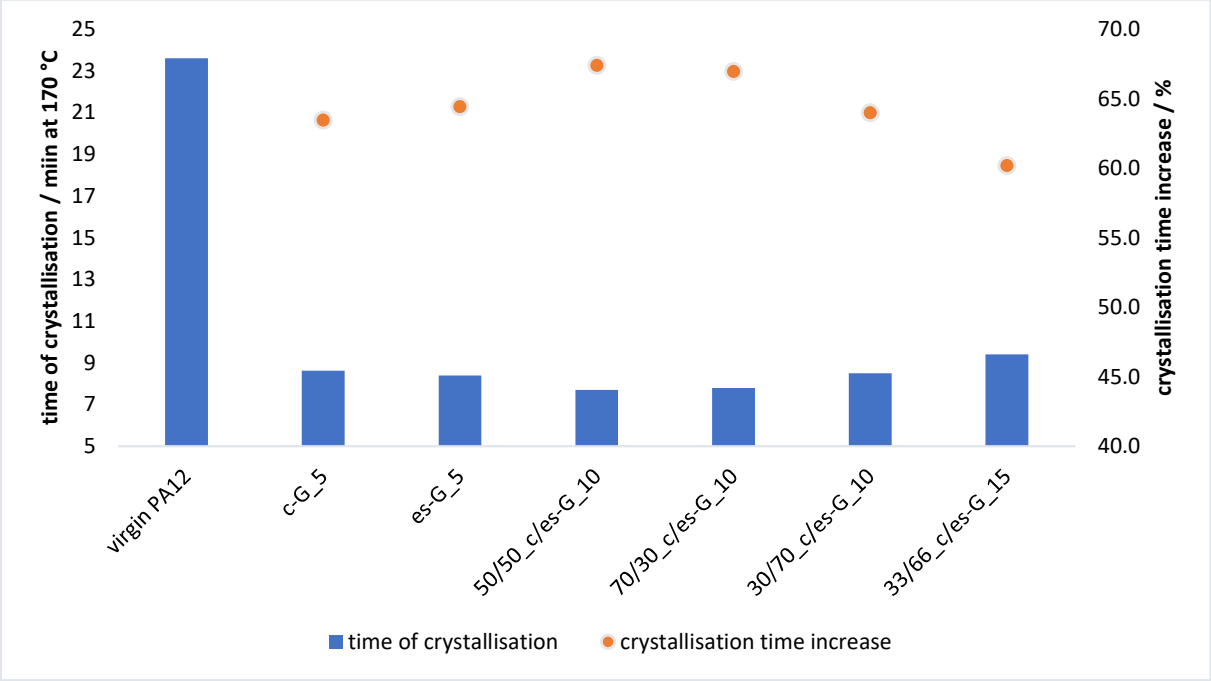

Figure 4-21. *Influence of the tested functional filler blends on the crystallisation time at 170 °C*

4.4 Combination of Bimodal Particle Size and Surface Modification of Ground Calcium Carbonate

The previous sections presented the influence of a calcium carbonate based mineral filler on the thermal properties in a PA12 matrix and how the thermal and flow properties can potentially be optimised by a precise amount of coarse in combination with a narrow size distribution fine calcium carbonate. Section 4.1 illustrated how the introduction of such a stiffening mineral filler resulted in a significant reduction of the mechanical ductility and how the surface modification of the mineral filler with typically up to ~3 mmol amino hexanoic acid per 100 m^2 of filler, up to 60 % of the lost ductility, can be re-gained.

To further control and optimise a functional filled PA12 compound with improved properties for a selective laser sintering process, the possibility to combine the precisely defined particle size ratio of a calcium carbonate filler and the surface modification with amino hexanoic acid has been studied. Optimised ratios of the contrasting particle size fillers were tested at different surface modifier content to evaluate the effect of each parameter on the thermal response as well as mechanical properties. The melt flowability at 190 °C, the melting speed, crystallisation time at 172 °C and the elongation at break were analysed for all developed samples, as defined in section 3.4.4.

***Table 4-5**. Single component GCC-mineral filler data*

Filler nomenclature	Filler type	d_{v10} / µm	d_{v50} / µm	d_{v90} / µm	SSA / m^2g^{-1}
c-G	coarse sized GCC	1 ± 0.5	5 ± 1.5	17 ± 2.0	2 ± 0.2
m-G	medium sized GCC	1 ± 0.5	2 ± 0.5	5 ± 0.5	4 ± 0.5
s-G	small sized GCC	0.5 ± 0.1	1 ± 0.5	3 ± 0.5	8 ± 0.5

***Table 4-6.** Mineral GCC-filler data after filler mixing*

Mixed filler nomenclature	Single components		Mix proportions		Specific surface area / m^2g^{-1}
	Coarse Filler	Fine Filler	Amount Coarse Filler / w/w%	Amount Fine Filler / w/w%	
70/30_c/s-G	c-G	s-G	70	30	3.6
33/66_c/s-G	c-G	s-G	33	66	5.7
50/50_c/m-G	c-G	m-G	50	50	2.7

***Table 4-7**. Tested GCC-filler loadings and introduced surface area of filler per given 100 g mass of polyamide 12*

Compound nomenclature	Filler used	Filler amount / w/w%	Total carbonate surface per 100 g polyamide 12 / m^2	Coarse Filler surface per 100 g polyamide 12 / m^2	Fine Filler surface per 100 g polyamide 12 / m^2
70/30_c/s-G_12	70/30_c/s-G	12	49	17	32
70/30_c/s-G_15	70/30_c/s-G	15	63	22	41
33/66_c/s-G_15	33/66_c/s-G	15	101	11	90
50/50_c/m-G_15	50/50_c/m-G	15	48	16	32

4.4.1 Influence of the untreated Functional Filler Ratio on the Melt Properties

The effect, which the pure, untreated functional filler blend had on the melt properties is shown in **Figure 4-22** and **Figure 4-23**. The melt flowability decreases with an increased amount of filler material compounded in PA12 (Section 4.2). By controlling the ratio of the coarse fraction, which shows a greater impact on the melt flow viscosity at high introduced filler surface levels than the same amount of fine particles, a further decrease of the mould flowability can be prevented. **Figure 4-22** shows how the melt transition width is manipulated with the introduction of filler. By implementing an optimised amount of coarse functional filler with a specific surface of < 2 m^2g^{-1}, in combination with a fine filler fraction with a specific surface of < 6 m^2g^{-1}, the melt transition process time can be reduced by up to 18 %.

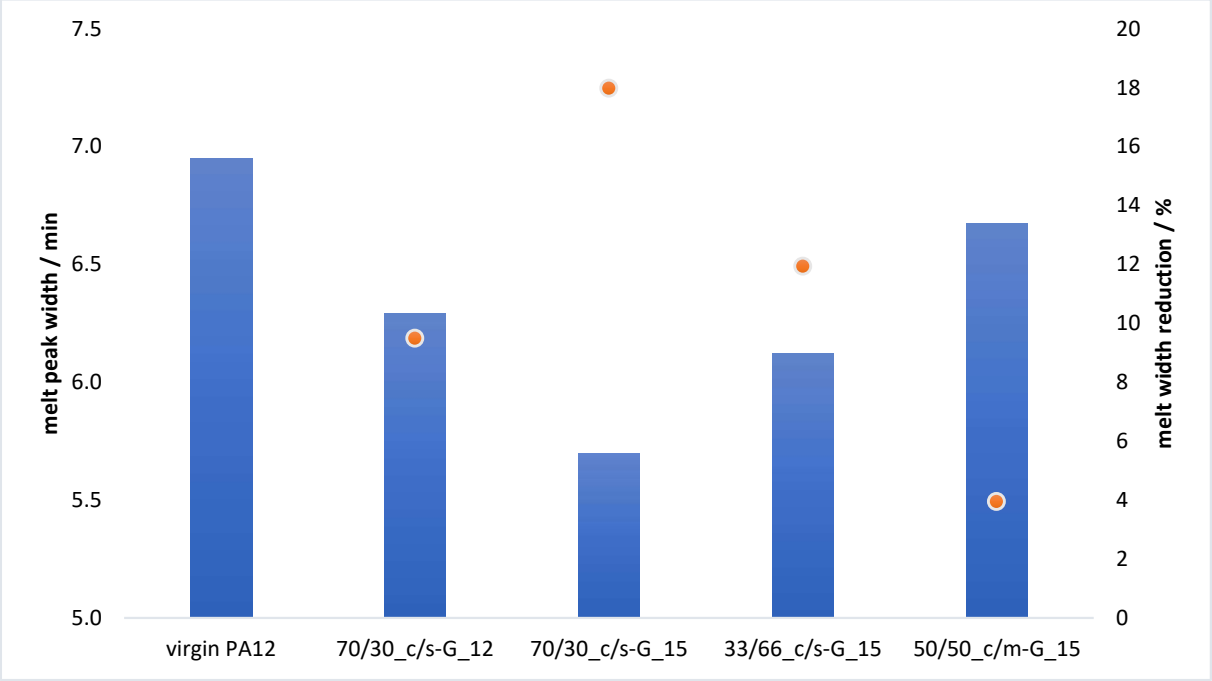

Figure 4-22. *Influence of the different untreated functional filler blends on the melt peak width at 5 °C min^{-1}*

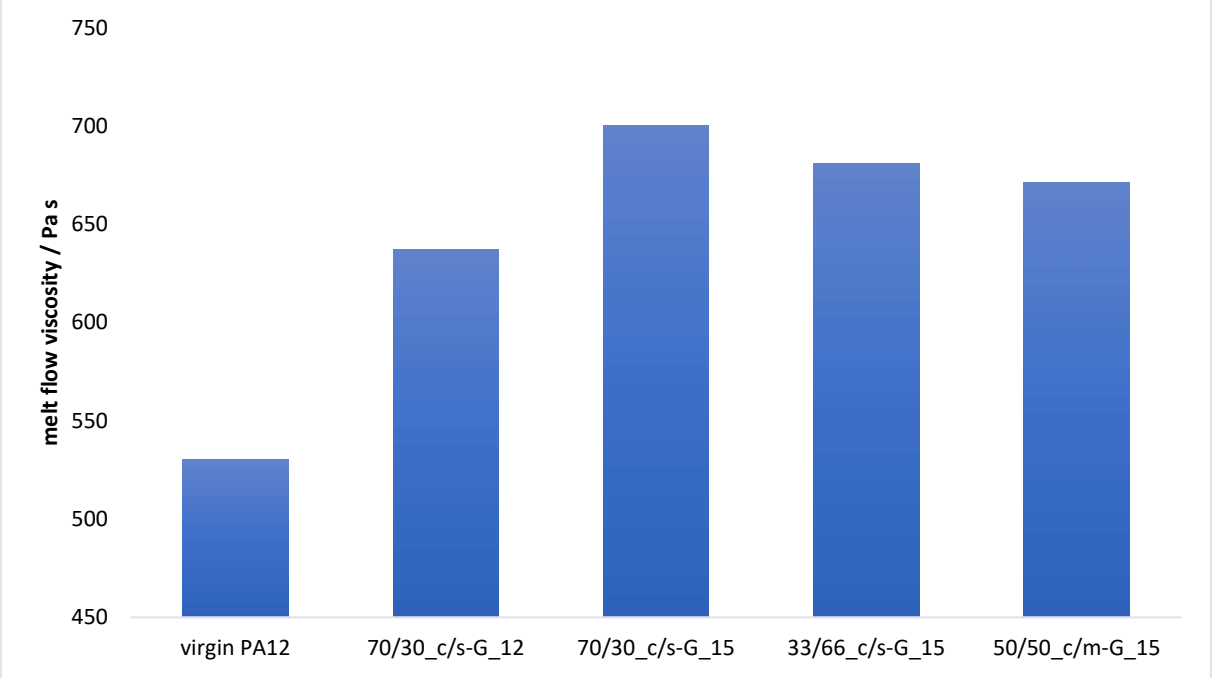

***Figure 4-23**. Influence of the different untreated functional filler blends on the melt flow viscosity at 190°C,2.16 kgf*

4.4.2 Effect of the Surface Modifier Amount on the Melt Properties

The beneficial energy transition, due to higher thermal conductivity and lower specific heat of the calcium carbonate filler material, is significantly reduced if the functional filler is surface coated with 3.05 mmol amino hexanoic acid per 100 g polymer matrix (**Figure 4-24**). The high coverage of the calcium carbonate surface through the surface modification results in a significant reduction of the thermal property difference between filler and polymer. Consequently, the energy is not taken up as quickly by the filler material and not released as rapidly to the PA12 as when the filler was untreated. Due to the organic nature of the surface modifier, the thermal properties of the surface modified functional filler behave more comparably to those of the pure PA12. **Figure 4-25** demonstrates how the improved melt transition width achieved with untreated filler can be slightly regained by reducing the surface modifier amount or only coating the finer filler fraction.

Figure 4-26 and **Figure 4-27** show how the surface modification beneficially influences the melt flowability, by reducing the total loss in flow viscosity resulting otherwise from filler loading. A reduction of the surface modifier to 2 mmol / 100 m^2 of filler material or the coating only applied to the fine filler particle fraction has no negative influence on this improved flowability response. This indicates that the reason for the improvement depends on the coated fine filler particles. This can additionally be confirmed if it is considered that the greatest reduction in 'melt flowability loss' can be achieved with the surface modified compounds '70/30_c/s-G.1_15' and '33/66_c/s-G.1_15', all of which had the higher fine filler fraction ratio. The presence of fine filler particles within the compound improves the melt flowability, the opposite being seen for the same amount of coarse mineral filler. The surface modifier on the fine filler fraction surface additionally improves this flowability of the mineral filler and the polymer matrix, by working as a lower molecular weight lubricant at the interface between them.

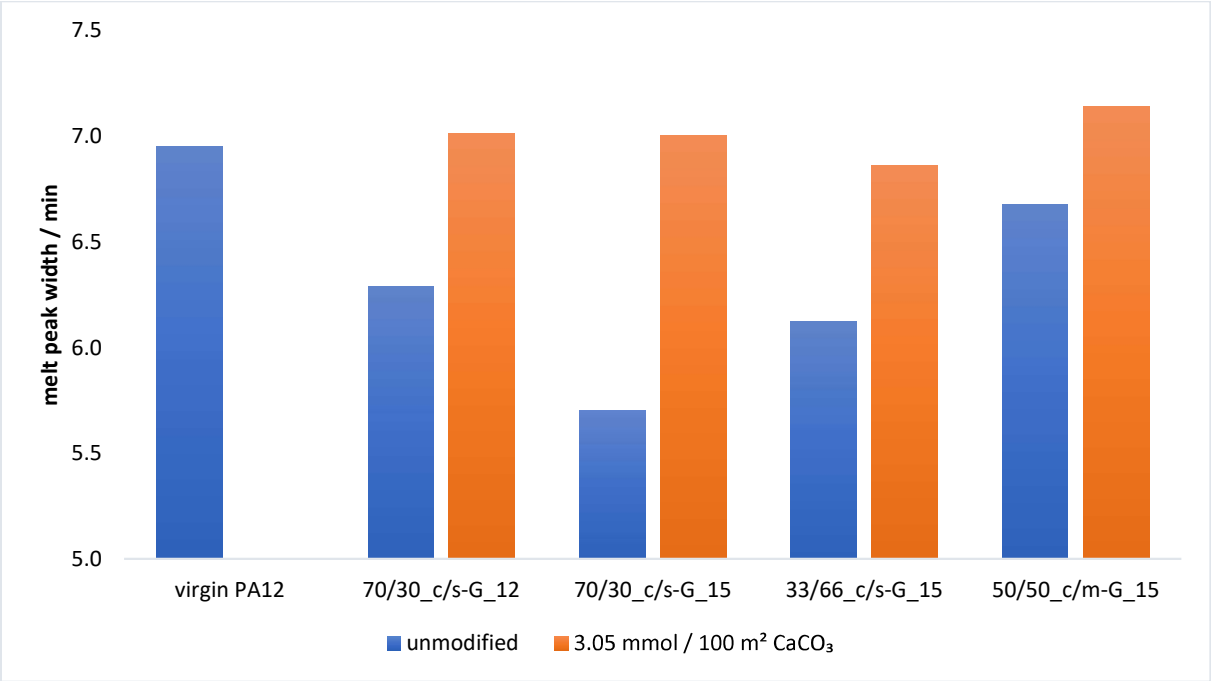

Figure 4-24. *Influence of the filler modification on the melt peak width at 5 °C min^{-1}*

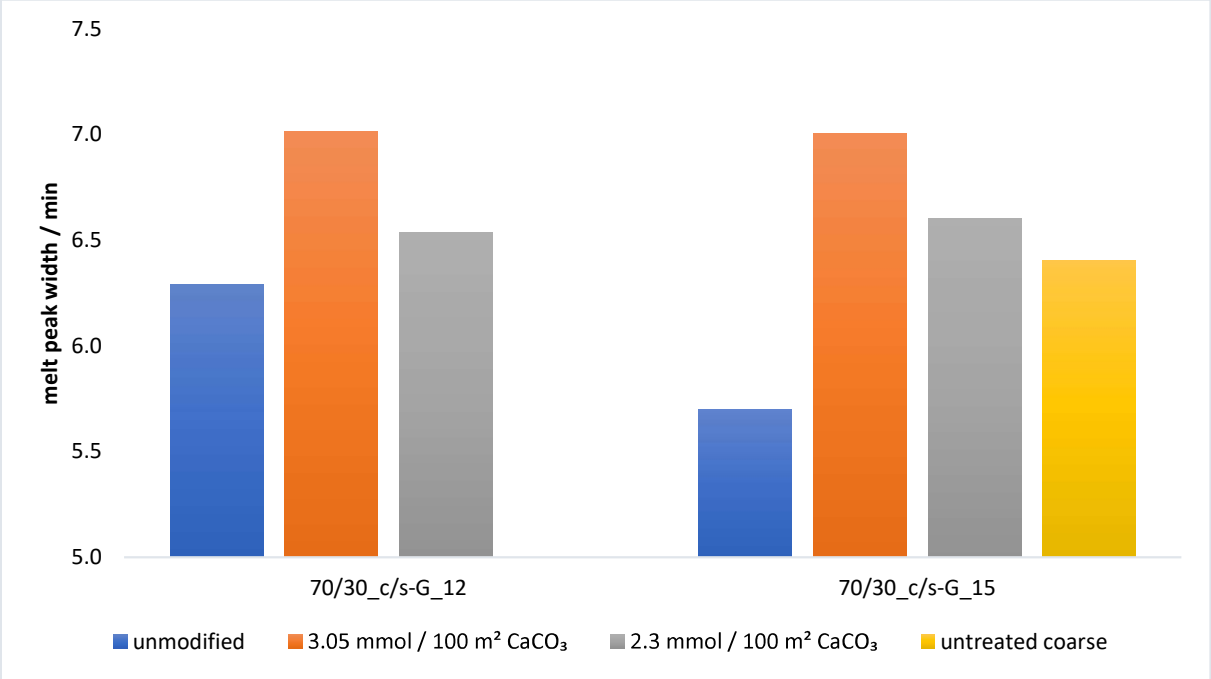

Figure 4-25. *Effect of the variation of surface modifier amount on the melt peak width at 5°C min^{-1}*

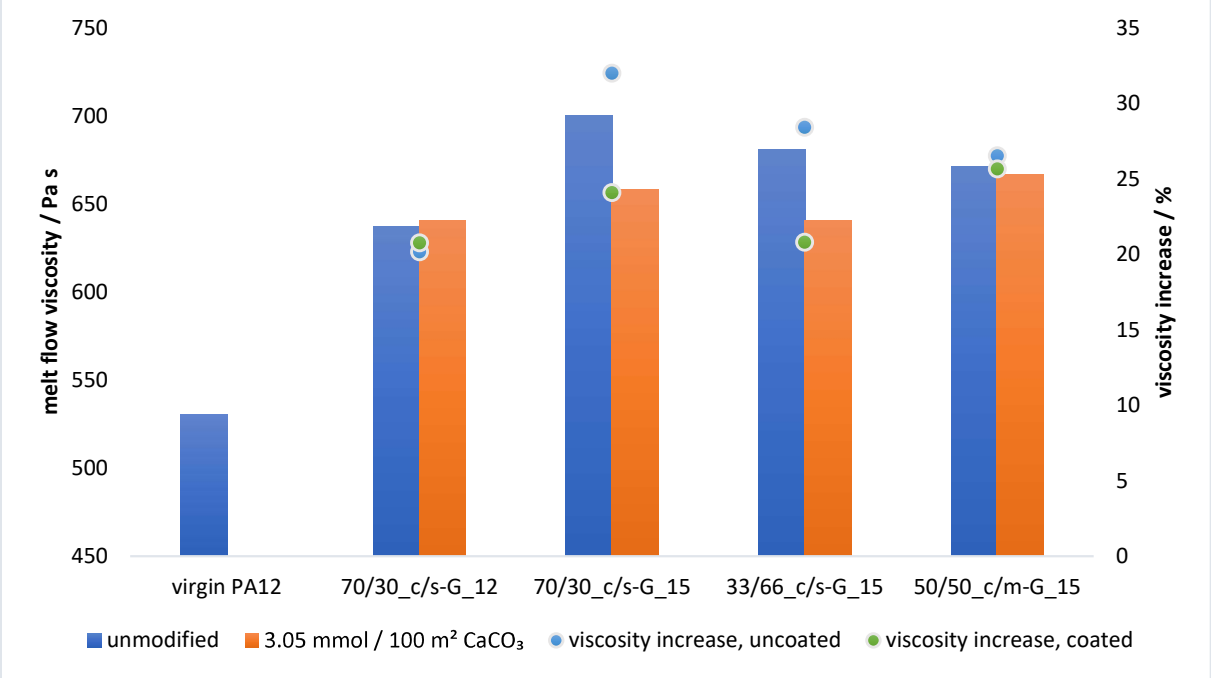

Figure 4-26. *Influence of the filler modification on the melt flow viscosity at 190 °C, 2.16 kgf*

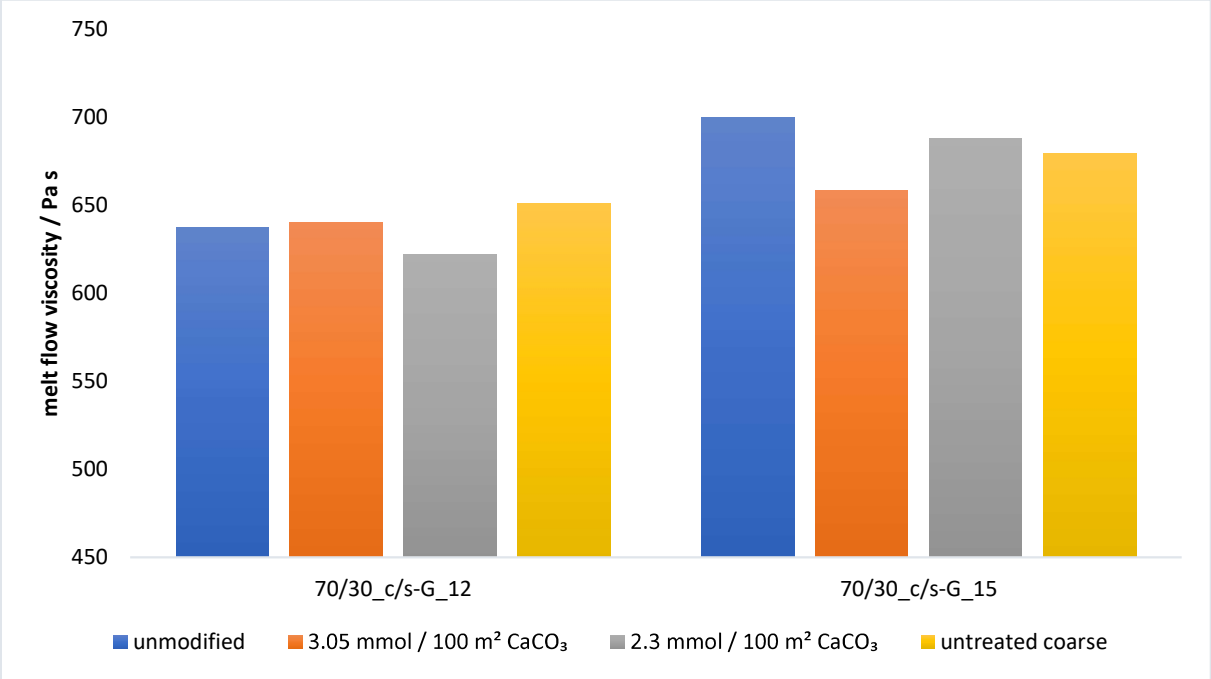

Figure 4-27. *Effect of the variation of surface modifier amount on the melt flow viscosity at 190 °C, 2.16 kgf*

4.4.3 Influence of the Untreated Functional Filler Ratio on the Crystallisation Properties

The higher crystallisation onset point, achievable by adopting an optimised amount of fine calcium carbonate particles within the compound is confirmed with **Figure 4-28**. The increase of the crystallisation onset point was not significant due to the lack of sufficient fine particles within the compound '50/50_c/m-G_15'.

Figure 4-29 reflects the results seen in previous sections. With the addition of an increased surface area of mineral filler in a PA12 compound, the crystallisation time at 172 °C can be significantly reduced. This reduction in the crystallisation time at 172 °C shows no dependency on the ratio of the filler blend. These findings support the hypothesis that the crystallisation onset point shows a strong dependence primarily on particle number, i.e. available nucleation points.

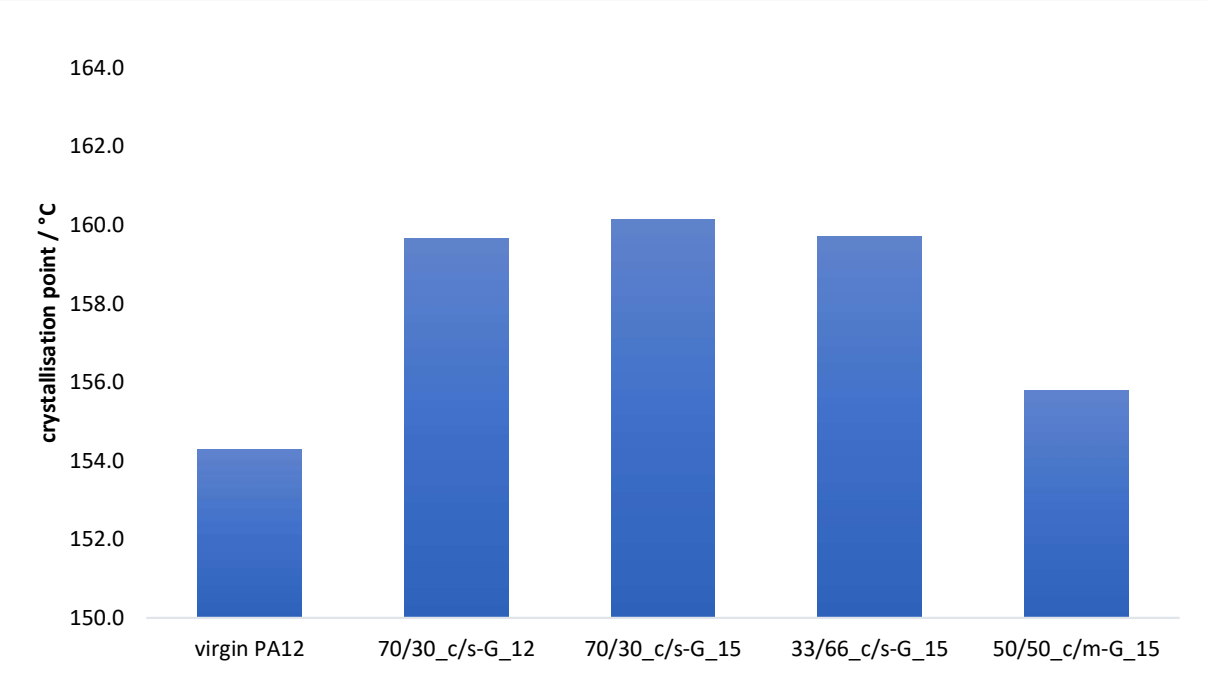

Figure 4-28. *Influence of the different untreated functional filler blends on the crystallisation point at 5 °C min^{-1}*

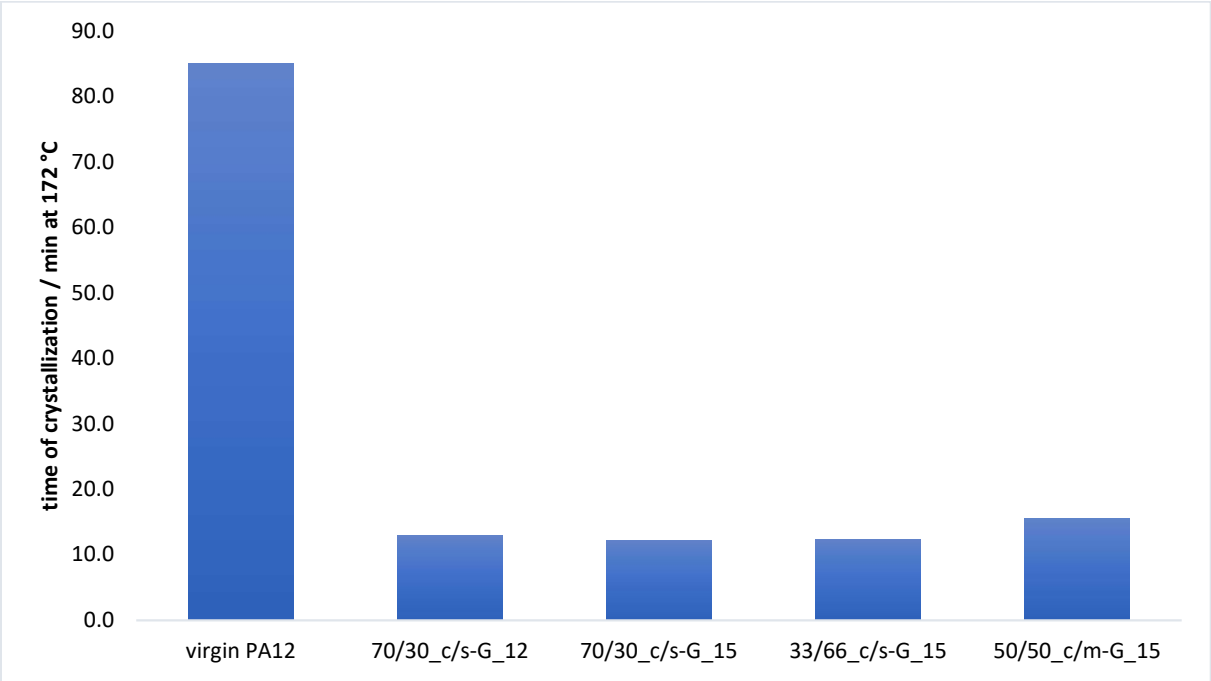

Figure 4-29. *Influence of the different untreated functional filler blends on the crystallisation time at 172 °C*

4.4.4 Effect of the Surface Modifier Amount on the Crystallisation Properties

Even with increased amount of surface modifier, the surface modification of the tested functional fillers showed no significant influence on the crystallisation properties during the temperature reduction phase at 5 °C min^{-1}. This is shown by the stable crystallisation point behaviour in **Figure 4-30**.

By conducting a more precise investigation of the crystallisation kinetics, i.e. determination of the crystallisation time at a constant temperature, in this case 172 °C, once the free surface of the fine functional filler particles is coated with the surface modifier they lose some of their nucleation inducing properties. This results in a significant increase of the measured crystallisation time toward that of the polymer alone. **Figure 4-31** shows that the achieved reduction of the crystallisation time by the addition of a GCC-based functional filler is from 85 % down to 66 %. The reduction of the surface modifier amount, or only a surface modification of the fine filler particles, leads to no regaining of this earlier achieved reduction with untreated material filler. These findings underline the statement that it is the larger amount of finer particles that results in an increased amount of nucleation points, which enables the positive manipulation of the crystallisation properties. However, by surface coating the fine filler fraction, the particles are effectively prevented from inducing nucleation within the crystallisation process.

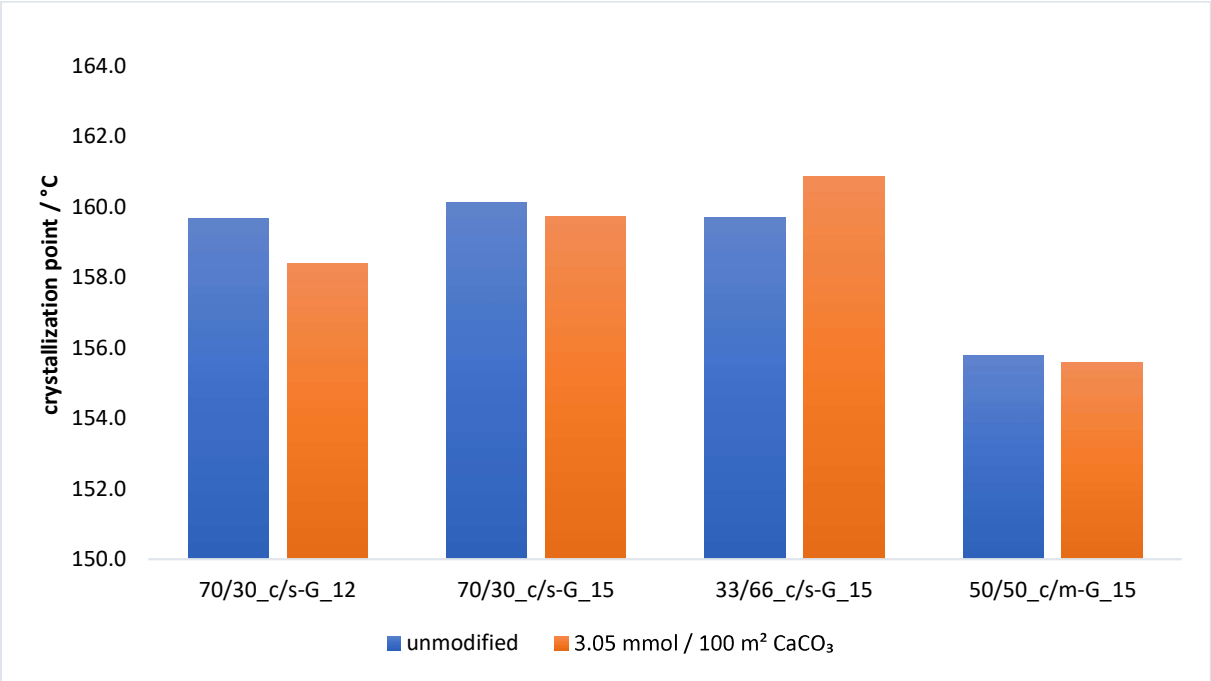

Figure 4-30. *Influence of the filler modification on the crystallisation point at 5 °C min^{-1}*

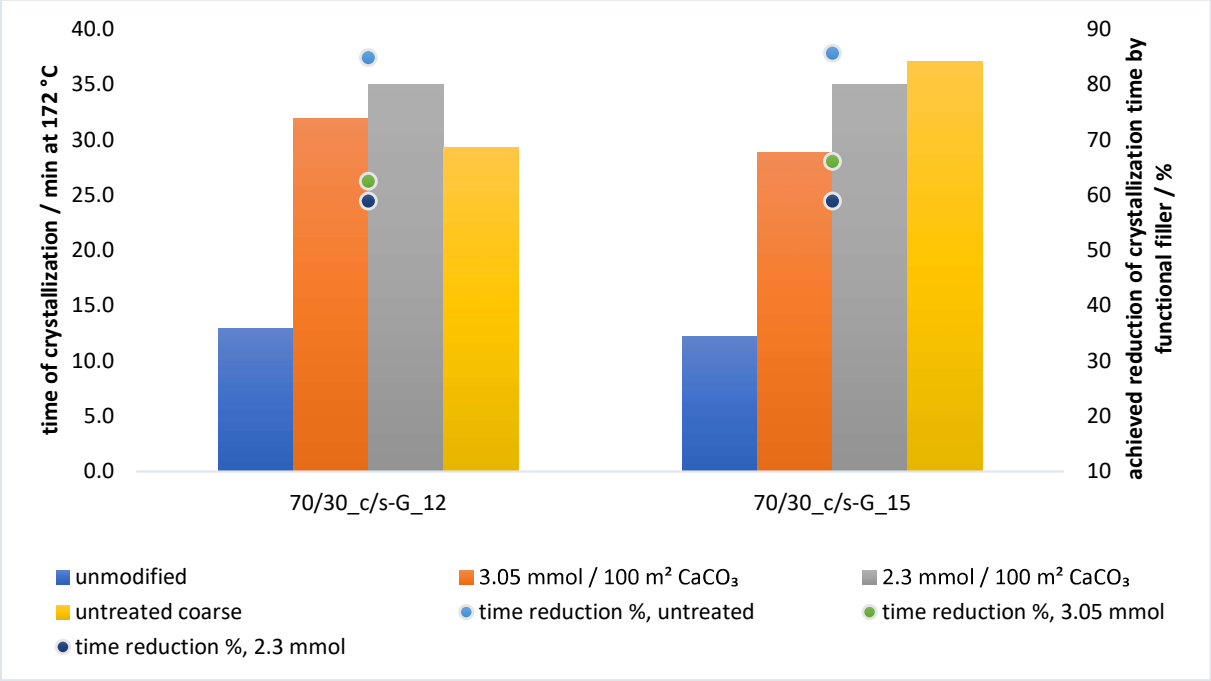

Figure 4-31. *Effect of the variation of surface modifier amount on the crystallisation time at 172 °C*

4.4.5 Influence of Untreated and Treated Functional Filler Ratio on the Ductility

Mineral filler additions act to stiffen filled polymer compounds. The ductility of the tested compound is significantly reduced. This effect is illustrated in **Figure 4-32**, by comparing the tensile elongation at break of pure PA12 against the tested filled compounds. At a filler loading of 15 w/w%, up to 70 % of the elongation is lost.

Relating to the findings, described in Section 4.1, the surface modification of the mineral filler with amino hexanoic acid results in a re-gain of up to 60 % of the lost ductility when implementing a solid mineral filler. **Figure 4-33** presents how the elongation at break of the compound can be improved whilst suffering loss of ductility of only ~30 %, independent of the filler blend used in the compound. **Figure 4-34** additionally shows how, by surface modifying the fine particle filler fraction only, the maximum optimisation of 30 % loss of ductility can be achieved for compound '70/30_c/s-G.3_15' as well.

The improvement reached through the optimised surface modification of a calcium carbonate filler, together with an optimised particle size ratio blend, is limited to a ductility loss of 30 % arising from as high as a 15 w/w% loading of solid mineral filler – a very significant finding.

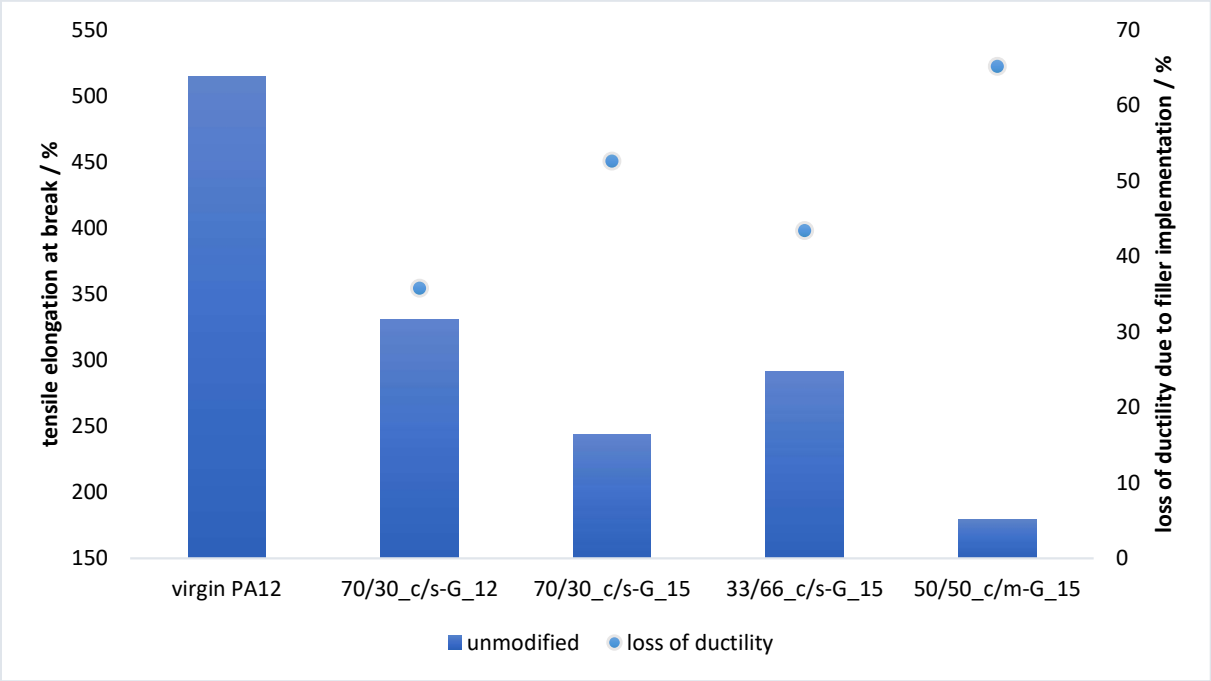

Figure 4-32. *Influence of the different untreated functional filler blends on the elongation at break*

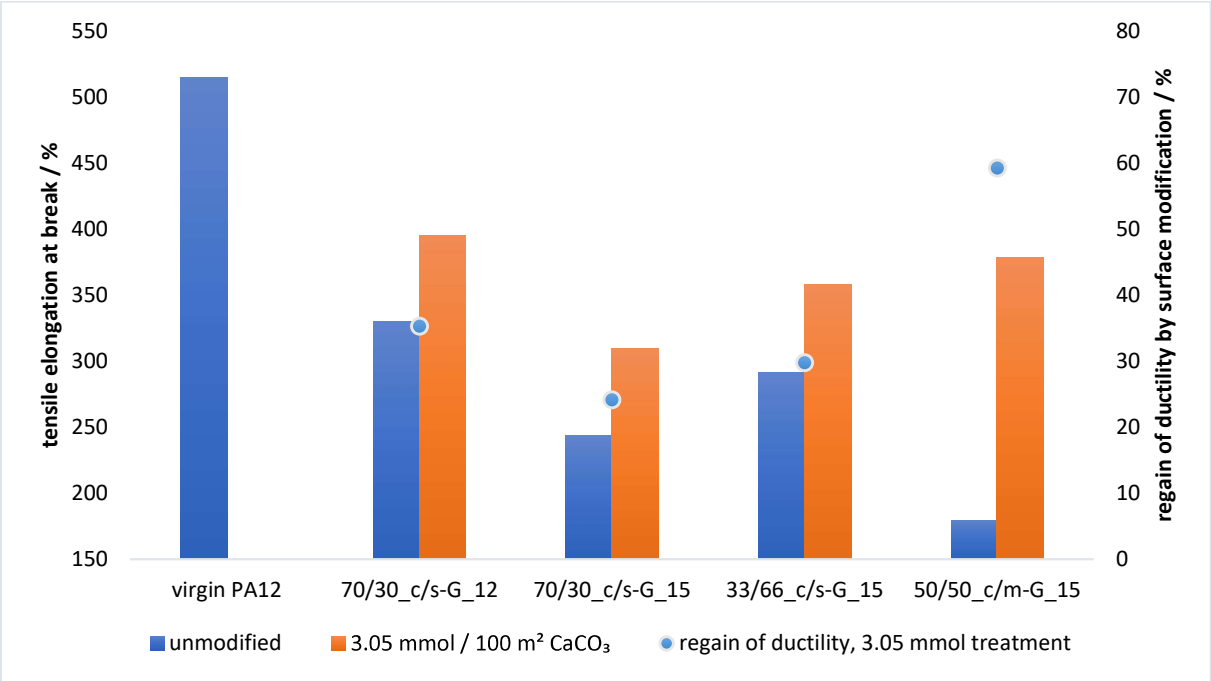

Figure 4-33. *Influence of the filler modification on the elongation at break*

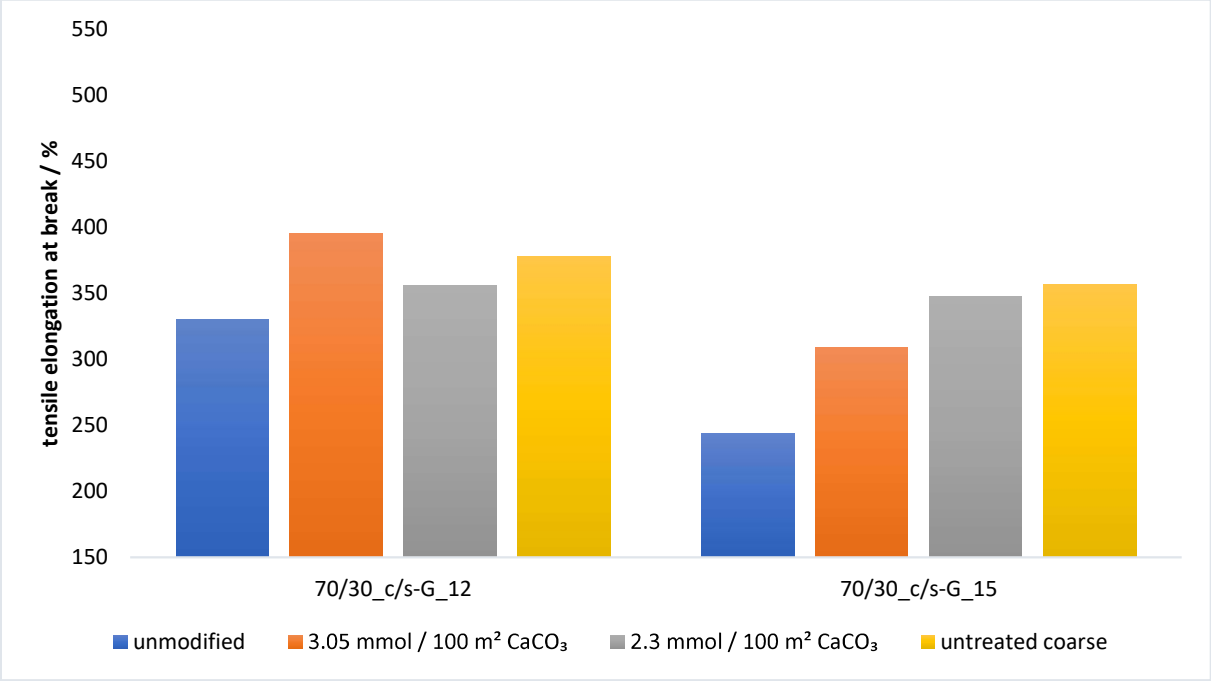

Figure 4-34. *Effect of the variation of surface modifier amount on the elongation at break*

4.5 Comparison of GCC and PCC

In addition to the particle size comparison shown in Section 4.4, the influence of the morphology of the mineral filler was investigated, by the use of controlled, synthesised precipitated calcium carbonate, as described in section 3.4.5. The produced compounds were analysed in the same way and compared with the samples from Section 4.4.

***Table 4-8**. Single component GCC-mineral filler data*

Filler nomenclature	**Filler type**	**d_{v10} / µm**	**d_{v50} / µm**	**d_{v90} / µm**	**SSA / m^2g^{-1}**
c-G	coarse sized GCC	1 ± 0.5	5 ± 1.5	17 ± 2.0	2 ± 0.2
m-G	medium sized GCC	1 ± 0.5	2 ± 0.5	5 ± 0.5	4 ± 0.5
s-G	small sized GCC	0.5 ± 0.1	1 ± 0.5	3 ± 0.5	8 ± 0.5

***Table 4-9.** Single component filler data of synthesized PCC*

Filler nomenclature	**Filler type**	**d_{v10} / µm**	**d_{v50} / µm**	**d_{v90} / µm**	**SSA / m^2g^{-1}**
pr-P	coarse sized PCC	1 ± 0.5	5 ± 0.5	9 ± 0.5	1 ± 0.3
sc-P	small sized PCC	0.5 ± 0.1	2 ± 0.5	4 ± 0.5	6 ± 0.5

***Table 4-10**. Tested GCC-filler loadings and introduced surface area of filler per given 100 g mass of polyamide 12*

Compound nomenclature	**Filler used**	**Filler amount / w/w%**	**Total carbonate surface per 100 g polyamide 12 / m^2**	**Coarse Filler surface per 100 g polyamide 12 / m^2**	**Fine Filler surface per 100 g polyamide 12 / m^2**
70/30_c/s-G_12	70/30_c/s-G	12	49	17	32
70/30_c/s-G_15	70/30_c/s-G	15	63	22	41
33/66_c/s-G_15	33/66_c/s-G	15	101	11	90
50/50_c/m-G_15	50/50_c/m-G	15	48	16	32

***Table 4-11.** Tested PCC-filler loadings and introduced surface area of filler per given 100 g mass of polyamide 12*

Compound nomenclature	**Filler used**	**Filler amount / w/w%**	**Total carbonate surface per 100 g polyamide 12 / m^2**	**Coarse Filler surface per 100 g polyamide 12 / m^2**	**Fine Filler surface per 100 g polyamide 12 / m^2**
30/70_pr/sc-P_15	30/70_pr/sc-P	15	86	7	79
70/30_pr/sc-P_15	70/30_pr/sc-P	15	50	16	34

4.5.1 Morphological Structure of the Developed Mineral Fillers

Figure 4-35 shows the morphological structure of the five main untreated single components functional GCC-fillers ‘c-G to s-G’ and the produced PCC-fillers ‘pr-P’ and ‘sc-P’, before blending the different mixtures. As it was already shown by the particle size distribution (**Figure 3-17**), the coarse ground calcium carbonate filler ‘c-G’ has a much higher presence of

ultrafine particles, than the precipitated calcium carbonate filler with a comparable median d_{v50}, ‘pr-P’. This can be explained by the nature of the wet grinding process, in which a dynamic dissolution and re-precipitation of such ultrafine particles occur, in addition of the grinding itself, in which a large amount of fines is produced from the desired larger particles. This broad particle size distribution seen in a GCC can be changed by subsequent processing, e.g. differential centrifugation, or avoided, by precisely controlling the nucleation and crystal-growth during the precipitation process of calcium carbonate out of calcium hydroxide [72].

Comparing the GCC-Filler ‘m-G’ with the PCC-Filler ‘sc-P’, even at comparable median d_{v50} there is a higher fraction of ultrafines in the GCC-Filler, and so the control of specific surface area of the filler can be enhanced in the PCC case through adjusting crystal-growth / structure build-up in the precipitation process. With the controlled ‘cigar/needle-like’ crystal-growth and agglomerated structure of the scalenohedral PCC, the inner-particle specific surface area can be almost doubled, compared to a regular wet ground calcium carbonate filler. This enhances the free surface implemented in the polymer matrix, available for energy absorption and quick energy release, without losing the benefit of having a high primary particle area for the set effect on cooling.

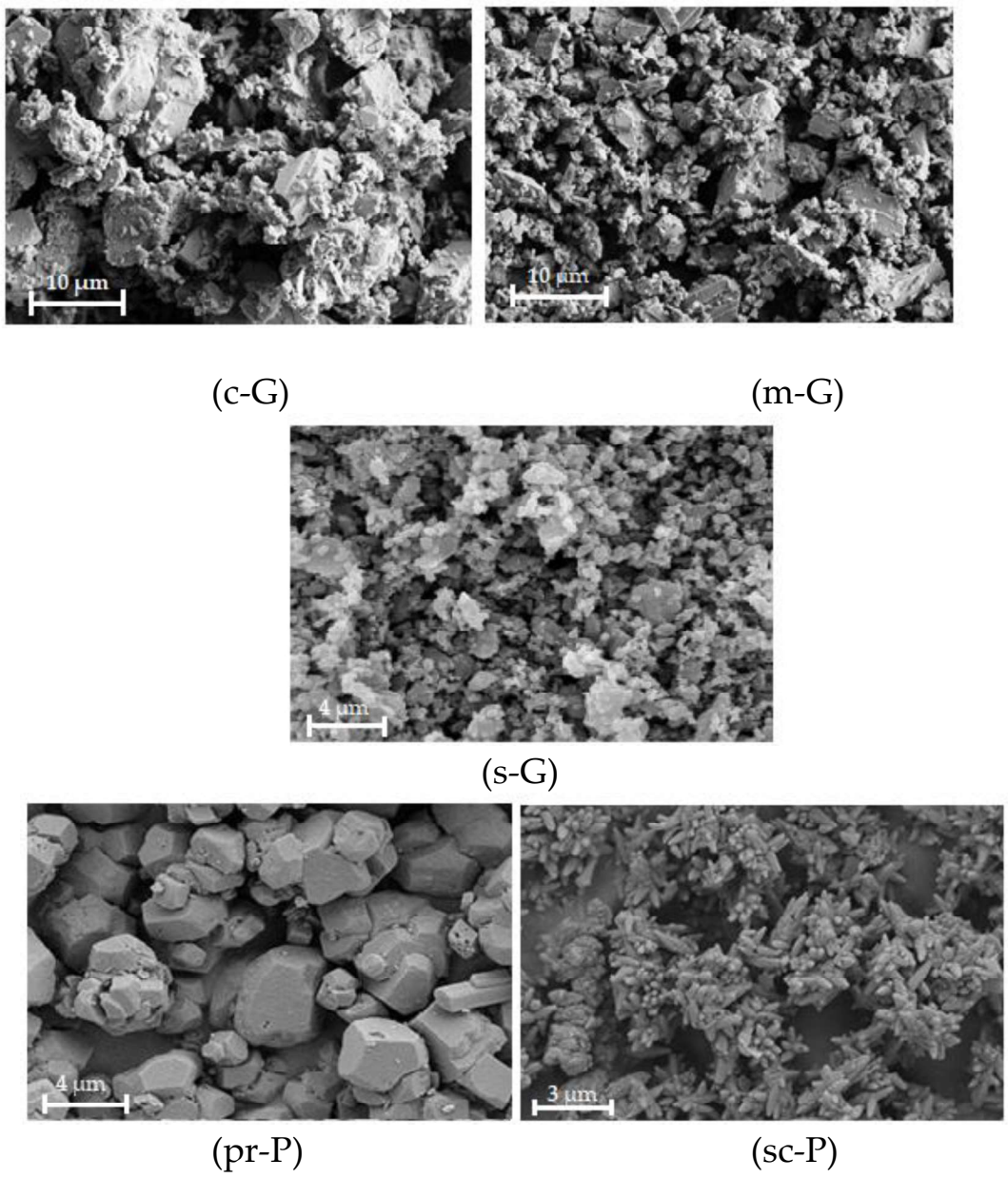

Figure 4-35. *Morphological structure of the main five untreated functional GCC and PCC fillers, before blending*

4.5.2 Influence of the Mineral Morphology on the Melt Properties

Sections 4.4.1 and 4.4.2 presented how the melt flowability decreases with an increased amount of filler material compounded in the PA12 matrix and how a controlled amount of fine particles prevents a further decrease. Additionally, the melt transition process time can be reduced by up to 18 %, by implementing an optimised amount of a coarse functional filler.

Comparing the untreated GCC compound version '33/66_c/s-G_15' and '50/50_c/m-G_15' with the PCC based functional fillers, the precipitated calcium carbonate functional filler has a more significant and higher impact on the melt flowability (**Figure 4-36**). This can be explained by comparing the morphology of the two used fine fillers. As illustrated in Section 3.1, the PCC

‘sc-P’ has a distinctive spiky structure, which increases the inner available particle surface for an improved energy transfer but reduces the smooth particle flowability versus the case for the GCC ‘m-G’ and ‘s-G’, which show a more spherical structure and better melt flowability.

Figure 4-37 compares the reduction that the untreated GCC ‘50/50_c/m-G’ had on the melt transition, with those of the untreated PCC ‘70/30_pr/sc-P’. The crystal structure of the fine functional filler and the steeper particle size distribution of the coarse filler particles play a significant role on the resulting melt properties. Even at the same weight-amount of filler and the same filler-area introduction of course and fine particles in the polymer matrix, the increased inner surface area and high amount of monosized coarse particles of the PCC ‘70/30_pr/sc-P’ reduces the melting transition peak much more significantly than ground calcium carbonate.

Surface modifying the GCC based mineral filler resulted in a significant reduction of the beneficial energy transition. Section 4.2 showed, that the main driver for the improved melt transition is the action of the coarser filler particles, which, due to their greater single-particle volume, can transmit more thermal energy in comparison with a multitude of single fine filler particles. The increased melt transition rate can be completely regained if the coarse PCC particles are completely uncoated and can operate as an optimised energy transmitter (**Figure 4-38**). The difference in the particle size distribution between the two coarse filler material ’c-G’ and ‘pr-P’ is shown in the property regain when using untreated coarse filler, (**Figure 4-38**). While both have similar d_{v50}, the difference in d_{v90} and specific surface area show that the PCC-Filler has a much coarser-steeper (close to mono size) curve, with much less fine fraction. This confirms the beneficial role of the correct amount of uncoated coarse particles on the melting properties of the compound.

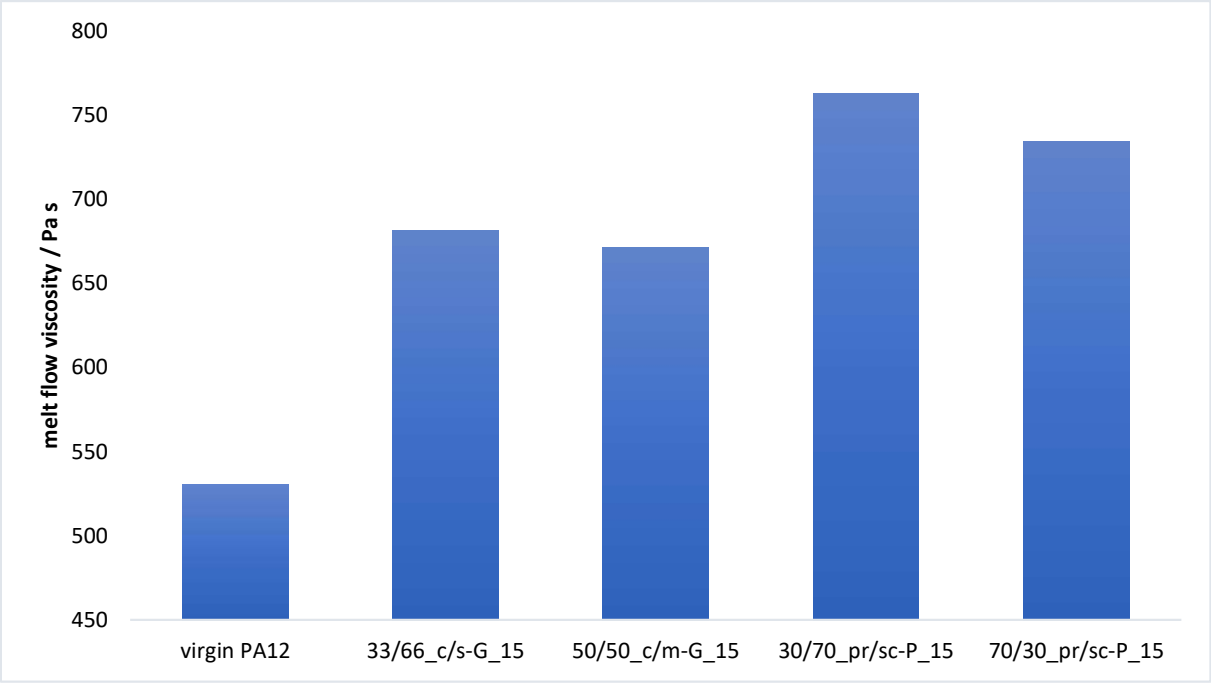

***Figure 4-36**. Melt flow viscosity at 190 °C, 2.16 kgf in comparison of the filler morphology variation*

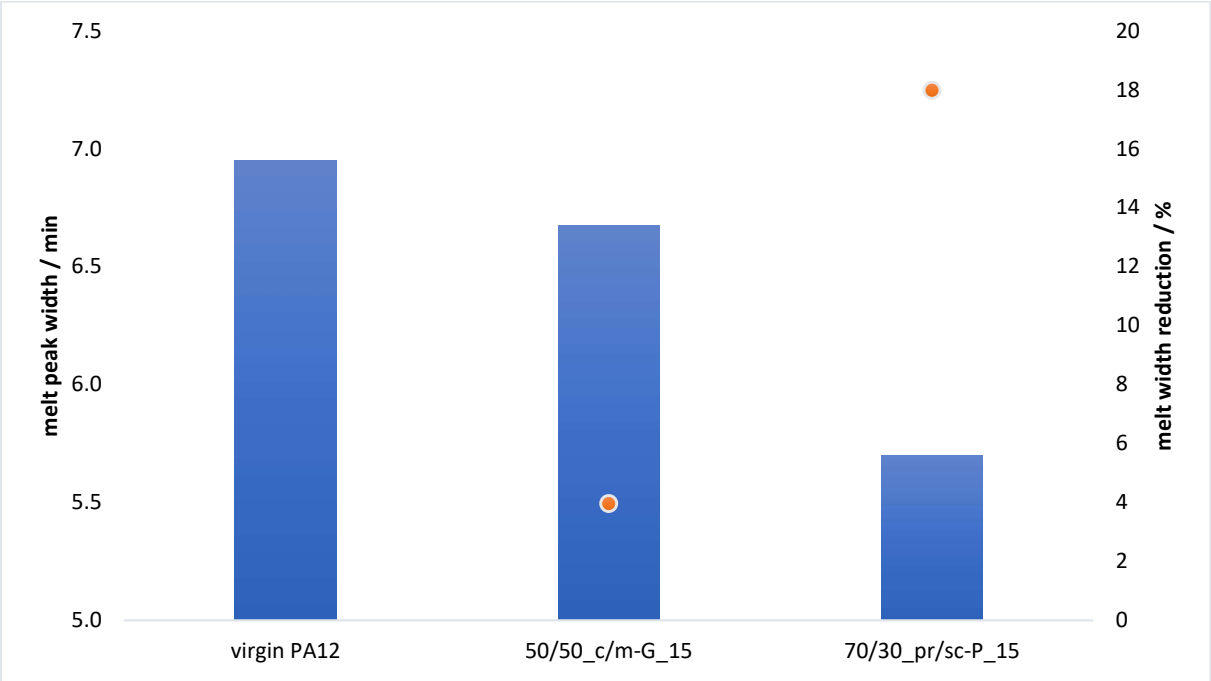

***Figure 4-37**. Influence of the functional filler morphology on the melt peak width at 5 °C min^{-1}*

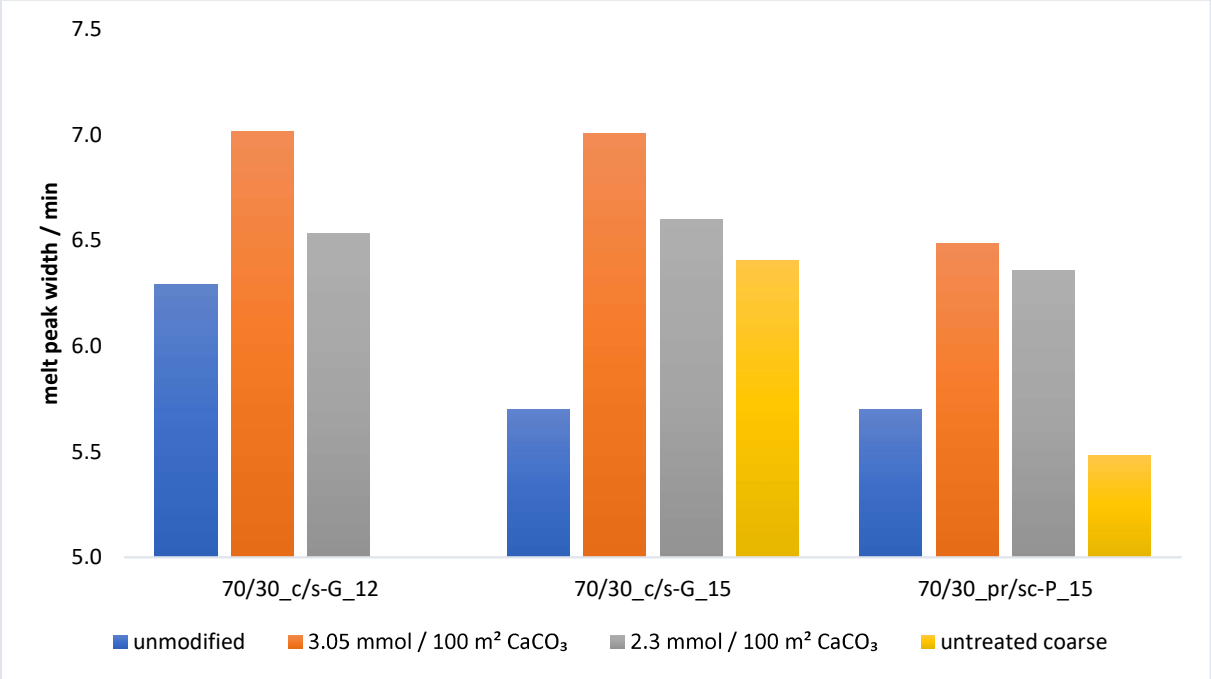

***Figure 4-38.** Effect of the filler morphology and surface modifier amount on the melt peak width at 5 °C min^{-1}*

4.5.3 Influence of the Mineral Morphology on the Crystallisation Properties

Independent of the unmodified filler morphology, the crystallisation onset point will be increased and the crystallisation time reduced, if an optimised amount of fine calcium carbonate particles are distributed within the compound (**Figure 4-39** and **Figure 4-40**).

As was underlined in Section 4.4.4, the surface modification of the finer filler particles effectively prevents them from initiating a nucleation effect within the crystallisation process and therefore lowers the overall effect the functional filler blend showed on the reduction of the crystallisation time.

This hypothesis is further confirmed by comparing the crystallisation time of the GCC-based compounds versus the PCC-based compounds in **Figure 4-41**. The morphology of the fine precipitated calcium carbonate reveals a high amount of cigar/needle-like anisometric structure compared with the more isometric ground calcium carbonate particles. Even if surface coated, the PCC particles present a greater amount of nucleation points, which explains why the achieved crystallisation time reduction is only reduced to 72 % when coating the PCC filler, instead of the 66 % for the GCC filler compounds. Additionally, the anisometric properties of the PCC are expected to lead to a greater patchwork of uncoated surface even after surface modification, which could also account, at least in part, for the less detrimental effect of coating on nucleation in the case of the PCC filler considered here.

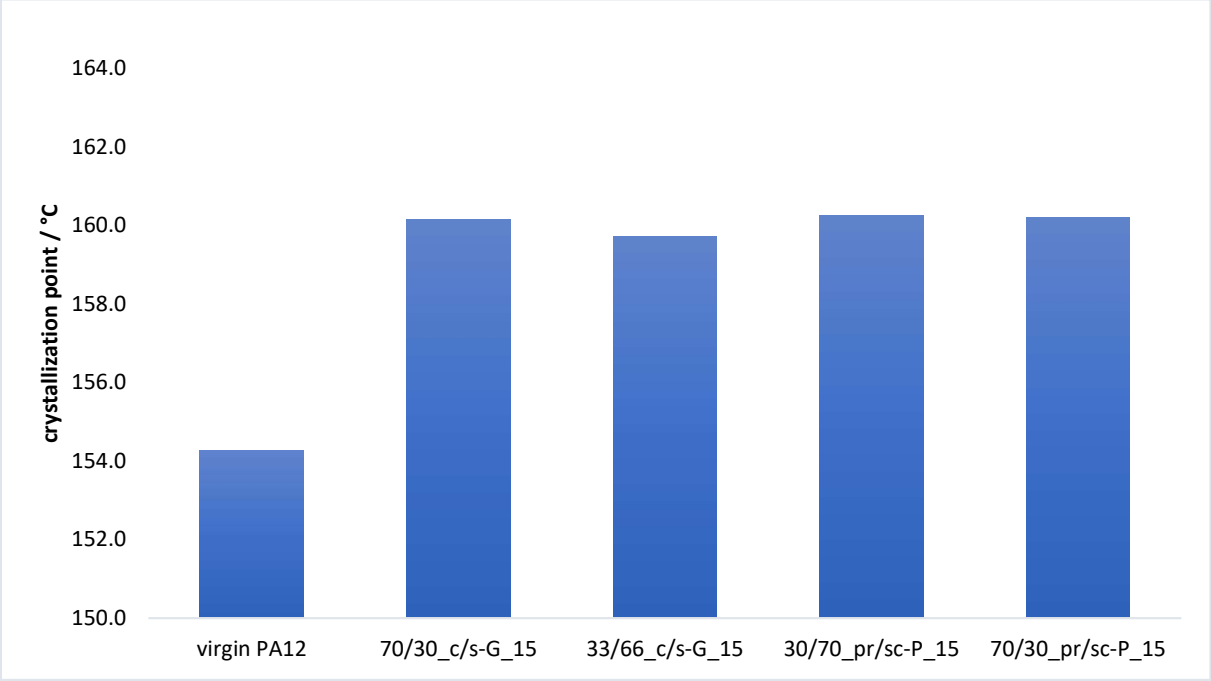

Figure 4-39. *Influence of functional filler morphology on the crystallisation point at 5 °C min^{-1}*

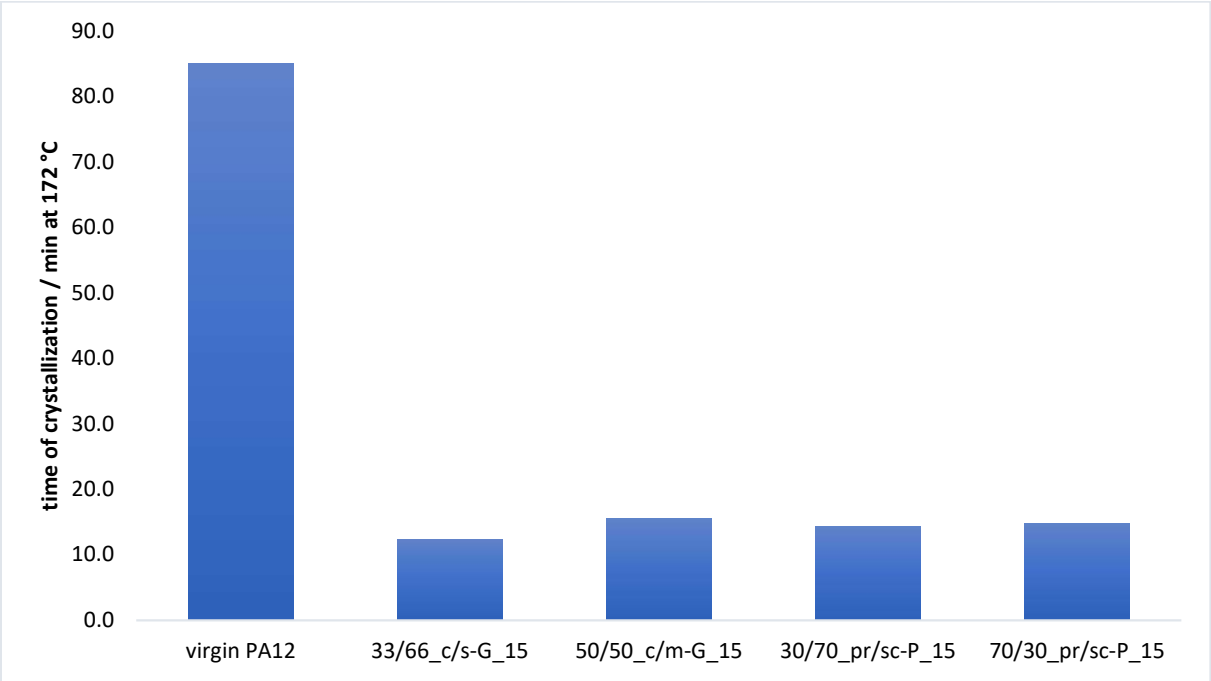

Figure 4-40. *Influence of the untreated functional filler morphology on the crystallisation time at 172 °C*

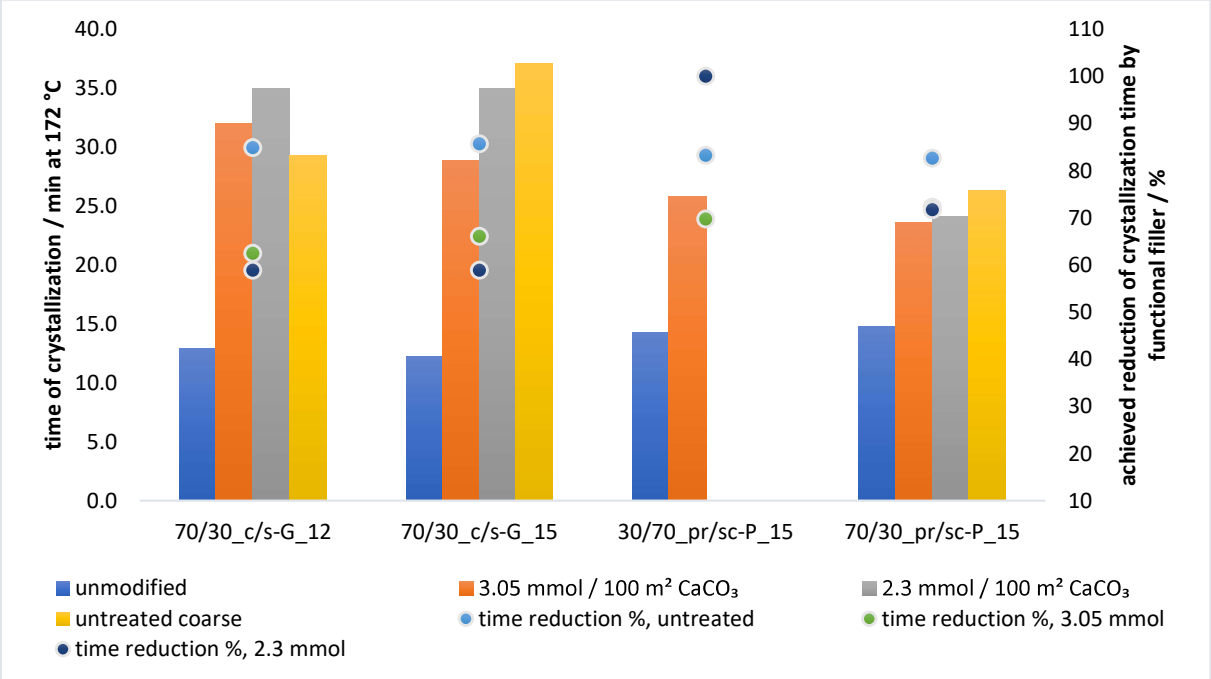

Figure 4-41. *Effect of the filler morphology and surface modifier amount on the crystallisation time at 172 °C*

4.5.4 Influence of the Mineral Morphology on the Ductility

Comparing the ductility results of the untreated GCC-based compound '50/50_c/m-G_15' and of the comparable PCC-based compound '70/30_pr/sc-P_15' shows that the loss of ductility can be significantly reduced by reducing an excess amount of ultrafine filler particles, (**Figure 4-42**). The comparison of both untreated PCC-based compounds '30/70_pr/sc-P_15' and '70/30_pr/sc-P_15' shows the same trend. By reducing the fine filler fraction and increasing the coarse filler fraction, effectively by narrowing the particle size distribution and so having a low amount of fines, the loss of ductility can be reduced from 68 % down to 30 %.

The results for compound '70/30_pr/sc-P.1_15' in **Figure 4-43** shows how the surface modification of the optimised PCC filler fails to give an additional re-gain of the ductility. As defined in Section 4.4.5, by surface modifying the fine filler fraction only of filler '70/30_c/s-G', the elongation at break of the compound can be improved whilst suffering only a limited loss of ductility of only ~30 % as well.

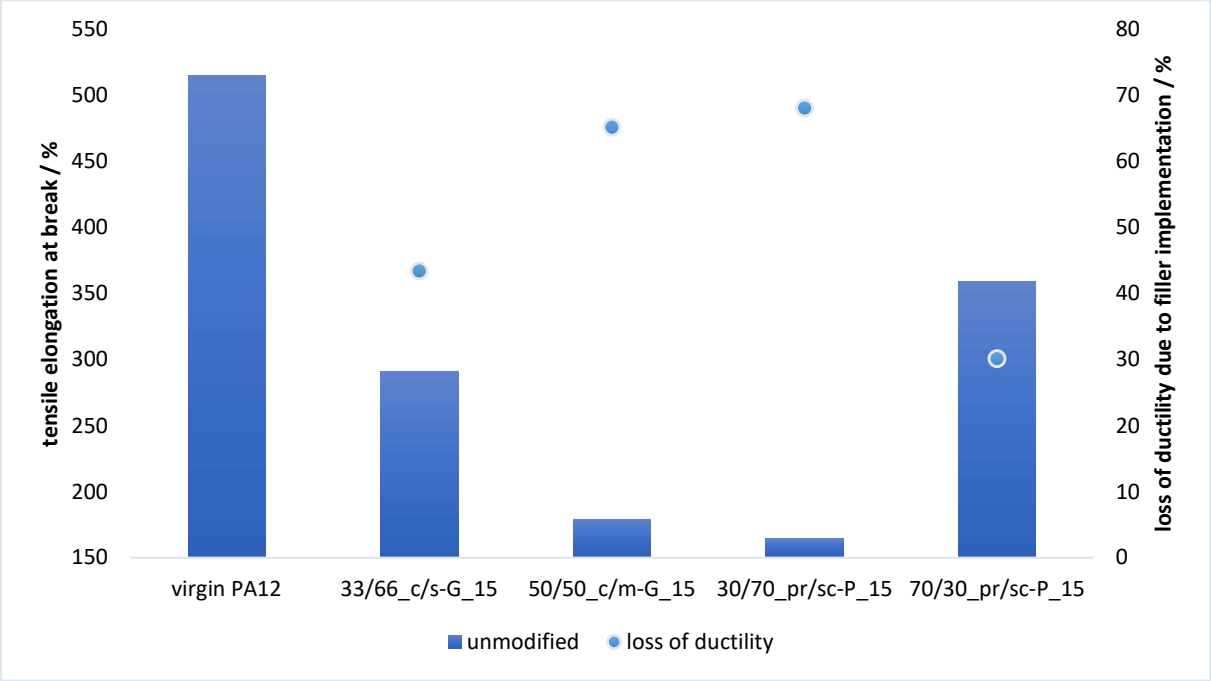

Figure 4-42. *Influence of the untreated functional filler morphology on the elongation at break*

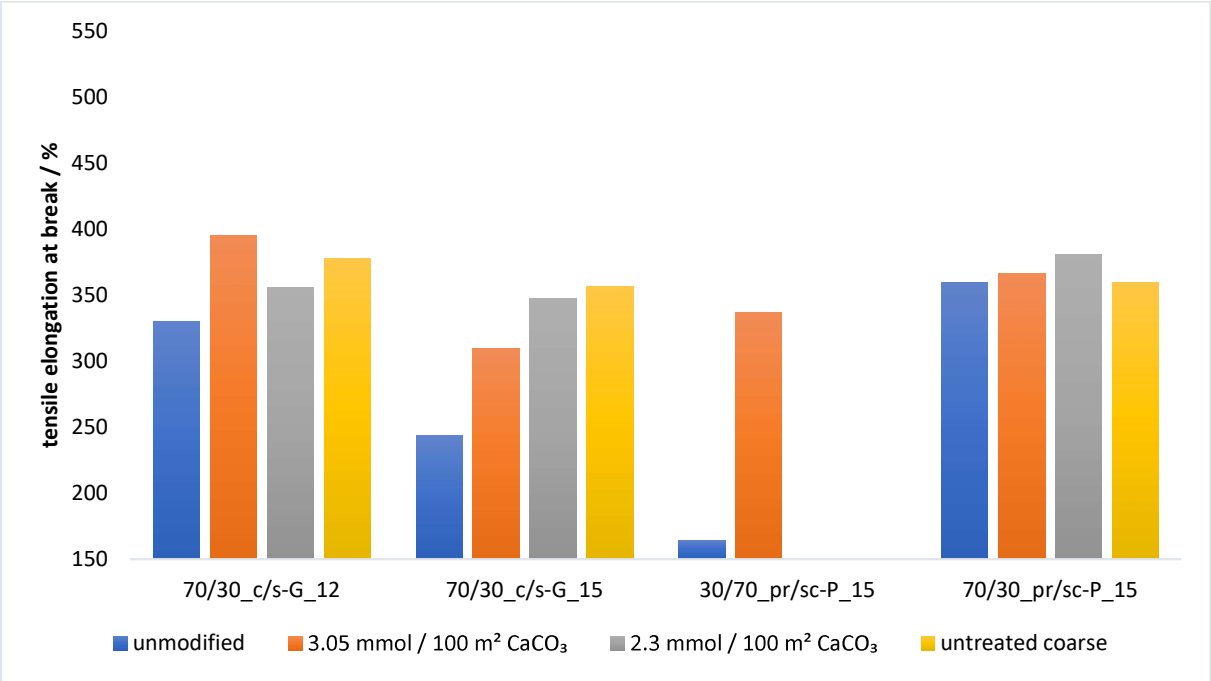

Figure 4-43. *Effect of the filler morphology and surface modifier amount on the elongation at break*

4.6 Closure

Calcium carbonate–polyamide 12 composites have been produced via twin-screw compounding using a calcium carbonate blend of different morphology as functional filler material. The filler particle size distributions and filler ratio were investigated and combined in such a way as to optimise the thermal response of the final compound. The mineral filler surface was modified with specific modification agents to improve the compatibility of the mineral filler material with the polar group in the polymer structure, hence reducing the loss in the resulted mechanical properties of the mineral filled PA12 compound.

The effect of the mineral filler on the thermal and mechanical properties can potentially be optimised with a combination of a precise amount in ratio of surface modified coarse and fine calcium carbonate filler, with an optimised morphology.

- With the introduction of a solid mineral filler within pure polyamide 12, the high melt flowability, needed for an optimized selective laser sintering process and proper layer-melt distribution [16], is significantly decreased. This reduction can be regained by up to 30 % by surface modification of at least the fine filler fraction with ~2 – 3 mmol amino hexanoic acid per 100 m^2 calcium carbonate filler. The surface modifier on the fine filler fraction additionally reduces the negative impact on flowability from the mineral filler in the polymer matrix, by working as a lubricant at the material interface.
- By implementing an optimised amount of coarse functional filler with a specific surface of < 2 m^2g^{-1}, in combination with a fine filler fraction with a specific surface of < 6 m^2g^{-1}, the melt transition process can be enhanced by up to 18 % (reducing time required in comparison with the virgin polymer). More thermal energy was transmitted due to the greater single-particle volume of the coarser calcium carbonate particles, in comparison with a multitude of single fine filler particles. This resulted in a greater influence on the melting behaviour of the compound with the inclusion of a few coarse filler particles in combination with fine calcium carbonate filler particles.
- By changing from isometric ground to anisometric precipitated calcium carbonate of agglomerated scalenohedral form, a greater surface area per unit particle plus a reduction of the amount of fine particles in a coarse filler fraction can be achieved. This resulted in an even more beneficial improvement in the melting transition (a reduced temperature range).
- By surface modifying the functional filler with amino hexanoic acid, the beneficial effect on the melting transition process is lost due to the high coverage of the functional filler surface with the organic modifier, effectively reducing the interfacial surface area.
- This loss can be largely re-gained if an uncoated coarse precipitated calcium carbonate filler with a narrow particle size distribution is used in the compound. The beneficial thermal response given by the coarser fraction is restored by not coating the coarse filler fraction and the transmitted energy will be better distributed throughout the surrounding polymer matrix.

- The introduction of sufficient additional nucleation points, independent of the ratio of coarse and fine filler material in the blend or the particle morphology, was found to have a significant impact on the rate of crystallisation.
- Uncoated filler particles accelerated the crystallisation process at 172 °C by approx. 80 % (in comparison with virgin PA12), while that effect is significantly reduced if the free

surface of the fine functional filler particles are coated with the surface modifier. These findings underline the statement that an increased amount of nucleation points enables the positive manipulation of the crystallization properties. However, by surface coating the fine filler fraction, the particles are effectively prevented from inducing nucleation within the crystallization process.

- The re-increase in the measured crystallisation time can be controlled by replacing fine ground calcium carbonate with precipitated calcium carbonate, which has a more anisometric needle-like structure in its morphology. Even if surface coated, the PCC particles present a greater number of surface nucleation points.

- As previously seen in literature, the introduction of a stiff/solid mineral filler within a polymeric system, will lead to a certain loss in certain mechanical properties [47-49].
- Up to approx. 70 % of its ductility is lost by loading PA12 with 15 w/w% ground calcium carbonate despite a beneficial increase in stiffness.
- By surface modification of the ground calcium carbonate functional filler with typically up to ~3 mmol amino hexanoic acid per 100 m^2 of filler, the compatibility between the nitrogen groups within the polyamide chain and the calcium carbonate surface can significantly be enhanced [37]. This resulted in a significant regain of the lost ductility.

The following summary table gives an overview of the most significant findings of this study.

	uncoated GCC blend	**modified GCC**	**reduced modification**	**uncoated coarse GCC**
melt flowability	reduced	improved	improved	improved
melt transition	enhanced	effect lost	slight regain	slight regain
crystallization point	Increased	increased	increased	increased
crystallization time	20% reduced	150 % regain	150 % regain	150 % regain
ductility	70 % lost	60 % regain	60 % regain	60 % regain

	uncoated PCC blend	**modified PCC**	**uncoated coarse PCC**
melt flowability	reduced	improved	improved
melt transition	enhanced	slight regain	high regained
crystallization point	increased	increased	increased
crystallization time	20% reduced	regain of 60 %	regain of 60 %
ductility	30 % lost	no effect	no effect

5 Conclusions and Future Work

This combination of dually optimised functional filler particle size ratio and surface modification showed how the melting as well as crystallisation behaviour of PA12 can be manipulated, whilst at the same time the typical loss of the mechanical properties on adding filler can be limited.

The thermal and flowability properties of a PA12 matrix can be manipulated beneficially with an introduction of a precise amount of coarse and fine calcium carbonate filler. The loss of the mechanical properties, caused by this introduction, can be re-gained partially by an optimised surface modification of the fine filler fraction with ~ 2 – 3 mmol amino hexanoic acid per 100 m^2 filler.

Out of all the tested combinations, a mixture of 70 %weight narrow coarse sized PCC-particles in combination with the increased inner surface area of 30 %weight of the scalenohedral structured fine particles resulted in the shortest melt transition time, highest ductility and minimised decrease in the melt flowability, hence the most improvements in the overall performance (70/30_pr/sc-P.3).

Future Work

The steepness of the particle size distribution was increased through the synthetic production of the mineral filler by precipitation, as well as the crystal structure. For future work each precipitated calcium carbonate morphology / crystal structure should be studied independently. However, the effect of narrowing size distribution can be considered to a first approximation as an extrapolation of the findings from the previous bimodal studies where different ratios and particle size distribution of GCC were used. To determine an extreme case, a narrow particle size, fine scalenohedral agglomerated calcite was used in this study.

The combined improvements, under twin-screw extrusion compounding of PA12, demonstrate the possible usage of optimised calcium carbonate as a functional filler in additive manufacturing, which can potentially be transferred via a subsequent investigation into the selective laser sintering process. The implementation process of such an optimised functional filler within PA12 and the production of spherical powder, suitable for a laser sintering process needs to be studied independently. An additional point of future investigations is the adjustment / improvement of the energy absorption of the functional calcium carbonate at a suitable wavelength of 10.6 µm.

This fundamental understanding of the interaction of a functional filler with the polymer surface can further be used and investigated for different inorganic filler materials, such as calcium phosphate for example, which shows a higher absorption rate at the given wavelength of 10.6 µm. By changing the nature of the filler, away from a pure basic pH nature, the impact of pH on an efficient surface modification reaction can also be investigated.

The core knowhow on the impact of a defined filler particle size distribution (and their controlled combination) on specific filled polymer composite attributes could be universally applicable and should also be investigated for different polymers.

The potential reduction of the laser energy during the laser sintering process, increase of printing speed due to the faster crystallisation process and the result of these parameter adjustments on the final part density are also candidates for future research.

Reference

[1] R.I. Campbell, R.J. Hague, B. Sener, P.W. Wormald, The potential for the bespoke industrial designer, The Design Journal 6(3) (2003) 24-34.

[2] R. Hague, I. Campbell, P. Dickens, Implications on design of rapid manufacturing, Proceedings of the Institution of Mechanical Engineers, Part C: Journal of Mechanical Engineering Science 217(1) (2003) 25-30.

[3] R. Hague*, S. Mansour, N. Saleh, Material and design considerations for rapid manufacturing, International Journal of Production Research 42(22) (2004) 4691-4708.

[4] N. Hopkinson, R. Hague, P. Dickens, Rapid manufacturing: an industrial revolution for the digital age, John Wiley & Sons (2006).

[5] N. Hopkinson, P. Dickens, Rapid prototyping for direct manufacture, Rapid prototyping journal (2001).

[6] C.K. Chua, K.F. Leong, C.S. Lim, Rapid prototyping: principles and applications (with companion CD-ROM), World Scientific Publishing Company (2010).

[7] L. Liu-Lan, S. Yu-Sheng, Z. Fan-di, H. Shu-huai, Microstructure of selective laser sintered polyamide, Journal of Wuhan University of Technology-Mater. Sci. Ed. 18(3) (2003) 60-63.

[8] T. Childs, M. Berzins, G. Ryder, A. Tontowi, Selective laser sintering of an amorphous polymer—simulations and experiments, Proceedings of the Institution of Mechanical Engineers, Part B: Journal of Engineering Manufacture 213(4) (1999) 333-349.

[9] M. Schmidt, D. Pohle, T. Rechtenwald, Selective laser sintering of PEEK, CIRP annals 56(1) (2007) 205-208.

[10] J. Koo, S. Lao, W. Ho, K. Ngyuen, J. Cheng, L. Pilato, G. Wissler, M. Ervin, Polyamide nanocomposites for selective laser sintering, Proc. SFF Symp., Austin (2006), 392-409.

[11] M. Schmid, A. Amado, K. Wegener, Polymer powders for selective laser sintering (SLS), ETH-Zürich (2014).

[12] J. Kim, T. Creasy, Selective laser sintering characteristics of nylon 6/clay-reinforced nanocomposite, Polymer Testing 23(6) (2004) 629-636.

[13] I.Y. Phang, T. Liu, A. Mohamed, K.P. Pramoda, L. Chen, L. Shen, S.Y. Chow, C. He, X. Lu, X. Hu, Morphology, thermal and mechanical properties of nylon 12/organoclay nanocomposites prepared by melt compounding, Polymer international 54(2) (2005) 456-464.

[14] Y. Guo, K. Jiang, D.L. Bourell, Preparation and laser sintering of limestone PA 12 composite, Polymer Testing 37 (2014) 210-215.

[15] C.R. Rambo, N. Travitzky, K. Zimmermann, P. Greil, Synthesis of TiC/Ti–Cu composites by pressureless reactive infiltration of TiCu alloy into carbon preforms fabricated by 3D-printing, Materials Letters 59(8) (2005) 1028-1031.

[16] M. Schmid, Laser Sintering with Plastics: Technology, Processes, and Materials, Carl Hanser Verlag GmbH Co KG (2018).

[17] L.E. Murr, S.M. Gaytan, A. Ceylan, E. Martinez, J.L. Martinez, D.H. Hernandez, B.I. Machado, D.A. Ramirez, F. Medina, S. Collins, R.B. Wicker, Characterization of titanium aluminide alloy components fabricated by additive manufacturing using electron beam melting, (2010) 1887-1894.

[18]M.C.Commons. https://upload.wikimedia.org/wikipedia/commons/3/33/Selective_laser_melting_system_schematic.jpg. (date of access: July 2021)

[19] W. Kaiser, Kunststoffchemie für Ingenieure: von der Synthese bis zur Anwendung, Carl Hanser Verlag GmbH Co KG (2021).

[20] A. Pfister, Neue Materialsysteme für das Dreidimensionale Drucken und das Selektive Lasersintern, Universitätsbibliothek Freiburg, (2005).

[21] R.D.F. Laska, An investigation of polyamide 6 and 12 synthesis in an oscillatory baffled reactor, Engineering and Physical Sciences, (2019).

[22] T. Chen, W. Li, J. Jun, J. Pen, J. Chao, Modification of nanometre calcium carbonate and its application on PVC composites in situ suspension polymerisation, Materials Science and Technology 26(7) (2010) 871-874.

[23] C. Yan, L. Hao, L. Xu, Y. Shi, Preparation, characterisation and processing of carbon fibre/polyamide-12 composites for selective laser sintering, Composites Science and Technology 71(16) (2011) 1834-1841.

[24] J. Schmidt, M. Sachs, S. Fanselow, M. Zhao, S. Romeis, D. Drummer, K.-E. Wirth, W. Peukert, Optimized polybutylene terephthalate powders for selective laser beam melting, Chemical Engineering Science 156 (2016) 1-10.

[25] J. Koo, L. Pilato, G. Wissler, J. Cheng, W. Ho, K. Nguyen, S. Lao, A. Cummings, M. Ervin, Innovative selective laser sintering rapid manufacturing using nanotechnology, Proceedings of Solid Freeform Fabrication, Austin (2005) 98-108.

[26] B. Lecouvet, M. Sclavons, S. Bourbigot, C. Bailly, Towards scalable production of polyamide 12/halloysite nanocomposites via water-assisted extrusion: mechanical modeling, thermal and fire properties, Polymers for advanced technologies 25(2) (2014) 137-151.

[27] K. Stoeffler, L.A. Utracki, Y. Simard, S. Labonté, Polyamide 12 (PA12)/clay nanocomposites fabricated by conventional extrusion and water-assisted extrusion processes, Journal of Applied Polymer science 130(3) (2013) 1959-1974.

[28] J. Pietschmann, Industrielle Pulverbeschichtung, Springer (2010).

[29] M. Schmid, R. Kleijnen, M. Vetterli, K. Wegener, Influence of the origin of polyamide 12 powder on the laser sintering process and laser sintered parts, Applied Sciences 7(5) (2017) 462.

[30] B. Lang, J.W. McGinity, R.O. Williams III, Hot-melt extrusion–basic principles and pharmaceutical applications, Drug development and industrial pharmacy 40(9) (2014) 1133-1155.

[31] C. Eloo, M. Rechberger, Neue Technologien zur Herstellung thermoplastischer Pulver, Teipel, U.(Hrsg.) 5 (2011) 353-366.

[32] D. Gysau, Fillers for paints: fundamentals and applications, Vincentz Network GmbH & Co KG (2006).

[33] W.F. Tegethoff, Calciumcarbonat: von der Kreidezeit ins 21. Jahrhundert, Springer-Verlag (2013).

[34] M. Kenny, T. Oates, Lime and limestone, Ullmann's Encyclopedia of Industrial Chemistry (2000).

[35] T. Kato, T. Suzuki, T. Amamiya, T. Irie, M. Komiyama, H. Yui, Effects of macromolecules on the crystallization of CaCO3 the formation of organic/inorganic composites, Supramolecular Science 5(3-4) (1998) 411-415.

[36] J. Broda, C. Slusarczyk, J. Fabia, A. Demsar, Formation and properties of polypropylene/stearic acid composite fibers, Textile Research Journal 86(1) (2016) 64-71.

[37] H. Goodman, surface-modified fillers for polymer resins compositions, GB, (2003).

[38] G.W. Ehrenstein, G. Riedel, P. Trawiel, Thermal analysis of plastics: theory and practice, Carl Hanser Verlag GmbH Co KG (2012).

[39] R.G. Kleijnen, M. Schmid, K. Wegener, Nucleation and impact modification of polypropylene laser sintered parts, AIP Conference Proceedings, AIP Publishing LLC, (2016), p. 100004.

[40] L. Madsen, C. Grøn, I. Lind, J. Engell, Adsorption of benzoic acid on synthetic calcite dispersed in cyclohexane as a function of temperature, Journal of colloid and interface science 205(1) (1998) 53-64.

[41] P.D. Kaempfe, Kristallisation, Modifikation und Adsorptionseigenschaften von Calciumcarbonat sowie Untersuchung eines oszillierenden Kristallisationssystems, Duisburg, Essen, Universität Duisburg-Essen, Diss., (2011).

[42] A. Wegner, G. Witt, Ursachen für eine mangelnde Reproduzierbarkeit beim Laser-Sintern von Kunststoffbauteilen, RTejournal-Forum für Rapid Technologie, (2013).

[43] S. Kumar, Selective Laser Sintering/Melting, Comprehensive Materials Processing, Editors: Hashmi S., Batalha G. F, Van Tyne C. J, Yilbas B, Elsevier, Oxford (2014) 93-134.

[44] P. Gane, M. Buri, D. Spielmann, B. Neuenschwander, H. Scheidiger, D. Bättig, Mechanism of Post-Print Laser Marking on Coated Substrates: factors controlling ink ablation in the application of high brightness calcium carbonate, Journal of Graphic Technology 1 (2002).

[45] R. Bollström, P. Gane, Spot Application of a Transparent Nanoclay Layer to Provide Post-print Laser Marking Functionality on High Brightness 100% Calcium Carbonate Coatings, Advances in Printing and Media Technology (2016) 33.

[46] M. Schmid, K. Wegener, Additive manufacturing: polymers applicable for laser sintering (LS), Procedia Engineering 149 (2016) 457-464.

[47] V. Hristov, J. Vlachopoulos, Effects of polymer molecular weight and filler particle size on flow behavior of wood polymer composites, Polymer composites 29(8) (2008) 831-839.

[48] J.Z. Liang, Melt rheology of nanometre-calcium-carbonate-filled acrylonitrile–butadiene–styrene (ABS) copolymer composites during capillary extrusion, Polymer international 51(12) (2002) 1473-1478.

[49] F. Zoukrami, N. Haddaoui, C. Bailly, M. Sclavons, R. Legras, Elongational and shear flow behavior of calcium carbonate filled low density polyethylene: Effect of filler particle size, content, and surface treatment, Journal of Applied Polymer Science 123(1) (2012) 257-266.

[50] O.A. Jimoh, K.S. Ariffin, H.B. Hussin, A.E. Temitope, Synthesis of precipitated calcium carbonate: a review, Carbonates and Evaporites 33(2) (2018) 331-346.

[51] N. Erdogan, H.A. Eken, Precipitated calcium carbonate production, synthesis and properties, Physicochemical Problems of Mineral Processing 53 (2017).

[52] R. Patel, M. Patel, A. Suthar, Spray drying technology: an overview, Indian Journal of Science and Technology 2(10) (2009) 44-47.

[53] C. Croitoru, A. Pascu, I. Roata, E. Stanciu, Obtaining and characterization of polyolefin-filled calcium carbonate composites modified with stearic acid, IOP Conference Series: Materials Science and Engineering, IOP Publishing, (2017), p. 012041.

[54] Z.S. Stojanović, S. Marković, D. Uskoković, Determination of particle size distributions by laser diffraction, Technics–New Materials (Special Edition) (2012) 11-20.

[55] S.J. Blott, D.J. Croft, K. Pye, S.E. Saye, H.E. Wilson, Particle size analysis by laser diffraction, Geological Society, London, Special Publications 232(1) (2004) 63-73.

[56] P. Sinha, A. Datar, C. Jeong, X. Deng, Y.G. Chung, L.-C. Lin, Surface area determination of porous materials using the Brunauer–Emmett–Teller (BET) method: limitations and improvements, The Journal of Physical Chemistry C 123(33) (2019) 20195-20209.

[57] J.-P. Kruth, G. Levy, R. Schindel, T. Craeghs, E. Yasa, Consolidation of polymer powders by selective laser sintering, Proceedings of the 3rd International Conference on Polymers and Moulds Innovations, (2008), pp. 15-30.

[58] Y. Zhang, L. Hao, M. Savalani, R.A. Harris, K. Tanner, Characterization and dynamic mechanical analysis of selective laser sintered hydroxyapatite-filled polymeric composites, Journal of Biomedical Materials Research Part A 86(3) (2008) 607-616.

[59] S. Clark Ligon-Auer, M. Schwentenwein, C. Gorsche, J. Stampfl, R. Liska, Toughening of photo-curable polymer networks: a review, Polymer Chemistry 7(2) (2016) 257-286.

[60] G.W.H. Höhne, W. Hemminger, H.-J. Flammersheim, Theoretical fundamentals of differential scanning calorimeters, Differential Scanning Calorimetry, Springer (1996), pp. 21-40.

[61] B. Wunderlich, Thermal analysis of polymeric materials, Springer Science & Business Media (2005).

[62] D. Drummer, D. Rietzel, F. Kühnlein, Development of a characterization approach for the sintering behavior of new thermoplastics for selective laser sintering, Physics Procedia 5, Part B (2010) 533-542.

[63] Y. Leong, M. Abu Bakar, Z.M. Ishak, A. Ariffin, B. Pukanszky, Comparison of the mechanical properties and interfacial interactions between talc, kaolin, and calcium carbonate filled polypropylene composites, Journal of Applied Polymer Science 91(5) (2004) 3315-3326.

[64] R. Goodridge, C. Tuck, R. Hague, Laser sintering of polyamides and other polymers, Progress in Materials Science 57(2) (2012) 229-267.

[65] S. Singh, A. Sachdeva, V.S. Sharma, Optimization of selective laser sintering process parameters to achieve the maximum density and hardness in polyamide parts, Progress in Additive Manufacturing 2(1) (2017) 19-30.

[66] I. Gibson, D. Shi, Material properties and fabrication parameters in selective laser sintering process, Rapid Prototyping Journal 3(4) (1997) 129-136.

[67] J.D. Williams, C.R. Deckard, Advances in modeling the effects of selected parameters on the SLS process, Rapid Prototyping Journal 4(2) (1998) 90-100.

[68] H. Ho, I. Gibson, W. Cheung, Effects of energy density on morphology and properties of selective laser sintered polycarbonate, Journal of Materials Processing Technology 89 (1999) 204-210.

[69] A.E. Tontowi, T. Childs, Density prediction of crystalline polymer sintered parts at various powder bed temperatures, Rapid Prototyping Journal 7(3) (2001) 180-184.

[70] Y. Shi, Z. Li, H. Sun, S. Huang, F. Zeng, Effect of the properties of the polymer materials on the quality of selective laser sintering parts, Proceedings of the Institution of Mechanical Engineers, Part L: Journal of Materials Design and Applications 218(3) (2004) 247-252.

[71] W. Zuiderduin, C. Westzaan, J. Huetink, R. Gaymans, Toughening of polypropylene with calcium carbonate particles, Polymer 44(1) (2003) 261-275.

[72] P.G. Koutsoukos, C.G. Kontoyannis, Precipitation of calcium carbonate in aqueous solutions, Journal of the Chemical Society, Faraday Transactions 1: Physical Chemistry in Condensed Phases 80(5) (1984) 1181-1192.